EXPERIMENTAL INVESTIGATION ON WELDING AND WELDABILITY OF 316L AUSTENITIC AND 430 FERRITIC STAINLESS STEELS DISSIMILAR METAL JOINTS

Thesis Submitted for the Award of the Degree of

DOCTOR OF PHILOSOPHY

in

Mechanical Engineering

By

TEMBHURKAR CHETAN KISHOR

41700265

Supervised By   **Co-Supervised by**

Dr.Ravinder Kataria   **Dr.Sachin Ambade**

LOVELY PROFESSIONAL UNIVERSITY
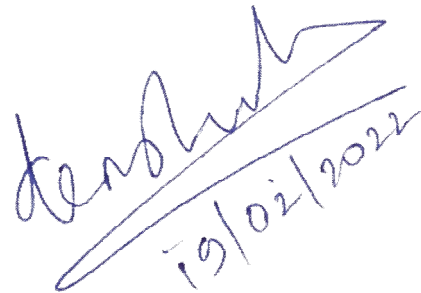*Transforming Education Transforming India*

LOVELY PROFESSIONAL UNIVERSITY

PUNJAB

2022

Declaration

I, hereby declare that the thesis titled **"Experimental investigation on welding and weldability of 316L Austenitic and 430 Ferritic stainless steels dissimilar metal joints"** submitted herein has been carried out by me in the School of Mechanical Engineering, Lovely Professional University, Phagwara, Punjab. The work is original and has not been submitted earlier as a whole or in part for the award of any degree/diploma at this or any other Institution/University.

TEMBHURKAR CHETAN KISHOR

Date: 19/02/2022

Certificate

The thesis titled **"Experimental investigation on welding and weldability of 316L Austenitic and 430 Ferritic stainless steels dissimilar metal joints"** submitted by **Tembhurkar Chetan Kishor** for the award of degree of Doctor of Philosophy, has been carried out under my supervision at the School of Mechanical Engineering, Lovely Professional University, Phagwara, Punjab. The work is comprehensive, complete and fit for evaluation.

Dr. Ravinder Kataria

(Supervisor)

Associate Professor

School of Mechanical Engineering,

Lovely Professional University, Phagwara,

Punjab

Dr. Sachin Ambade

(Co-Supervisor)

Assistant Professor

Department of Mechanical Engineering,

Yeshwantrao Chavan College of

Engineering, Nagpur, Maharashtra

ABSTRACT

Austenitic Stainless Steel (ASS) is a kind of stainless steel that is extensively used. Its welding and corrosion behavior with similar and dissimilar metals has been extensively studied and is well documented. For better economic alternative, high heat resistant and good sustainability in chloride environment, industries are looking ferritic stainless steel (FSS) than ASS. For example, ASS was extensively used in constructions of boilers, valves, pipelines, etc in chemical, petrochemical, oil, gas, shipbuilding, defense, railways and nuclear industries. As the price of nickel is rising, the nickel in austenitic stainless steel may make it a more expensive material to use. So, manufacturers are looking for better alternative of ASS. However, due to the lack of phase transformation, FSS has low weldability and grain growth in the heat affected zone (HAZ) and weld zone (WZ), resulting in low ductility and toughness. Therefore, a careful selection of fillers and welding processes is more important to provide sound weld joint for dissimilar welding. The dissimilar welding of ASS and FSS by conventional welding process consist a welding defect called "spattering". To overcome this welding defect, the dissimilar welding should be done with advanced welding processes where these welding defects is minimized or does not occur. Welding with this advanced welding processes gives better mechanical and corrosion properties than conventional welding processes. The dissimilar welding of ASS and FSS shows precipitation of martensite during cooling when heat input is higher and cooling rate is lower. This may change the microstructure, corrosion and mechanical characteristics of the weld metal. Welding processes, welding parameters, weld heat input, affect the sensitization and pitting resistance of the weld joint. The chemical composition of rods or fillers plays an important part in pitting resistance. Therefore, special attention in welding processes and selection of fillers is required for the dissimilar weld joint. The present investigation takes care of all these and aims to highlight this systematically.

The thesis has been structured into chapters including an Introduction, Literature Review, Experimental work, Results and Discussion and Conclusions.

It is found that, welding with ER 316L filler increases tensile strength (~ 573 MPa), toughness (~ 47 J) of the welded joint as compared to ER 309L (~ 27 J) and autogenous weld (~ 20 J) joint whereas hardness is greater in autogenous weld (avg.317.0 HV). It is found that the dissimilar weld joint shows a microstructure which contains martensite and chromium carbide precipitation in the welded joint which increases the hardness of the weld joint. It is found that the dissimilar weld joint shows passivity in 0.5M H_2SO_4 and 0.01M NH_4SCN.It is attributed to formation of film of $Cr_{23}C_6$ (Chromium carbide) on the surface of welded joint. The degree of sensitization is greater in autogenous weld (45.6233 %) as compared to ER 309L (4.9504 %) and ER 316L filler (3.5073 %). The pitting potential found highest in ER 309L filler (0.086077 mV) as compared to ER 316L (0.021578 mV) and autogenous weld (-0.018582 mV) due to the solid solution strengthening weld joint and chemical composition of fillers used in welding. In advanced welding process such as Cold Metal Transfer (CMT) welding with GTAW mode increases tensile strength, toughness, pitting potential and decreases degree of sensitization of the weld joint.

ACKNOWLEDGEMENT

TABLE OF CONTENTS

LIST OF TABLES

LIST OF FIGURES

LIST OF SYMBOLS

A	Ampere
c.d	Current density
E_{bd}	Breakdown potential
E_{corr}	Corrosion potential
E_{pass}	Passive potential
E_{ppp}	Primary passive potential
E_{pit}	Pitting potential
i_{corr}	Corrosion current density
i_{crit}	Critical current density
i_{pass}	Passive current density
OCP	Open circuit potential
HI	Heat input
η	Efficiency of welding
I	Welding Current
W	Welding Speed
SCE	Saturated calomel electrode
SEM	Scanning electron microscopy
V	Volts
βa	Anodic Tafel slope

βc	Cathodic Tafel slope
μ	Micro

CHAPTER 1: INTRODUCTION

1.1 Preamble

Austenitic stainless steel has an excellent corrosion resistance and a high tensile strength which is often utilised in many industries. Its welding with similar and dissimilar metals and its corrosion behaviour has been widely studied and well documented. The most common austenitic stainless steel (ASS) used in industries are 304L and 316L stainless steel (SS). Among these, 316L austenitic stainless steel have greater strength and better resistance to corrosion. However, 316L composition by weight (%) contains high amount of nickel (Ni) and the price of nickel increasing day by day, which breaks the spine of manufacturers and consumers. Thus, the field of research has been the replacement of austenitic stainless steel with another stainless steel. Among industries, ferritic stainless steel (FSS) shows high heat resistant and good durability in chloride environments and also shows an economic alternative than austenitic stainless steel. But dissimilar joining of FSS with ASS is difficult as both the stainless steel has different physical, mechanical and metallurgical property. Due to the lack of phase transformation, ferritic stainless steel has low weldability and low grain growth in the weld zone and in the heat affected zone, which leads to poor toughness and ductility. Therefore, to make the sound weld joint the proper selection of fillers and parameters for welding processes is important.

1.2 Austenitic Stainless Steel (ASS)

Austenitic stainless steel can be widely used in various industries such as chemical, petrochemical, oil and nuclear industries which can be variedly used to produce storage tanks, pressure cups and furnace equipment's due to higher corrosion resistance and mechanical properties at elevated temperature [1]. Any fusion process, such as GTAW, SMAW, or GMAW, can easily weld austenitic stainless steel. However, in current situation, the major concern in various industries is to search alternative material, as the cost of Nickel (Ni) content in austenitic stainless steel is high [2]. Low carbon austenitic stainless steel 316L, which has high resistant to intergranular corrosion, is often employed in applications that require this feature [3].

1.3 Ferritic Stainless Steel (FSS)

Ferritic stainless steel is a heat resistant material and can be used in shipbuilding, defence, railways and nuclear industries to produce pressure vessels, bridges, building structures, aircraft and space crafts, railway coaches and general applications [4]. Welding of ferritic stainless steel displays the issue of coarse grains in the weld zone and heat affected zone of the fusion welds and consequent low toughness and ductility due to the absence of phase transformation during which grain refinement can occur [5]. The importance of delta-ferrite influence besides the metallurgical and microstructural properties which must be controlled which affects the mechanical properties of the material [6]. Ferritic stainless steel AISI 430 is used mainly for household utensils to oil, automotive trim, nuclear, fasteners, power, pressure vessels and petrochemical industries [7,8].

1.4 Welding of Stainless Steel

Welding is a permanent bonding process in which various materials, such as metals, alloys, and plastics are joined to contact surfaces by applying heat and/or pressure by means of with or without filler material. The component to be joined will be welded at the interface and a permanent joint will be created after solidification [9]. In certain instances, a filler is used to produce a weld pool of molten material which is firmly attached between the components after solidifying. The material's weldability depends on different factors such as changing the metal during welding, changing the hardness of the weld due to rapid solidification, the degree of oxidation due to the material and oxygen interaction in the atmosphere and the tendency to formation of the crack at a welded joint [10].The metallurgical changes at the heat affected zone (HAZ) of the weld are very important because they directly affect the mechanical characteristics of the weld and the performance of the weld. The metallographic structure (HAZ) of the base metal varies slightly with respect to distributions of pearlite, ferrite and grain size depending on the accepted welding conditions. In just one pass of welding gun, the material heats up quickly to its maximum temperature and cooled slowly by transferring heat to base materials. Depending on the temperature reached, a phase change may occur. If the distance from the welding pool is adequate, the material will not be affected. The region adjacent to the molten area where microstructural changes take place without affecting the melting of the underlying material

2

is termed as heat affected zone (HAZ). These variations in the microstructure may impact and must be regulated on the mechanical and corrosion characteristics of the weld.

The microstructure of the molten metal is mainly controlled by the cooling cycle. The lower the energy consumption (i.e., lower the current), the shorter the solidification time. Fine grains grow due to quenching. The more energy is supplied, the less time it takes to solidify, the slower the cooling rate and the bigger the grain size. The coarse grain in the microstructure specifies low hardness and low tensile strength. The welding arc heats above the critical temperature (955^0C), causing the ferrite grains to grow rapidly. Of course, the heat input of the weld may be reduced by preventing overgrowth of the grain. In the present research the difference between the conventional and advanced welding techniques are compared. Firstly, the Gas Tungsten arc welding (GTAW) uses a non-consumable tungsten electrode and an inert gas and a separate filler material [11]. In this process, an electric arc is formed between the tungsten electrode and the base metal. However, GTAW is subject to limitations if a thickness more than 3 mm joint edge preparation exists and the entire GTAW welding process requires multiple passes to fill the joint [12]. Secondly, Cold Metal transfer (CMT) which is an advanced metal inert gas welding process which is based on short-circuiting transfer process and it result in spatter-free MIG/MAG robot welding of ultra-light gauge sheets from 0.3 mm in either computerized or manual process [13].

1.5   Parameters affecting welding of Stainless Steel

Ferritic stainless steel can be used in applications such as shipbuilding, defence, railways and nuclear industries to produce pressure vessels, bridges, building structures, aircraft and space crafts. Grain coarsening within the heat-affected zone and the weld zone of fusion welds is a concern with ferritic stainless steels. As a result, welded joints lose toughness and ductility, limiting their applicability in engineering applications. As a result, ferritic stainless steel can be used in place of austenitic stainless steel in a variety of applications. This application required use of welding and therefore, weldability of ferritic stainless steel has received attention [14]. Many researchers have examined the effects of various welding processes under various welding conditions, as well as changes in the microstructure and mechanical characteristics of ferritic stainless steels [15-18]. Typically, heating due to welding will cause grain growth and refinement depending upon the temperature reached,

heating time and cooling rate. Upon cooling after welding, chromium carbide ($Cr_{23}C_6$) is deposited at the grain boundaries. If titanium or other alternative particles are used, titanium nitride is also precipitated along the grain boundaries. During quenching, martensite is also formed along the edges of the quenched ferrite particles. The formation of molten metals from stainless steel to low/medium chromium ferrite and martensite is common in HAZ. All of these microstructural changes are detrimental to corrosion resistance.

To maintain the correct weld size, several important parameters affect the welding of stainless steel and it need to be analyzed and adjusted during welding. There are five important parameters such as electrode size, current or heat, electrode angle, travel speed and arc length.

1.5.1 Electrode size

The size of the electrode affects the penetration depth at a fixed current and the shape of the weld. The rate of deposition is determined by the electrode size. The smaller diameter electrode has a greater current density and faster deposition rate as compared to the larger diameter electrode at any given current. However, larger diameter electrodes are better since they carry more current, which means they deposit the material quicker. Location and type of weld also affect the size of the electrode. The next successive pass is made with a larger electrode. Electrodes that are too large may become clogged or difficult to remove. The final bead is usually convex and overlapping. Electrodes that are too small will dissolve and wear out too quickly, making it difficult to maintain a stable arc length [102,103-107].

1.5.2 Current

The welding current is the most important parameter because it impacts the melting rate and current density of the filler and base metal [108]. This welding current has an effect on the mechanical and microstructural properties of the weld by changing the size of the weld pool and the heat affected zone (HAZ). With increasing welding current, penetration and gain increase. If the current intensity at a given welding speed is too high, the penetration will be too great, and the weld melts. High currents will induce undercutting and digging

arc. This may result in the use of unnecessary electrodes in the form of over-enhancement. This welding will enhance the shrinkage of the weld and produce more deformation.

In the DCEP polarity, the shape of the weld increases as the welding current reaches a critical value and then begins to decrease [109]. However, when using DCEN polarity, the shape of the weld increases as the current in the entire area increases [109]. If the same flux is used, the heat-affected zone will increase as the welding current increases. Too low current will cause inadequate penetration and incomplete melting [95]. Too low current can also cause overlapping and unstable arcs. The shape of the weld, the welding speed, and the weld quality are all affected by the current [95].

1.5.3 Electrode angle

The shape of the weld is greatly influenced by the clamping angle. Deep groove welds, in particular, need this. The electrode angle is made up of two positions: working angle and travel angle. The working angle is the angle of the horizontal plane, defined as the measurement of an angle at 90 degrees in relation to the welding direction. Depending on the welder's preference and circumstances, the angle in the welding direction varies from 5 to 20 degrees. Weld bead size will be affected by the width of the welding travel path that deviates from the surface of the plate. Choosing the wrong angle may result in unequal leg length, bad fusion, and an undercut in the upper leg. Fillet welds in particular rely on the right working angle. Small changes in working angle often did not affect the weld's appearance or quality [96, 99-101].

1.5.4 Travel speed

The welding speed is the linear speed of the arc as it advances along the weld. The impact of speed on welding quality varies with the various welding parameters and demonstrates the broad nature of the variables involved. The use of less filler material in the weld means that as the welding speed increases, less reinforcement is needed in the weld. This means that the weld bead is smaller. Other than current, welding speed is the most influential factor on weld penetration. In these situations, the molten pool must be lower than the welding electrode. The amount of slag in the weld metal increases.

1.5.5 Arc length

The arc length constantly varies when the electrode is consumed. A lengthy arc will be impossible to control, and will likely end up stopping the arc entirely. A wide, spattered, and irregular deposit forms when the welded base metal melts with the rest of the base metal. The electrode sticks to the base material when the arc length is too small, and forms uneven deposits, since the heat is insufficient to melt the base material. The rod will not function correctly if the arc length is too short.

For best results, one must use the suggested arc length, which corresponds to the diameter of the electrode tip that will be exposed. Arc length varies on the kind of welding electrode, and the type of welding used. Therefore, smaller electrodes require shorter arcs than larger electrodes [99- 101].

1.6 Welding defects

Weld defects can be caused by improper process selection, improper joint design, improper welding parameters, improper technique, improper suspension and inadequate consumables. Defects such as inclusions, under filling, cracks, lack of penetration, porosity, spatter, cracks, undercuts and overlaps. These defects decrease the weld joint's strength and efficiency and are prone to premature failure. Some defects such as shrinkage/rupture, lack of melting and pore expansion are unacceptable. However, some defects such as imperfect penetration, slag inclusion, and microporosity are acceptable within acceptable limits [19]. The multi-pass welding results in inclusions which is shown by dark etching particle near position D shown in figure 1.1 due to the incomplete slag removal from the weld. The other weld defects such as lack of fusion (A), lamellar tearing (B), poor profile (C) and undercut (E) is shown in figure 1.1. The increase in welding current also influences the welding defects. As the welding current increases it leads to increase in coarse grain formation which leads to lack in penetration [18]. The increase in welding speed also leads to weld defects. As the welding speed increases the delta-ferrite formation takes place which increases the chances of failure of the joint [133].
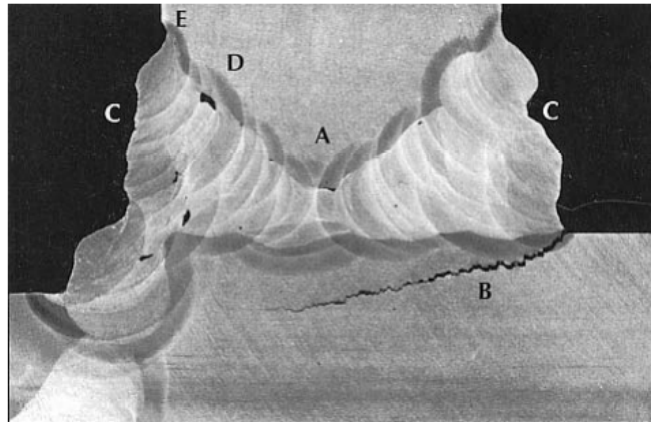
Figure 1.1: Weld defects:(A) lack of fusion; (B) lamellar tearing;(C) poor profile;
(D) inclusions; and (E) undercut [20]

1.6.1 Welding defects due to welding current

The weld metal is often of lower quality than the base metal due to segregation of solutes and/or microstructural inhomogeneities. The ultimate microstructure of the weld metal influences mechanical characteristics, corrosion resistance, and high temperature cracking behaviour. The weld metal microstructure is influenced by both solidification behaviour and subsequent solid-state changes at room temperature [35]. All ASSs can solidify as primary ferrite or primary austenite depending on the composition of alloy. Primary ferrite converts entirely to austenite under equilibrium conditions, which is stable at ambient temperatures. This transformation is hampered by rapid cooling after welding and there may be residual ferrite in the final microstructure. Variable cooling rates can influence the quantity of delta-ferrite in the weld metal microstructure at ambient temperature, and small differences in composition within an alloy can cause a transition from primary ferrite to primary austenite [35,133]. The thermal characteristics of ASS are detrimental to the entire thermal cycle during the entire welding process and after cooling. An uneven heating and longer exposure to high temperatures can lead to changes in metallurgical phenomena in the fusion zone (FZ) and heat affected zone (HAZ), which can damage the weld's characteristics and cannot be suitable for a variety of applications.

1.6.2 Welding defects due to welding speed

Fine dimples can be visible in the weld pool at low weld speeds, while elongated dimples can be seen at high weld speed [8]. The grains are curved to grow perpendicular to the pool's boundary because the trailing portion of the elliptical weld pool's boundary is curved. In contrast, the trailing portion of the extended weld pool has an essentially straight boundary, and the grains are equally straight, growing virtually perpendicular to the boundary of the pool. As a result, for weld metals free of heterogeneous nuclei, columnar grains should curve and develop in the direction of welding at low welding speeds, while growing straight towards the weld centreline at high welding speeds. As a result, at high welding speed, changes in growth directions occur, which might compromise weld toughness by increasing the possibility of segregation near the weld centreline. This limits the maximum welding speed that can be utilised in particular circumstances [133].

1.7 Corrosion of weld joint

Intergranular corrosion is associated with a highly active grain boundary effect that causes localized damage to adjacent grain boundaries with a relatively small corrosion of grains in stainless steel [21,22]. This can result in strength loss due to impurities at the grain boundaries, alloying element enrichment, or depletion of one of these elements in the grain boundary area [21]. Ferritic stainless steels have significantly reduced corrosion resistance due to welding. These steels can be exposed to a various form of corrosion including intergranular corrosion (IGC), crevice corrosion and pitting corrosion. Because of the lack of nickel, these materials are generally resistant to stress corrosion cracking and represent a viable alternative to austenitic stainless steels in chloride-containing environments. IGC is very sensitive to the weld process and post weld adjustments, but with the right alloy selection, crevice and pitting corrosion can usually be prevented.

The issue with FSS welding is that HAZ is susceptible to intergranular corrosion due to low chromium content in the weld matrix, which is a severe issue. Regardless of its economic attractiveness, its moderate strength combined with good corrosion resistance in corrosive and acidic environments influences its employment in specific engineering applications. This susceptibility is known as sensitization. It is widely thought that stress corrosion cracking occurs as a result of sensitization in some ferritic stainless steels [23].

1.8   Dissimilar metal welding (DMW) (ASS and FSS)

Dissimilar metal joints in structural materials have become important for numerous industrial applications such as the chemical, petrochemical, oil, and shipbuilding industries. Dissimilar metal welding (DMW) has received increasing attention in recent years in order to reduce material prices and usage [24]. In addition, they are expected to provide good results; DMW is a useful way to combine metals for different purposes [25]. Dissimilar joints usually experience different conditions of use, especially temperature variations, which will affect their performance [26]. As a result, according to the conditions of use, the weld metal must have reasonably good features such as oxidation, heat transmission capabilities, mechanical properties, and corrosion resistance at high temperatures [27]. DMW is more difficult to weld than similar metals in general due to the base metal's unusual physical, mechanical, and metallurgical properties [28]. These differences make it difficult to choose a suitable filler material because the physical properties of the two base materials are different [29]. The choice of joining method for this combination of materials is difficult due to its physical and chemical properties. This method is often useful when mechanical or service characteristics need to be conveyed. The joining of austenitic stainless steel with ferritic stainless steel is problematic due to the development of chromium carbide in various locations of the junction [28]. The austenitic stainless steel can be welded with ferritic stainless steel with the help of different filler material such as 308L, Inconel 182, ERNiCu-7 and ERNICr-3 [31]. Therefore, for a sound joint the selection of filler material should be proper. When a significant heat input occurs, such during a welding technique like GTAW, it may create brittleness in the metal [32]. For joints created with dissimilar metal joint, the mechanical properties of the joints should not be lower than of the weaker base metal [33].

The next chapter addresses the literature review of dissimilar joint of ASS and FSS by GTAW and Cold Metal Transfer (CMT) welding. The dissimilar joints were discussed with different types of fillers used for joining. The different types of corrosion tests are discussed for dissimilar metal joints. The microstructure of dissimilar joints was studied using an optical microscope, as well as mechanical tests such as tensile, impact, and hardness tests.

CHAPTER 2: LITERATURE REVIEW

2.1 Preamble

Stainless steels are utilized in a wide variety of applications and are widely used in different types of industries. The various types of stainless steels include martensitic, duplex, austenitic, ferritic and age hardening precipitation stainless steel. These stainless steels are used in a wide range of applications, including the chemical, petrochemical, pharmaceutical, dairy and food processing industries. The austenitic stainless steel is classified into 200-series and 300-series. Among these two types, 300-series has more corrosion resistance, strength, hardness and formability than 200-series austenitic stainless steel due to increased content of chromium percentage in 300-series stainless steel. Sensitization occurs as a result of chromium depletion in stainless steel caused by continuous heating of stainless steel over a specified temperature range.The carbon, chromium, nickel, manganese is used as alloying elements to improve strength, hardness and sensitization. The 316L Austenitic Stainless Steel can be welded by gas tungsten arc welding (GTAW), shielded metal arc welding (SMAW), flux cored arc welding (FCAW), electron beam welding (EBW), laser beam welding (LBW) and plasma arc welding (PAW). It can be also welded by advanced welding processes such as cold metal transfer (CMT), friction, explosive and ultrasonic welding. The sound weld joint is due to the important parameters such as electrode size, current or heat, electrode angle, travel speed and arc length. The 316L ASS weld metals can be analyzed by means of microstructural development, mechanical and corrosion properties. The welded 430 FSS can be analyzed by means of delta-ferrite formation, microstructural, mechanical and corrosion properties. Thus, the 316L ASS and 430 FSS dissimilar weld can be analyzed by means of microstructural, corrosion and mechanical properties.

2.2 Stainless Steel (SS)

Stainless steels (SSs) are broadly utilized in various types of industries and environments. Stainless steels are production substances for corrosion-resistant equipment in chemical, petroleum, shipbuilding and nuclear industries [34-35]. Since the beginning of stainless-steel production, the number of grades with significant chemical composition and mechanical properties has increased rapidly over the years.

All stainless steels have iron, which is combined with 10.5% chromium. Chromium (Cr) reacts with oxygen and ambient moisture in this percentage of chromium to produce an adherent protective and consistency oxide layer that covers the whole material surface and offers good resistance to corrosion. Corrosion resistance may be further improved by adding up to 8 percent or more nickel, while providing different physical properties. The addition of molybdenum increases corrosion resistance, while nitrogen increases the mechanical strength and pitting resistance.

Since microstructure has a decisive influence on physical properties, stainless steels are classified according to their microstructure at room temperature. The stainless-steel family's key feature is corrosion resistance. The most important alloying element is chromium, which requires more than 10.5 %. This amount of chromium is thought to be sufficient to make a passive chromium oxide layer (Cr_2O_3), which protects base metal from corrosion and oxidation under environmental circumstances [36-37] (the state in which stainless steels shows a very low corrosion rate is known as passive state). However, stainless steel is susceptible to pitting, cracking, and intergranular corrosion (IGC) in certain corrosive conditions (such as chloride and fluoride environments). This form of corrosion weakens the self- healing barrier and reduces corrosion resistance [36-37]. The various types of stainless steels are chemically dependent and have unique corrosion resistance, mechanical properties and cost. The right stainless steel should be choosen according to the needs [37]. Stainless steel used in applications such as household appliances, chemical storage tanks, electronic and decorative materials to clean and hygienic items in industries such as pharmaceutical, dairy, food processing etc. [34-35].

Stainless steel is exposed to various temperatures during manufacturing processes (such as welding) and operations such as pressure vessels or reactors. Since the microstructure of

the material can change, so that manufacturing process must be carefully controlled. These changes can reduce the corrosion resistance and mechanical properties of the stainless steel after fabrication [9,38].

2.3 Classification of Stainless Steel

The stainless-steel types can be distinguished in different ways, for example with regard to their use, the alloying elements used in their manufacture or in particular. As a result, these kinds of stainless steels are classified as austenitic, ferritic, and martensitic stainless steels. Further, duplex stainless steel and precipitation-hardening (PH) types of stainless steel are included in the stainless-steel family corrosion-resistant stainless steel [36-37]. Such a classification is shown in figure 2.1.
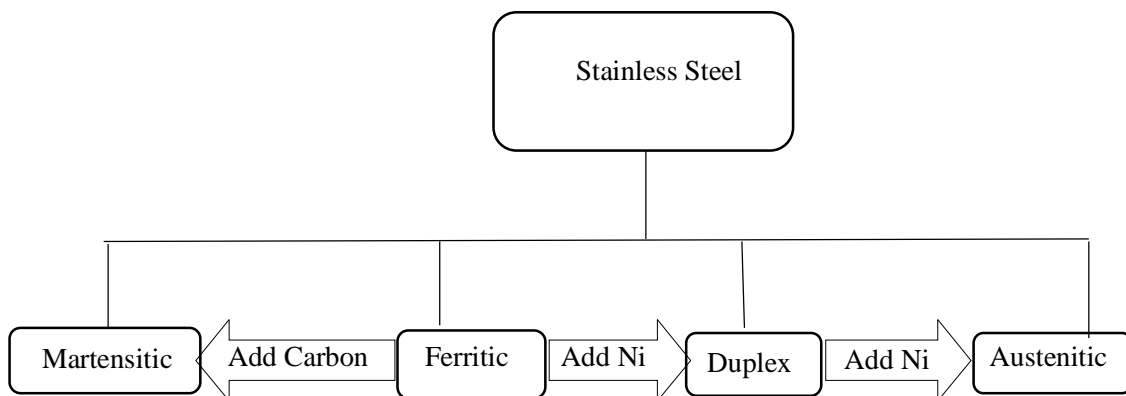
Figure 2.1: Classification of Stainless Steel

2.3.1 Martensitic Stainless Steel (MSS)

Martensitic stainless steel can be hardened with the same heat treatment as ordinary carbon steel. This steel mainly consists of Iron (Fe) – Chromium (Cr) – Carbon (C) ferrous alloy system that induces strength and ductility in a unique microstructure that can be controlled by heat treatment. The greater the hardness, the greater the strength and the lesser the ductility. The corrosion resistance of these steels is usually lower than ferritic, austenitic and duplex stainless steels. Corrosion resistance may be better in the hardened state than in the annealed or soft state. Martensitic stainless steel (MSS) can be heat treated to increase tensile strength. MSS is utilized for applications with moderate resistance to corrosion and high strength or toughness. Due to their excellent mechanical properties and corrosion

12

resistance, they are used in water and steam valves, turbines, pumps, shafts, bearings, cutting devices, and appliances. MSS can also be used in application like valve parts, ball bearings and surgical instruments, valve steams, nut, bolts and other parts [34, 39, 40]. AISI 403, 410, 420 and 431 are types of martensitic stainless steel [35-37,41-43].

2.3.2 Duplex Stainless Steel (DSS)

Duplex stainless steel has a duplex microstructure made up of ferritic and austenitic grains, which are both utilized in the material. Ferrite and austenite phases are usually in approximately equal volume fractions in the ferrite range of 30–70%. Duplex stainless steel is stronger than austenitic stainless steel and has greater resistance to corrosion and a better stress resistance for cracking [44]. The oil and gas, pulp and paper, petrochemical gas, desalination, and pollution control industries all make extensive use of duplex stainless steel. Duplex stainless steels are divided into three categories based on the number of alloying elements: thin, medium, and high [45]. The duplex microstructure provides an interesting combination of properties to the family of stainless steels. The strength of duplex stainless steels is approximately double that of austenitic or ferritic stainless steels. Duplex stainless steel is much tough and more ductile than ferritic stainless steels. The pitting and crevice corrosion resistance in term of chloride environment are affected by the chromium, molybdenum and nitrogen content. When compared to austenitic stainless steels, the duplex stainless-steel grades have comparable or greater corrosion resistance. Duplex stainless steels have excellent resistance to stress corrosion cracking inherited from ferritic stainless steel. Duplex steels with the same corrosion resistance are less expensive than other stainless steels, given that the amount of nickel and molybdenum is less. As duplex stainless steel has a lower alloy content, it can be cheaper, especially for high alloys [46]. DP3W, Zeron100, SAF2502, 2250 and S32550 are types of duplex stainless steel [36-37, 41-43].

2.3.3 Austenitic Stainless Steel

Austenitic stainless steel has a wide range of applications, including boilers, chemical pipelines, chemical containers, and heat exchangers for the petrochemical, chemical, petroleum, nuclear, and shipbuilding industries [1]. Austenitic stainless steel is used in 60 to 70 percent of industries. There are two distinct types of austenitic stainless steel (ASS): 300-series stainless steel and 200-series stainless steel. The 300-series (mainly 304L and 316L stainless steel) is the most normally used type of ASS. In comparison to 304L ASS, 316L austenitic stainless steel has increased resistance to corrosion and strength [47]. To produce the austenitic structure, the 300-series alloy utilises alloying elements such as nickel (Ni), nitrogen (N), copper (Cu), manganese (Mn), and carbon (C) as well as iron chromium (Fe-Cr) alloy [35]. Nickel is an important component in the stabilization of the austenitic structure, which makes metals more ductile, tougher, and resistant to corrosive environments. The ASS series will begin to precipitate Chromium carbide ($Cr_{23}C_6$) in the temperature range of 450^0 C to 900^0 C if it is slowly heated or cooled [35-37]. This results in chromium depletion near the grain boundaries. If the chromium concentration in the matrix is less than 10-11 wt %, it will be more susceptible to intergranular corrosion (IGC), also known as sensitization, since Cr_2O_3 layer is not passive enough to protect ASS [48-50]. ASS is excellent in tensile strength and in many corrosive environments. It contains a minimum of 16 to 18 % chromium which is helpful to develop protective (passive) film and corrosion resistance properties. It is excellent in tensile strength and in many corrosive environments. Though, stainless steel has a problem with corrosion, it also suffers from cracking, decay, and pitting [51]. These corrosive environments weaken the protective film in the material as discussed above and lower the corrosion resistance. So, there are broad ranges of stainless steel available in the market such as AISI 201, 202, 304, 316, 310, 321, 347 etc. and these types of materials can be used as per the requirement. [36-37, 41-43].

2.3.4 Ferritic Stainless Steel

Ferritic stainless steel is commonly used in petroleum refining equipment, furnace parts, heat exchangers, oil burner parts, protection tubes, storage vessels, chemical processing equipment, electrical appliances, solar water heaters, and household appliances [52]. About half of the stainless steels in the AISI 400 series are made up of ferritic stainless steel (FSS). These steels include metals such as molybdenum, which helps give them added strength. In chloride environments, FSS is known for its strong resistance to stress corrosion cracking (SCC), pitting, and crevice corrosion [18]. It is the second most frequently used stainless steel because of its good corrosion resistance and cheaper cost [53]. Ferritic stainless steels have excellent properties and low nickel content, making them an excellent alternative to Fe-Cr stainless steel in many industries [54]. During the production process, various processes such as rolling, heat treatment and welding are performed. Welding makes microstructure weaker, reduces mechanical characteristics, and has the ability to directly impact corrosion resistance. During welding, chromium is deposited at the grain boundaries, causing corrosion between grains in case of stainless steel.

Moreover, there are several ways to control this intergranular corrosion in the stainless steel viz. (1) control the interstitial elements (2) control the ferritic factor (3) by using the stabilization technique (4) control the weld heat input and cooling rate [55]. Ferritic stainless steels (FSS) are used, which exhibit high heat resistance and good durability in chloride environments, and are also an economical alternative to austenitic stainless steel (ASS). Some applications, however, require the joint integrity of FSS and ASS [56], but FSS has low weldability and grain growth in the WZ and HAZ, resulting in low ductility and toughness due to a lack of phase transformations. AISI 405, 409, 409M, 410S, 430, 434, and 446 etc. are some typical steels in this category [36-37,41-43]. There are various stainless steels for industrial and domestic construction according to customer needs, and each with specific alloying elements added according to the purpose and application based on weldability, strength and durability [56].

430 FSS are used in applications such as household utensils, vehicle exhaust, road and rail vehicles, oil, gas, petrochemical, nuclear and power industries [7]. 430 FSS is a low-cost

15

alloy with high strength and resistance to corrosion. The main problem with FSS welding is the lack of ductility in the heat affected zone. Coarse grain growth in the HAZ of fusion welds causes this problem. The temperature in this region reaches a critical temperature (955^{0}C), causing rapid growth of ferrite grains [57]. Furthermore, despite FSS's low carbon content, fast cooling can result in the development of martensite at grain boundaries and/or low chromium concentration areas along HAZ's grain boundaries. The formation of martensite in the HAZ reduces ductility and toughness even in small amount. Carbide precipitation can expose steel to intergranular corrosion.

2.3.5 Age hardening precipitation Stainless Steel

Age hardening stainless steel grades may be hardened at a very high temperature since they are age hardening Cr-Ni types. These grades can have an austenitic, semi-austenitic or martensitic structure. Adding components like copper and aluminum will give this steel its strengthening effect. These elements form intermetallic compounds with aging. When annealed in solution, this grade has properties similar to those of austenitic grade. The hardening of the deposits should not be exposed to higher temperatures during welding or during service as the deposits decreases strength. S17400, S17700, and S14800 etc. are types of age hardening precipitation stainless steel [34-36,41-43].

2.4 Types of Austenitic Stainless steel

Austenitic stainless steels are generally intended for usage in corrosive conditions ranging from mild to severe. It is also used in applications requiring high hardness (e.g., cryogenic temperatures) and other applications requiring good oxidation resistance (at temperatures above 600^{0}C) [34-35]. Austenitic stainless steels are non-magnetic and can also be used where magnetic materials are unacceptable. Austenitic stainless steels at a temperature equal to 1400^{0}C have a single-phase FCC structure over a wide temperature range. This structure is the result of an alloy equilibrium that stabilizes the austenite phase from high to cryogenic temperature. In order to strengthen these alloys, they need to either be solid solution strengthened or work hardened. Since they're primarily single-phase, neither of these options is ideal [58]. The austenitic stainless-steel fall into two main categories such as 200- series and 300-series.

2.4.1 The 200-series

The standard 200- series stainless steels are also referred to as Cr-Mn austenitic stainless steels [59]. They typically contain 15-19 % Cr, high Mn (5-15%) and low Ni content (less than or equal to 5%). The most common types of chromium and manganese are often listed by their nickel content (e.g., 4% Ni and 1% Ni). The stainless-steel chemical composition is shown in the table. In recent years, the cheaper Cr-Mn steels with slightly different chemical composition has increased drastically. As shown in table 2.1, China specifically calls them new 200-series, even though the name has been widely used throughout Southeast Asia [59].

Table 2.1: Chemical composition of 200-series stainless steel [60]

Grades		Chemical composition (wt %)					
AISI	UNS	C	Cr	Mn	N	Ni	Cu
201	S20100	0.15 max	16.0-18.0	5.50-7.50	0.25 max	3.50-5.50	-
202	S20200	0.15 max	17.0-19.0	7.50– 10.0	0.25 max	4.00 – 6.00	
204 Cu	S20430	0.15 max	15.5 – 17.5	6.50 – 9.0	0.05 – 0.25	1.5 - 3.5	2.0– 4.0
205	S20500	0.12– 0.25	16.5 – 18.0	14.0 – 15.50	0.32 – 0.40	1.0 – 1.75	

2.4.2 The 300-series

The 300-series is a replacement of 18/8 (18 % Cr / 8 % Ni) stainless steel that has been extensively used as a corrosion- resistant material for decades. In applications needing corrosion resistance and ductility, grade 304 is often utilized in the 300 series. Grade 304L is a modification of 304 SS to improve weldability (reduce carbon content). Lower carbon levels result in reduced carbide and intergranular corrosion (IGC) in the heat affected zone. Another modification of grade 304 is 304N with the addition of nitrogen (N) for increased strength [34-35]. Grade 316 contains Molybdenum (Mo) and is more resistant to marine pitting than grade 304.Grade 316 is further categorized as 316L (low carbon) and 316N (nitrogen containing). For 316LN (low C, N) and 304LN grades, a decrease in C decreases strength, which is compensated by the addition of nitrogen. This nitrogen (N) enhanced

grades are more resistant to sensitivity. AISI 321,347 and 348 stainless steels are types which can be steadied by Ti, Nb + Ta and Nb for welded structures and for high temperature applications [61-62]. Table 2.2 shows the various chemical composition of 300 series ASS.

Table 2.2: Chemical composition of 300 series ASS [60]

Material	Chemical Composition (wt %)									
	C	Cu	Cr	Si	Mo	Mn	Ni	S	P	Others
304L	0.016	0.5	18.2	0.376	0.254	1.451	8.63	0.0251	0.028	
316L	0.023	0.415	16.55	0.37	2.13	1.44	10.05	0.0067	0.0311	
321	0.022	0.402	17.251	0.325	0.271	1.279	9.100	0.0012	0.0315	Ti-0.2856
347	0.044	0.423	17.474	0.409	0.262	1.308	9.116	0.0010	0.0303	Nb-0.6610

2.4.3 Difference between 200 series and 300 series

The differences in corrosion resistance, strength, hardness and formability between 200 and 300 series are described below:

a) Corrosion resistance

Stainless steel has an exceptional corrosion resistance because of the presence of Chromium (Cr), which creates a protective layer on the surface. This layer protects it from the external environment. The high chromium content of steel requires more stabilizing elements than austenite to stabilize its structure. The 200-series stainless steels require less chromium (Cr) than 300-series stainless steel because the Ni content is reduced to reduce the cost of 200-series stainless steels. Due to the low Cr content in 200-series stainless steel, the corrosion resistance is lower than that of 300-series stainless steel. By adding nitrogen (N) as austenite stabilizer chromium can be added to improve the corrosion resistance. 200-series stainless steels have very high C content (0.15 %), which increases sensitivity (Cr carbide precipitation at grain boundaries). This drastically reduces the Cr matrix of 200-series stainless steels, making them more susceptible to intergranular

corrosion (IGC). Nickel (Ni) has also been replaced by magnesium (Mn) in the 200-series to reduce manufacturing costs.

b) Strength and hardness

The 200-series stainless steel has a higher nitrogen (N) content than 300-series. Nitrogen (N) acts a hardening and strengthening agent. Therefore, 200-series stainless steel is typically stronger and harder than 300-series stainless steel and 201 has yield strength which is 30% higher than 304.

c) Formability

In general, 200-series grades are more difficult to manufacture because of their higher strength than 300-series stainless steels. However, 200-series soft stainless steel obtained by adding copper and improves formability. Copper (Cu) enhances formability by increasing stacking fault energy, slowing work hardening, and slowing the rate of work hardening. The production of copper containing grades requires less energy, allowing for pre-installed production equipment originally developed for the ductile 300-series. The austenitizing properties of copper also reduce the Nickel (Ni) content of 200-series stainless steels.

2.5 Sensitization of Stainless Steel

Continuous heating or cooling of stainless steel over a specific temperature range causes grain boundaries of chromium rich carbides (usually Fe, $Cr_{23}C_6$) occurs. As a consequence of this deposition of a carbide that is high in chromium, the adjacent area of the grain boundaries will see a depletion of chromium. This phenomenon is called sensitization. Figure 2.2 shows a chromium carbide precipitation along grain boundaries [63]. For austenitic stainless steels, the sensitivity temperature is approximately $450\text{-}850^0C$ [34-36,64]. Stainless steel is vulnerable to IGC and intergranular stress corrosion cracking due to its vulnerability to corrosive conditions. Premature component failure arises as a result of this. These errors arise because the sensitive effect on corrosion behavior is not taken into account during production. Most of these errors are related to welding. Repetitive component failures due to intergranular corrosion (IGC) are of increasing interest in the sensitive behavior of stainless steels [34-36,64,9,38]. The following sections describe some

important sensitivity mechanisms, time-temperature-sensitization (TTS) and various tests to obtain sensitivity (qualitative / quantitative).
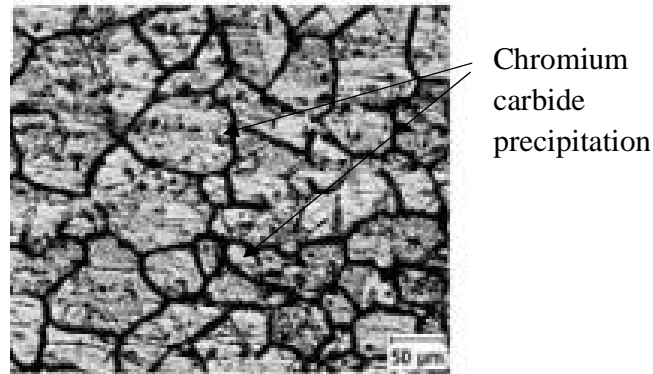
Figure 2.2: Microstructure of the specimen sensitized at 700^0C for 60 min [63]

2.5.1 Mechanism of Sensitization

Three theories on the mechanism of sensitization have been proposed in the literature. These are i) the theory of noble metal carbide, ii) the theory of segregation and iii) the theory of chromium depletion theory. Among these theories, Cr depletion theory is the most widely used theory to explain IGC and is further discussed [37,64].

2.5.1.1 Chromium depletion theory

Chromium-depleted areas near grain boundaries are susceptible to corrosion because they do not have sufficient corrosion resistance to withstand exposure to corrosive environments [65]. During this phenomenon, interstitial carbon atoms diffuse extremely quickly to the grain boundaries at sensitive temperatures; subsequent deposition lowers the matrix and grain boundaries surrounding the much slower Cr carbide diffusion. The primary element in stainless steels that resists corrosion is chromium, and having this element reduced may make a stainless steel more susceptible to corrosion at grain boundaries. The actual distribution of chromium (Cr) in the carbohydrate environment of stainless steels has been extensively studied using thermodynamic models [66-69]. Stawstrom and Hillert [66] suggested that stainless steel is susceptible to corrosion only if the Cr content is less than 13 wt.% and the grain boundary is greater than 20 nm. They made an effort to explain the recovery of stainless-steel corrosion resistance through an established method which

requires extended periods of time in a hot environment that encourages sensitization known as healing process. During healing, re-chromization is performed by removing Cr from the particles on the surface of the carbide matrix at the grain boundaries [70]. They discovered that variations in the carbon activity of the steel caused an increase in the Cr content of the matrix at the carbide matrix contact, which explained the healing. To determine the distribution of Cr at the grain boundaries between the carbide grains and the line perpendicular to the grain boundaries, Tedmon et al. [71] utilised a more comprehensive method. They anticipated that there could be a large Cr gradient in the grain boundary area, which would have a major impact on the sensitization process. To verify their finding, the researchers utilised scanning transmission electron microscopy (STEM) to identify a chromium-depleted area, which ranged from 25 to 200 nm [64]. Chromium depletion theory explains several properties of IGC, such as the influence of elements such as C, Cr and stabilizing elements (Ti, Nb) and heat treatment parameters (cooling, desensitization and sensitivity). The Cr depletion theory also predicts that the oxidation rate at high temperatures rises at grain boundaries owing to the deposition of Cr carbide, lowering the Cr content of the alloy in this region.

2.5.1.2 TTT sensitization curve

The sensitivity of various stainless steels depends primarily on the exposure temperature and storage time. For austenitic stainless steels, temperature range of 450-850^{0}C provides the highest sensitivity to corrosion. Time and temperature are two important variables that determine intergranular corrosion (IGC) sensitivity. To demonstrate how heat treatment affects carbon-rich stainless steels across a wide temperature range, Binder et al [72] created the temperature versus time curves. Time temperature sensitivity (TTS) plots were generated based on different test methods for different stainless steels (ASTM standard A-262 practice A and E tests/DLEPR) [73-77]. TTS plots were processed using ASTM A-262 practice A and E test and/or DLEPR to determine susceptibility to IGC and isothermal annealed samples of materials at various temperatures and times. This graph plots the sensitivity test results as a function of temperature (Y-axis) and logarithmic absorption time (X-axis) and plots a line separating the sensitive and non-sensitized regions [34,35,64]. The information in this diagram is crucial for designers and manufacturers because it

demonstrates that heat treatment on the left side of the figure has no impact on the alloy's sensitivity, while heat treatment on the right side of the diagram causes the alloy to become more sensitive. Figure 2.3 shows the schematic of TTS diagram. The diagram focuses primarily on the sensitive and non-sensitive areas during aging. It also shows the high and low temperature (T_H and T_L) ranges of sensitivity, nose temperature and minimum time (T_{min}) required for sensitivity.
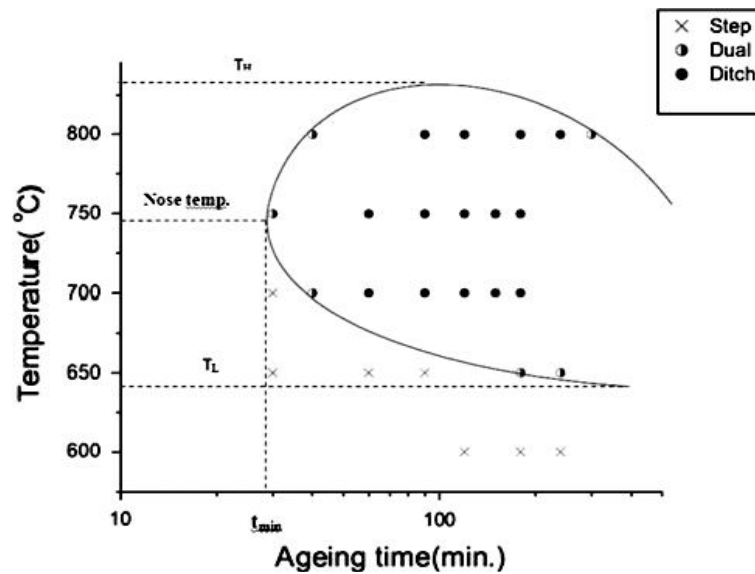
Figure 2.3: TTS schematic diagram

2.6 Influence of alloying elements

Austenitic stainless steel is an iron-based alloy containing 50 to 80% by weight of iron. The most important alloying additives for austenitic stainless steels are Cr, Ni, Mn and C. Other alloying elements (Mo, Nb, Ti, Al, Cu, W and N, etc.) are also added to stainless steel to improve strength, corrosion resistance and precipitation hardening (sensitivity) or resistance to intergranular corrosion effects, pitting resistance or influence microstructure [34-36]. C and Cr are the main alloying elements to control sensitization along with time and temperature. Due to the deposition of carbides, an added benefit of the Cr in austenitic stainless steels increased sensitivity [64,78]. The influence of various alloying elements on the sensitivity behavior of austenitic stainless steels is as follows.

22

2.6.1 Carbon

As the C content in stainless steel decreases, the C content in austenite is no longer sufficient to convert carbides (especially Cr carbides i.e $Cr_{23}C_6$) at the grain boundaries, which increases the time taken to initiate the process of sensitization [64,78-80]. Figure 2.4 shows the TTS 304 SS diagram showing the effect of C slowing down the process of sensitization [9]. The nose of the TTS curve shifts to right with the decrease in C content.
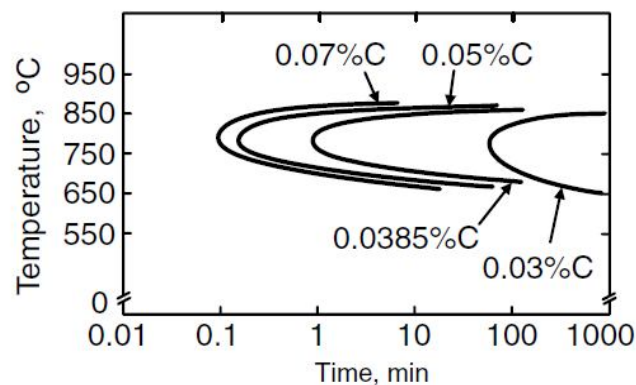
Figure 2.4: TTS 304 SS diagram showing the effect of C for sensitization process

2.6.2 Chromium

Cr is an important element that provides excellent corrosion resistance to stainless steel. This significantly affects the passivation properties of stainless steels. Because it's more strongly attracted to oxygen than iron, Cr helps stabilize the oxide layer. Higher Cr content is required for oxidation stabilization in more aggressive environments. C must also be present in sufficient amounts in the stainless steel for the damaging effect of Cr to occur. As Cr has a high carbide formation rate, it generally interacts with C at grain boundaries to produce Cr carbides, which improves sensitivity. R K Dayal et.al. [50, 62] also reported that an increase in Cr content delays the onset of IGC for a longer time. The higher Cr content in the matrix promotes Cr diffusion to the grain boundaries, since alloys with a higher Cr content are more sensitive. This moves the upper limit of the IGC range to a lower temperature.

2.6.3 Nickel

Nickel is weak cemented carbide; therefore, it isn't advantageous to intermetallic compound production. [64,81]. Some researchers suggest that it is important to strike a balance between C, Cr and Ni concentrations to prevent sensitivity to 304 stainless steels [64,78]. Increasing chromium content will cause an increased need for nickel, which is necessary to keep stainless steels stable during austenite formation. However, increasing the nickel (Ni) content in stainless steel reduces solubility and increases carbon emissions. Figure 2.5 shows the dependence of C, Ni and Cr on the sensitive behavior. Higher nickel content significantly reduces the allowable C concentration to prevent sensitization.
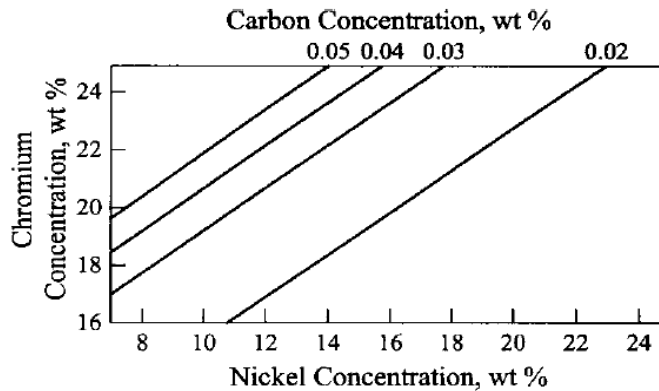
Figure 2.5: The relationship between Ni and Cr contents at C concentration needed to prevent sensitivity after 1 hour heat treatment at 650^{0}C [64].

2.6.4 Manganese

As an austenitic stabilizer, Mn is used instead of Ni in the production of inexpensive austenitic stainless steels [59,82-87]. Therefore, the effect of manganese (Mn) on sensitization and its kinetics is a very important issue. When manganese (Mn) is added to stainless steel, carbon (C) activity and solubility are both reduced. As a result, the carbide precipitation rate decreased [64]. However, the literature has shown an adverse effect of Mn on sensitivity. When testing the sensitivity of stainless-steel types 201,202 and 304, the authors [34,88] found that high Mn type 202 are more susceptible to IGC than low Mn alloys. Therefore, it has been shown that the 200-series stainless steel is more sensitive to IGC than that of 300-series. Manganese (Mn) is usually regarded an improving element of

austenite and the level of concentration is dependent on the presence of nickel and its composition [88]. It extremely efficiently stabilizes austenite at low temperatures and inhibits its martensite transition. The strength of which austenite is supported at high temperatures depends on the alloy composition.

2.6.5 Other alloying elements

The effect of Molybdenum (Mo) on the sensitivity kinetics is very similar to that of Cr. Mo remains in solution and promotes passivation, increasing corrosion resistance during sensitization. According to Beneke and Sander Berg [89], increasing the Mo content of stainless steel (from 0.07 to 2.27 %) delayed $M_{23}C_6$ deposition and increased the alloy's passivation characteristics, resulting in better sensitivity resistance. The decrease in N (0.16 wt.%) in stainless steel and increase in the amount of N (up to 0.25 wt.%) reduces the sensitivity kinetics. This gradually increases due to the precipitation of Cr_2N [90]. The calculation of Cr volume diffusion coefficient based on N indicates that the addition of N lowers Cr diffusion coefficient and thus slows down the nucleation and growth of carbides. Even in the presence of N, the passivation behavior of the alloy is very good, so that the existence of IGC requires more Cr depletion [91]. Based on thermodynamic study, the addition of N raises the concentration of Cr along the grain boundary during sensitisation process, thus decreasing the concentration gradient of Cr and reducing carbide formation [64]. In addition, other elements (Nb, Ti, W, Ta and vanadium (V)) are added to stainless steel to avoid the formation of chromium carbide. Ti additions (type 321) or Nb + Ta additions (type 347) binds C through forming their carbides at better temperature in order that little C is left to shape chromium rich grain boundary carbides during cooling. The inclusion of Ti and Nb thus decreases C detrimental impact on susceptibility. A small amount of Nb will cause a significant shift in the aging time at the nose of the TTS curve [64,78].

2.7 Welding of 316L Austenitic Stainless Steel

Austenitic stainless steels (ASS) are generally the most weldable stainless steels. However, the welding behavior of 316L ASS is very different from that of 430 ferritic stainless steel. The most widely used welding processes are gas tungsten arc welding (GTAW), submerged arc welding (SAW), gas metal arc welding (GMAW), shielded metal arc welding (SMAW) and flux cored arc welding (FCAW). In addition, electron beam welding (EBW), laser beam welding (LBW) and plasma arc welding (PAW) are the most common techniques in higher power fusion welding techniques. The advanced welding processes include cold metal transfer welding, friction, explosive and ultrasonic welding.

2.7.1 Gas Tungsten Arc Welding (GTAW)

A non-consumable tungsten electrode is used in the gas tungsten arc welding technique to create an arc between the workpiece and the electrode. The welding arc produces heat that heats the workpiece and produces a weld pool. Weld pools are protected from the elements by using an inert gas (Ar or He) or a gas combination [19]. If small amounts of non-inert gas are employed to shield the mixture, this method is known as tungsten inert gas (TIG). The GTAW can be used as without filler material for thin sheet (up to 3 mm) and is called as autogenous welding. The preparation and application of the filler material is required for thicker sections. This method is frequently used to weld thin parts made of stainless steel, aluminum, magnesium, and titanium alloys, as well as carbon and low alloy steels [9]. This process precisely controls the dissipation of high-quality, low strain and spatter free weld joints. The slower welding speed, lower deposition rates and a windy environment are less expensive than any other welding method because of the difficulties in preserving a weld pool. Filler or base metal is also less resistant. Figure 2.9 shows the schematic diagram of Gas tungsten arc welding with (a) complete process and (b) welding area/zone.
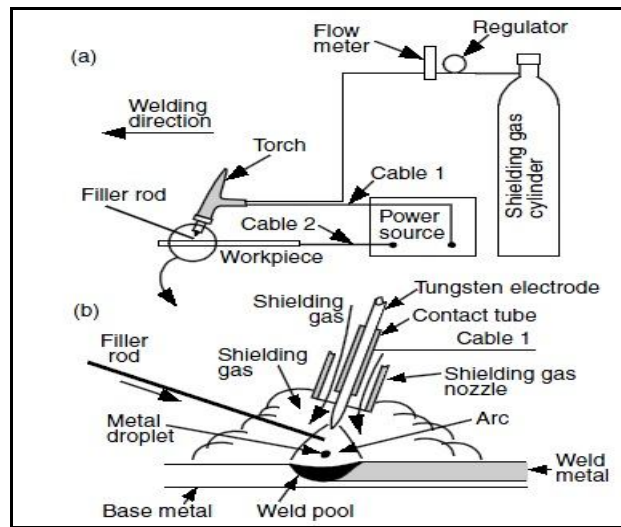
Figure 2.6: Gas–tungsten arc welding: (a) process; (b) fusion zone [9].

2.7.2 Cold Metal Transfer (CMT) Welding

The CMT technique (a short-circuiting transfer process) creates a clean MIG/MAG robot welding of ultra-light gauge sheets. This is accomplished through a procedure based on the short-circuiting transfer process. This works well on thin metal that tend to twist, distort and the weld defects due to welding. This sort of welding is more efficient than other metal inert gas welding. It is also additionally being utilized for thicker material where better sound weld joint is required. It isn't precisely cold, but its temperature is lower than GMAW processes like MIG. It is amazingly low heat input and an exceptionally stable arc welding process. There are numerous variations of CMT Welding like CMT Advanced, CMT Twin, CMT Pin, CMT Braze+. Different CMT Welding models include TPS 400i, TPS 320i, TPS 500i, TPS 600i etc. Figure 2.10 shows the manual cold metal transfer welding process.
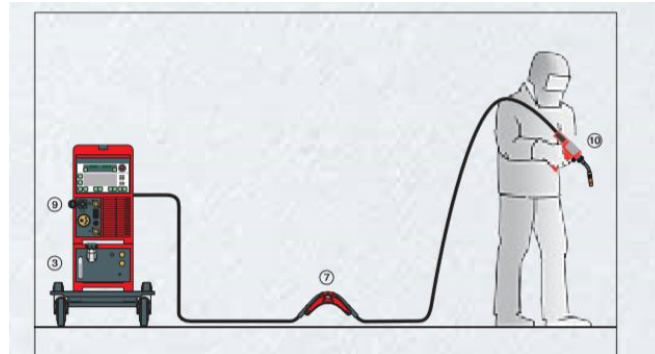
Figure 2.7: Manual CMT configuration

2.8 Welding electrode

The protective electrode consists of a thick coating of various chemicals such as cellulose, sodium and titanium dioxide, low sodium hydrogen and iron powder. There is a particular purpose for each chemical in the coating; the purpose is in the welding process. The major function of this protective electrode is to begin the arc, sustain the arc, refine the shape and penetration of the weld, and reduce spatter. The main purpose of this electrode is to start, sustain, and strengthen the arc, to refine the shape and penetration of the weld, and to decrease spatter. As the electrode melts, a thick coating of non-flammable gas surrounds the molten metal, protecting it from further oxidation. Combustion slag forms in the metal owing to the slag left behind by the coating, and this slower cooling may result in stronger weld beads. Welds are created via a process that involves melting iron particles with a very hot electrical arc. "300" series stainless steel electrodes are primarily used for most steel welding applications. These electrodes form strong but ductile weld. Stainless steel is a poor thermal conductor, which causes the electrode to overheat. As a result, improper arcs are created by high currents. There is a difference in temperature between the weld and the rest of the work in the base metal. The plate deforms as a result of the difference in temperature. A rule of thumb when welding steel is to avoid high current, high temperatures and carbon to avoid sensitive parts of the weld.

When choosing a filler, the properties of the filler and the properties of the base material should be well matched. The electrode is composed of a metal core and a flux layer. The core is usually a strong steel wire. The layer, which plays an important role is extruded into the core. It has three main functions: electrical, physical and metallurgical. Electrical performance is related to arc initiation and stabilization, while physical performance is related to slag viscosity and surface tension which control the metal droplet transfer, effective weld pool protection and weldability. The role of metallurgy involves chemical exchange between the weld pool and the slag that refines the weld metal. There are two types of flux coatings for stainless steel electrodes: lime and titanium. The lime is designated 15 for stainless steels and 16 for titanium. Lime coated stainless steel electrodes are highly permeable and harden quickly, making them suitable for welding. It should only work with DC polarity. Titanium coated stainless steel electrode provides a very smooth and stable arc and good welding effect. They work with AC and DC polarity. Due to its higher deposition, it is a good choice for all applications. According to the classification of the American Welding Society (AWS), the welding electrode may be named EXXX-YY. E for electrode, XXX for stainless steel grade, YY for coating type. For example, code E 308L -16 refers to a 308L electrode with titanium flux. Table 2.3 shows the guide for selection of welding parameters [102,103].

Table 2.3: Guide for selection of welding parameters [103]

Type	AWS Class	Current Type	Welding Position	Weld Results
Mild Steel	E6010	DCR	F, V, OH, H	Fast freeze, deep penetrating, flat beads, all-purpose welding
	E6011	DCR, AC	F, V, OH, H	
	E6012	DCS, AC	F, V, OH, H	Fill-freeze, low penetration, for poor fit-up, good bead contour, minimum spatter
	E6013	DCR, DCS, AC	F, V, OH, H	
	E6014	DCS, AC	F, V, OH, H	
	E6020	DCR, DCS, AC	F, H	Fast-fill, high deposition, deep groove welds, single pass
	E6024	DCR, DCS, AC	F, H	
	E6027	DCR, DCS, AC	F, H	Iron powder, high deposition, deep penetration
	57014	DCR, DCS, AC	F, V, OH, H	Iron powder, low penetration, high speed
	E7024	DCR, DCS, AC	F, H	Iron powder, high deposition single and multiple pass
Low Hydrogen	E6015	DCR	F, V, OH, H	Welding of high-sulphur and high-carbon steels that tend to develop porosity and crack under weld deposit
	E6016	DCR, AC	F, V, OH, H	
	E6018	DCR, AC	F, V, OH, H	
	E7016	DCR, AC	F, V, OH, H	
	E7018	DCR, AC	F, V, OH, H	
	E7028	DCR, AC	F, H	
Stainless Steel	E308-15,16	DC, AC	F, V, OH, H	Welding stainless steel301,302,303,304,308
	E309-15,16	DC, AC	F, V, OH, H	Welding 309 alloy at elevated temperature application and dissimilar metals
	E310-15,16	DC, AC	F, V, OH, H	Welding type 310 and 314 stainless steel where high corrosion and elevated temperatures are required
	E316-15,16	DC, AC	F, V, OH, H	Welding type 316 stainless and welds of high quality. Contains less carbon to minimize carbon transfer in the weld. Type 316 reduces pitting corrosion.
	E347-15,16	DC, AC	F, V, OH, H	For welding all grades of stainless steels
Low Alloy	E7011-A1	DCR, AC	F, V, OH, H	For welding carbon moly steels
	E7020-A1	DCR, DCS, AC	F	For low alloy, high-tensile strength
	E8018-C3	DCR, AC	F, V, OH, H	For low alloy, high-tensile steels
	E10013-G	DCS, AC	F, V, OH, H	

DCR- Direct Current Reverse Polarity, DCS- Direct Current Straight Polarity, AC- Alternating Current, F-Flat, V- vertical, OH- overhead, H- horizontal

2.9 Microstructure development during welding in 316L ASS

Due to dissolution segregation and/or microstructure inhomogeneities, ASS weld metals are generally of poorer quality than the base metal. The final microstructure of the weld metal influences mechanical properties, corrosion resistance and high temperature cracking. ASS, a small weld, exhibits solidification behavior and solid-state transformations that are influenced by its room temperature microstructure [35,58]. Depending on the alloy composition, ASS may be turned into primary ferrite or primary austenite. Primary ferrite, which is in equilibrium, becomes austenite, which is resistant to environmental effects. In the quenching process after welding, this change is suppressed, and in the finished microstructure, there may be some residual ferrite. Because the amount of δ-ferrite in the weld metal microstructure can be affected by cooling rates, any changes to the composition of a specific alloy should be thoroughly investigated [35,110-111]. ASS interferes with the whole thermal cycle; thus, it negatively affects both welding and cooling. Uneven heating, as well as extended exposure to high temperatures, may lead to metallurgical phenomena such as lower weld performance in the heat affected zone (HAZ) and fusion zone (FZ).

2.10 Mechanical properties of welded 316L ASS

Mechanical properties are important characteristics of welding, so the scope and functional requirements of welding must be determined. These include yield strength, hardness, ultimate tensile strength, percentage elongation and impact strength (toughness). These mechanical properties are influenced by the weld's microstructure, cooling conditions, base metal composition, electrode wire composition, and flux composition. Furthermore, the welding process parameters have direct and indirect impacts on the mechanical characteristics and microstructure of the weld. M.Zietala et.al [112] evaluated the structural homogeneity and the isotropy of the mechanical properties of 316L ASS. The microhardness measurement of the parallel and perpendicular directions is taken for the joint and found that the microhardness value for the perpendicular directions is higher than measurements taken for parallel direction. A higher value was due to the greater fragmentation of the microstructure, where the size of the fine sub-grains is less. The electrode is very essential in influencing the weld's tensile strength. Because of the higher solid solution strength of the weld, the weld joint possessed by different electrode has

adequate strength than the base metal [113]. The impact energy absorbed by the weld joint by different electrodes is more than the base metal due to the composition of nitrogen in the electrodes. If the composition of nitrogen in the electrodes is higher, than the impact energy and tensile strength of the welded joint is higher than the base metal [114].

2.11 Corrosion behavior of welded 316L ASS

There are frequently local sensitive regions while welding stainless steel (i.e areas prone to corrosion). The production of Cr carbides at grain boundaries reduces depletion in grain boundary regions. When the Cr value of the depleted region reaches less than 12 wt% by weight (required for the formation of strong negative films), this region is exposed to corrosion and results in IGC attack. It is most readily found in HAZ of austenitic stainless steels [34,37,9]. When intergranular corrosion develops at the grain boundary, the weld joint is less ductile and strong [115]. The corrosion behavior of the weld joint is affected by the number of passes and the amount of heat used. The rate of corrosion increases as the amount of heat increases and the number of pits is increased [116] whereas as the number of passes increases, the pitting resistance at the weldment increases [117].

2.12 Welding of 430 Ferritic Stainless Steel

2.12.1 Welding Metallurgy of 430 Ferritic Stainless Steel (FSS)

In addition to other alloying elements, especially molybdenum,430 FSS contains 10.5 % to 30 % chromium. The welding arc increases the temperature of the base metal region above its critical temperature (955^0C), causing ferrite grains to grow rapidly. Excessive grain growth, on the other hand, may be avoided by reducing the heat input during welding. The formation of coarse grains in the weld zone and the heat-affected zone of the fusion zone will be a concern when welding ferritic stainless steel. The lack of phase transformation leads to lower ductility and toughness, resulting in grain refinement. Strength, toughness, and hardness are affected by the microstructure and chemical composition of the weld metal, which are two critical features of ferritic stainless steel [16]. The microstructure of most ferritic chromium steels is a mixture of ferrite and carbides. Many metallurgical reactions can occur when this microstructure is heated to a high temperature in the HAZ around the fusion zone. All carbides and other deposits are dissolved during the heating

cycle. If martensite is present, it melts and reverts back to ferrite (carbide formation) or austenite during reheating by subsequent passes. Formation of martensite is common in weld metal and HAZ in stainless steels that have low and medium chromium in the ferritic stainless steel [118]. The presence of martensite in stainless steels with low chromium and ferrite content reduces corrosion resistance [35]. The microstructure of the fusion zone can consist entirely of ferrite or a mixture of ferrite and martensite, where martensite is found at the boundaries of the ferrite grains [54, 119].

2.12.2 δ- ferrite formation in weld metal

In power generating and associated sectors, stainless steel is extensively utilized. The welds of this steels usually have a dual- phase structure (i.e., ferrite + austenite) with different amounts of δ-ferrite [35]. Small amounts of δ-ferrite are used to minimise cracking while welding austenitic stainless steels [120]. A lot of precision is necessary to effectively regulate the austenitic stainless steel weld metal's ferrite concentration. High δ-ferrite content (> 10 vol%) reduces ductility, hardness and wear resistance, and very low δ-ferrite content (< 5 vol %) resulting cracks during weld metal solidification. δ- ferrite is the most important solidification product. It is formed directly from molten metal. At the start of solidification, the chromium concentration is very high of δ- ferrite in dendritic nuclei; nevertheless, the Cr level continues to decrease during solidification.

2.12.3 Effect of welding on corrosion behavior of FSS

Welding may substantially decrease the corrosion resistance of ferritic stainless steels. These steels can be exposed to many types of corrosion, including intergranular corrosion (IGC), crevice corrosion and pitting corrosion. Due to lack of nickel, these materials are generally resistant to stress corrosion cracking, making them a promising alternative to austenitic stainless steels in chloride-containing environments. IGC are very sensitive to welding technique and post-weld condition, but crevice and pitting corrosion can usually be avoided by choosing the right alloy. The difficulty with FSS weld is that the intergranular corrosion in the weld matrix near the HAZ is caused by a lack of chromium. Some engineering applications may face issues independent of financial concerns, corrosion resistance, corrosion and acid resistance, and the quality of their FSS because to a common

problem that affects all applications. This susceptibility is often called sensitization. Sensitization is assumed to be a reason for stress corrosion cracking in certain ferritic stainless steels, which may lead to a failure [55,120].

2.12.4 Microstructural properties of FSS HAZ

Ferritic stainless steel containing 12 % Cr has a ferrite phase of 100% delta ferrite when heated to above 1200^0C and passes through the $\delta + \gamma$ stable zone when cooled, which means that part of the δ- ferrite is transformed into austenite. After further cooling, the austenite is converted to martensite at Ms temperatures (especially after welding due to fast cooling rate). Because of the low cooling rate, the carbides have enough time to separate along the boundaries of the austenite grains. This means that carbon leaves the austenite to form carbides, so if the austenite cools slowly, it has less carbon and therefore the hardness of the martensite is lower. If the cooling rate is faster, no carbides are formed, and the martensite is harder. The HAZ area near the fusion line is heated above A3, so it has larger ferrite grains and grain boundaries of carbides and martensite. This HAZ is usually referred as high temperature HAZ (HTHAZ) [23]. HAZ that has not been heated above A3 has a smaller grain size and a ferrite and martensite in microstructure. This area is called the low temperature heat affected zone (LTHAZ) [121].

2.12.5 Mechanical properties of welded 430 FSS

Ferritic stainless steel shows poor weldability and low grain growth at fusion zone, which results in poor toughness and ductility due to lack of phase transformation. Therefore, careful selection of fillers and processes is essential for a good weld joint [7]. Weld joints produced with austenitic stainless-steel electrodes have greater tensile strength and hardness than those created with ferritic stainless-steel electrodes due to grain coarsening and the development of martensite in the HAZ [122]. Adding aluminum, titanium or a mixture (Al + Ti) reduces the grain size and increase the microhardness of the welded joint [122]. The mechanical characteristics of the joint rely on the welding current, which has a huge impact on the fusion zone. The fusion zone for the welded joint gets larger when the heat input is increased and the welding current is higher [123].

2.13 Welding of dissimilar metals

Dissimilar metal joints, which combine strength and corrosion resistance at a reasonable cost, have come to be used for many industrial applications, offering a wide range of capabilities, which have opened up new avenues of manufacturing. Recently, dissimilar metal welding (DMW) has been gaining attention in terms of cost reduction and material cost reduction [24]. DMW can also be used to combine different alloys to meet different property requirements [25]. Dissimilar joints are often subjected to different operating conditions that affect performance, especially temperature changes [26]. As a result, the welded metal is fairly well compatible with conditions such as temperature transfer capabilities, oxidation and corrosion resistance, and high-temperature mechanical properties [27]. Due to the physical, mechanical, and metallurgical characteristics of the base materials, the DMW is more difficult to weld than similar metals [28]. This change can make it difficult to select a filler that is compatible with two base materials [29]. These materials physical and chemical properties make it difficult to decide on a joining process. This approach is primarily used when a transition to mechanical properties or service is required. A.M.Barrios et.al [124] examined the 316L ASS and 430 FSS dissimilar welds for corrosion and mechanical characteristics. Gas Metal Arc Welding (GMAW) process is used and immersed in 10 %v/v hydrochloric acid solution for 24 and 72 hours. In the microstructure of HAZ of 430 FSS found acicular ferrite, martensite and coarsened ferrite grains. The corrosion, such as pitting and intergranular corrosion, increases in severity as the immersion time increases. The immersion time of weld joints influence the tensile strength of the dissimilar weld joint [124]. Figure 2.8 shows microstructural changes in dissimilar welded joint.
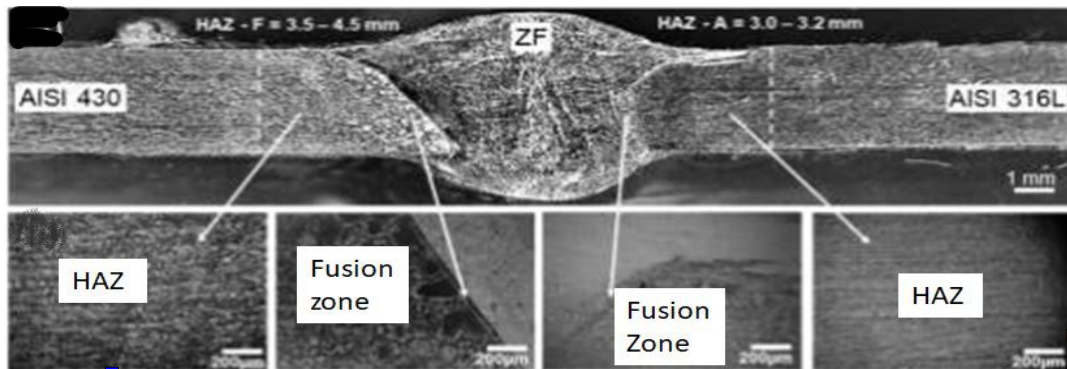
Figure 2.8: Microstructural structures of HAZ-430FSS, Fusion Zone-430 FSS,Fusion Zone- 316L ASS and HAZ-316L ASS [124].

2.14 Electrochemical techniques

(Test parameters of DLEPR by various researchers)

Electrochemical techniques have been developed to quickly access degree of sensitization (DOS) in order to achieve fast, quantitative, and non-destructive testing.

2.14.1 Electrochemical potentio-kinetic reactivation (EPR) technique

Electrochemical potetio- kinetic reactivation (EPR) technique has been standardized for many years and is included as per ASTM G108 standard. Two EPR techniques are primary available: single loop EPR (SLEPR) and double loop EPR (DLEPR) [64]. In SLEPR method, the analyzed sample is exposed to a de-aerated solution of 0.5 M H_2SO_4 + 0.01 M KSCN at room temperature. For passivation, the sample is then anodically polarized to the potential in the middle of the passivation area. In this area, the applied potential drops rapidly to the corrosion potential. After keeping for minutes, the applied potential quickly drops to the corrosion potential. The schematic diagram shown in figure 2.9. If the Cr concentration in the alloy is between 12-13 %, the metal will develop a protective Cr oxide layer on its surface. The oxide layer protects the alloy against corrosion (passive state). The protection of the oxide film is decreased if the concentration is less than this. As a result, the chromium depleted region is more susceptible to dissolving than the un-depleted zone. Higher current may be generated by sensitized stainless steel than by non-sensitized stainless steel. The sensitive area's reactivation is represented in the potentials vs. current

36

plot by the anode peak. The charge (Q), which is a measure of DOS, is proportional to the area below the reactivation peak [64,92]. The charge (Q) depends on the surface and grain size, and is normalized to the total area of the grain boundary. The normalization factor (Pa) can be chosen to be an acceptable level of sensitization for a given application. Clark et al. [93] have proposed that the P_a can be obtained from the empirical relationship: $P_a = Q/GBA$ (where GBA -total grain boundary area).
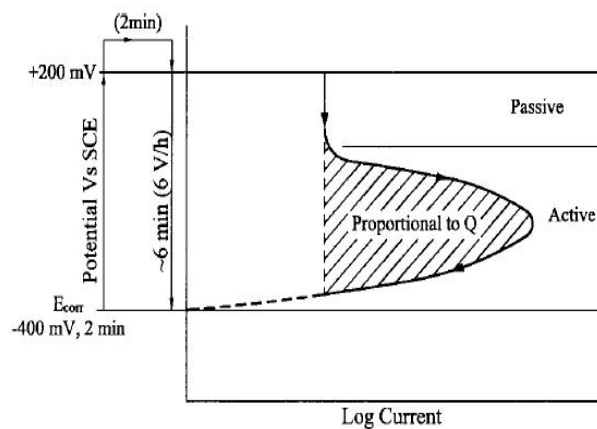
Figure 2.9: Schematic diagram of SLEPR test method [64].

In DLEPR method, the sample is first anodic polarized through the active area, and then scanned in the opposite direction for reactivation. The corrosion potential (Ecorr or E_{OC}) and its impact on corrosion are both dependent on velocity to potential relationship and its effects. Anodic reactions may occur across the whole surface in the passivation zone, which causes the polarisation curve to peak (E vs logi). The formation of the passivation layer takes place over the whole surface. The passivation film ruptures at the chromium-depleted area, which causes a current peak due to the anodic reaction at low-chromium samples. Schematic diagram of double loop electrochemical potentiokinetic reactivation loop is shown in figure 2.10.

The values of (Ia) the anodic peak current density, and the values of, the reactivation peak current density (Ir). To assess the DOS, the DLEPR test uses a ratio of Ir/Ia as the measuring tool [63,77,93,94]. High intergranular corrosion sensitivity will be anticipated if the ratio is higher than 0.05 [96]. In standard DLEPR, data scattering is larger than the

difference between typical Ir/Ia levels in DOS materials. The test becomes more selective, due to the changes in parameters such as scan rate, peak potential, and electrolyte content. A high scan rate will result in a loss of sensitivity while a low scan rate will lead to general corrosion and pitting, The scanning rate of 3 V/h is very suitable for cast steel. Doubling the concentration of KSCN will increase aggressiveness and reproducibility. The potential of non-sensitized samples may resist aggressive test conditions and maintain lower levels of I/Ia by extending the passive range from -300 mV to 450 mV [64].

The test temperature greatly affects the results of the EPR test, which explains why the reactivation charge increases as the test temperature increases [97]. Table 2.4 shows test parameters used by various researchers to obtain DOS of austenitic stainless steels.

Table 2.4: DLEPR test parameters by various researchers [64,92,98,99]

Grade	Electrolyte	Potential range, mV (SCE)	Scan rate (mV/sec)
AISI 304 and 304L	0.5 M H_2SO_4 + 0.01 M KSCN	-400 to +300 Back to -400	1.67
AISI 304LN and 316LN	0.5 M H_2SO_4 + 0.01 M KSCN	-600 to +200 Back to -600	1.67
AISI 316L	1)0.5M H_2SO_4 + 0.01 M KSCN	-450 to +250 Back to -450	1.67
	2)0.1M H_2SO_4 + 0.01 M NH_4SCN	-400 to +300 Back to -400	0.5
AISI 321,347	0.5M H_2SO_4 + 0.01 M KSCN	Eoc to +300 Back to Eoc	1
AISI 308L	0.5M H_2SO_4 + 0.01 M KSCN	-500 to 300 Back to -500	1.67
AISI 202	0.5M H_2SO_4 + 0.01 M KSCN	Eoc to +300 Back to Eoc	1

In the case of sensitization by welding, DOS depends on several parameters, namely, heat input, cooling rate, number of passes material composition and thermal conductivity. In this instance an EPR experiment should be conducted and comparable with the DOS obtained by the welding simulation research in order to assess if the HAZ of the welding is sensitized. Otherwise, DOS should be set to maximum temperature, cooling rate, composition and thickness under continuous cooling circumstances and those tests should correspond with the ASTM immersion test [64].
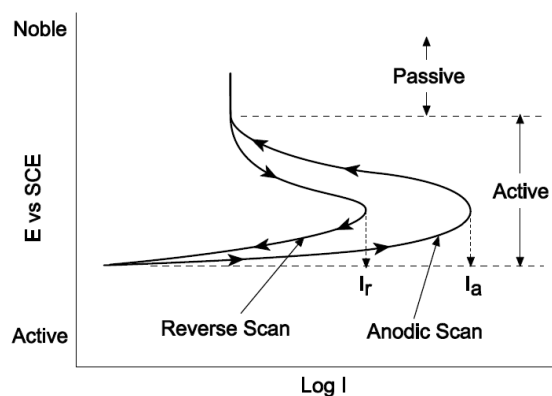
Figure 2.10: Schematic diagram of DLEPR test method [64].

2.15 Selected Techniques for Corrosion Measurements

2.15.1 Polarization methods

This method employs a three-electrode system that automatically adjusts the working electrode's potential (mV/s) and controls the current in accordance with its potential. These measurements provide a potential relationship with the current. Cathodic-anodic polarisation, anodic polarisation, and linear polarisation are three of several applications of polarisation. Diagrams of polarisation may give useful information about different electrochemical processes and their influences on corrosion rate in electrolyte systems. Cathodic polarisation plots enlighten on the related cathodic reaction and the contribution it makes to the overall rate of corrosion. The figure gives fundamental information on the characteristics of anodic corrosion products, metal or alloy solubility, passivity, passivity stability, passive breakdowns, etc. The relative paths of the cathode and the anode curves offer information as to whether anode or cathode controls corrosion. Reverse scanning

according to anodic polarization plots is often used to create hysteresis loops and determine trends in metals and alloys.

(a) Tafel extrapolation method

This technique utilises data from cathodic or cathodic anodic polarisation studies to estimate the correlating corrosion current (icorr). This is because there are areas where the E-log (I) experimental dependency of 50mV is linear. This area is known as the 'Tafel region' and slope is known as 'Tafel slope'.The area of the Tafel is notlinear with anodic passivation thus the corrosion rate is calculated using the cathodic part only when the Tafel line is linear. Figure 2.11 shows a polarization curve of a corroding metal showing Tafel extrapolation. In this figure, the evolution of hydrogen as well as the cathodic and anodic polarization curves of the metal solution are shown with dotted lines. To estimate the corrosion rate, the researchers calculated the corrosion potential for the Tafel region and then extrapolated the corrosion data. The evolution rate for hydrogen for the corrosion potential (Ecorr) is equal to the dissolving rate for metals which is the current density (icorr) rate of corrosion in the system.
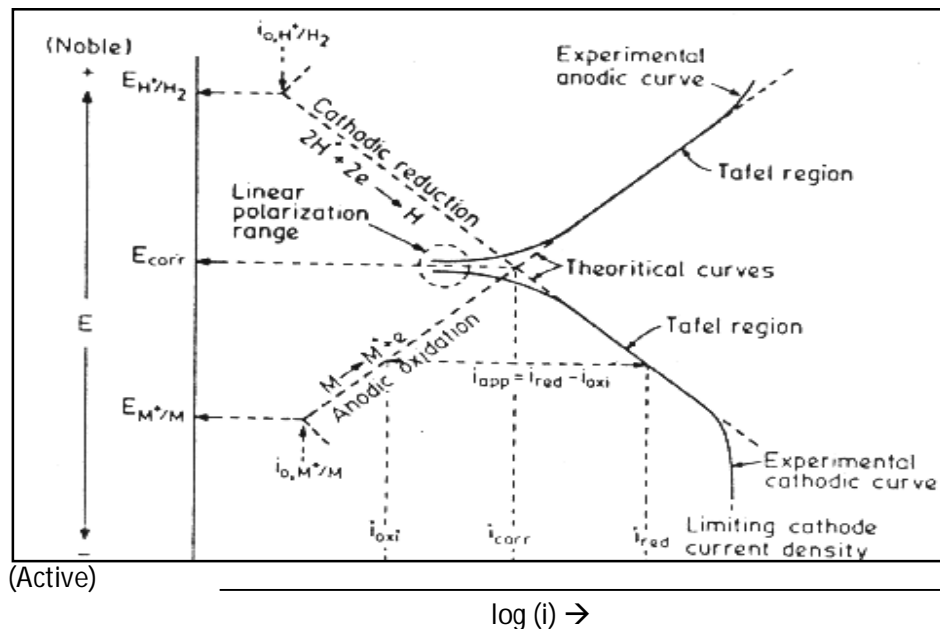
Figure 2.11: Polarization curve of a corroding metal showing Tafel extrapolation

40

(b) Anodic polarization

This method shows the passivation properties of the test metal using the potential- current ratio in the form of E-log (i). These diagrams are used to obtain various electrochemical parameters for comparison and to highlight the effect of test parameters on passivation properties. A characteristic anodic polarization plot of metal exhibiting passivity is presented in Figure 2.12. Initially, the melting rate of the metal (and thus the anodic current) increases with increasing potential and the log-potential (current density) relationship is similar to that of a linear Tafel region. As the potential increases, the rate of dissolution decreases slightly. This is due to the metal's breakdown in the active area and the formation of a corrosion layer on the metal's surface. As the film covers the metal surface, metal ions must pass through to reach the metal / film surface. This is a slow process, the rate of dissolution of the metal slows down and the anode current density drops to a low level known as the passivation current (i_{pass}). This is the situation when the current density is unaffected by the potential limit. The primary passive potential (Epp) is the potential at which current flows from the active to the passive area, and the critical current density (i_{crit}) is the corresponding current density.
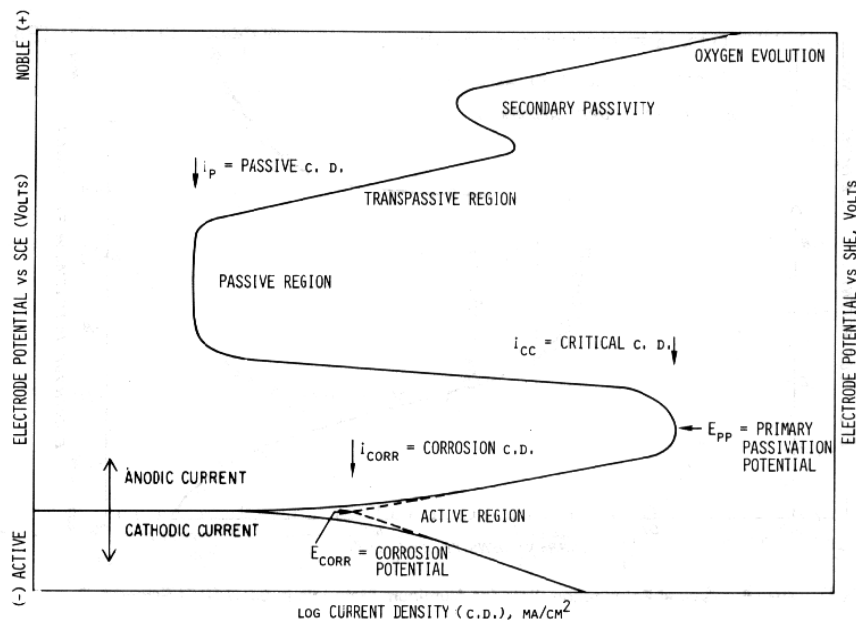
Figure 2.12: Characteristic anodic polarization curve of metal exhibiting passivity.

41

Finally, with noble potential, the dissolution rate increases as potential increases this area is trans passive region. The ability of the film to break and the potential at which film to begin to break is called the breakdown potential (E_b). Advantages of polarization method are; (i) simplicity (ii) fast, and (iii) minimum effect of changing surface conditions during corrosion [125].

2.15.2 Single and Double Loop Electrochemical Potentiokinetic Reactivation Technique (SLEPR / DLEPR)

Steel is also exposed to a phenomenon called sensitization. Chromium carbide deposition results in the depletion of chromium on grain boundaries. This detrimental deposition of cemented carbides is frequently the consequence of thermal cycling in welding processes. [126]. As a result, chromium depleted areas are less resistant to corrosion and predominantly grain boundary corrosion. Single loop and double loop electrochemical Potentiokinetic reactivation methods (SLEPR and DLEPR, respectively) are methods that use a potentiodynamic scan to determine the sensistivity level. Both tests were carried out in a solution of 0.1 M H2SO4 + 0.4 M Na2SO4 + 1000 ppm KSCN at room temperature [120].
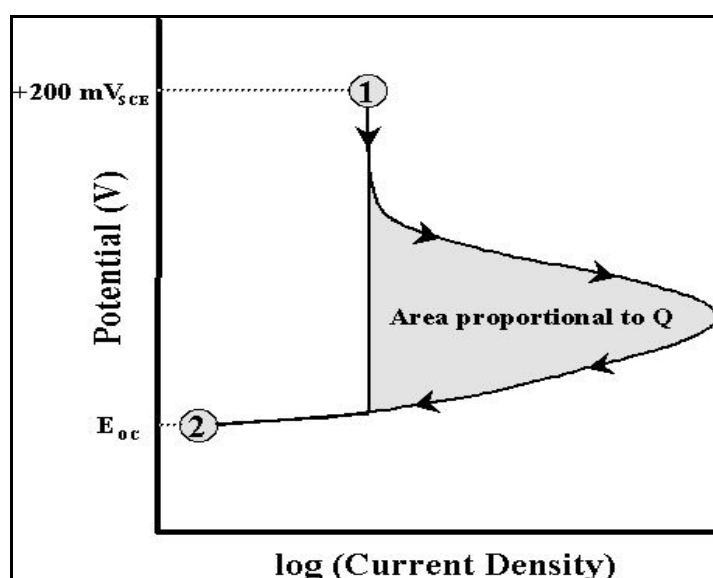
Figure 2.13: Single Loop Electrochemical Potentiokinetic Reactivation [126].

During a single loop technique, the sample first stabilizes in the solution and reaches the open circuit potential, which is usually about -600mV SCE (Point 2 in the figure 2.13). After the sample is stabilized, +200 mV SCE potential is applied to passivate the steel (Point 1 in the figure 2.13). Then, scan the potential to +200 mV SCE potential to the previously set open circuit potential (Point 2). When the potential decreases, the grain boundaries are mainly activated. Therefore, as the potential decreases, the total anode current (or charge Q) flowing at a fixed rate is proportional to the area of the activated grain boundary, which indicates the degree of sensitization. The double loop EPR method is similar to the single loop method in many respects. Here, the sample is also allowed to stabilize in an open circuit (Point 1 figure 2.14). Then, instead of the potentiostatic passivation of the sample, the potential is dynamically scanned from the open circuit (usually 400 mV SCE) to +300mV SCE (Point 2 figure 2.14), and then scanned back to the original open circuit potential. At this point, the comparison is done with the peak current of the anodic nose from the first anodic polarization (Ia) to the peak current on the return scan (Ir). The reverse scan current is believed to be mainly related to the reactivation of the low chromium grain boundary. Therefore, the ratio Ir/Ia is used to determine the degree of sensitization.
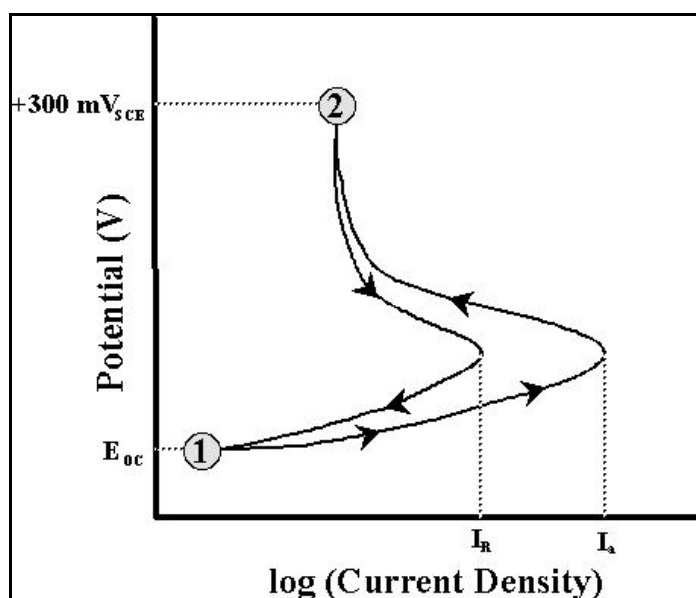
Figure 2.14: Double loop Electrochemical Potentiokinetic Reactivation [126].

2.16 Mechanical Testing of dissimilar welded joint

The mechanical properties such as the yield strength, maximum tensile strength, percentage elongation, hardness and impact energy were evaluated by the Universal Testing Machine, Charpy impact test and Vickers hardness tester respectively. The mechanical characteristics of a welded joint are determined by the microstructural features of the weld, which are influenced by welding processes and circumstances. ASTM standards E8 M-04 for the tensile specimen are shown in figure 2.15. Table 2.5 shows ASTM standard specification for tensile specimen. The charpy impact test with ASTM A 370, with specimen 45^0 V notch of 2mm depth are shown in figure 2.16
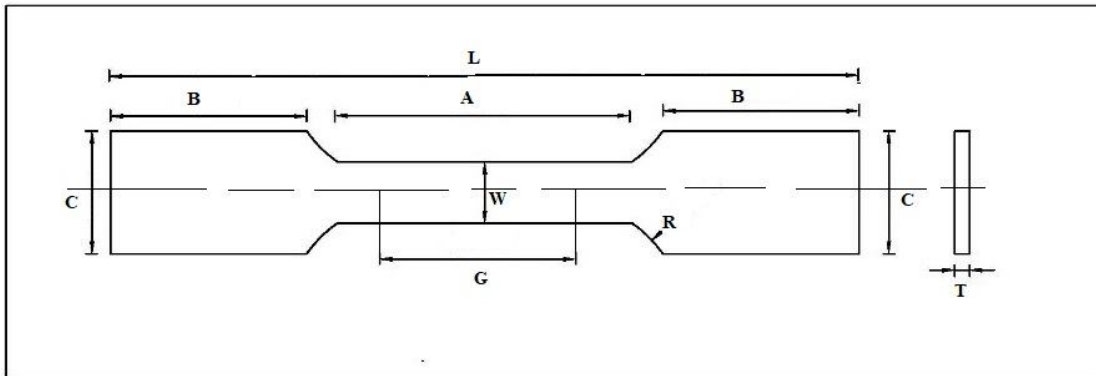
Figure 2.15: ASTM standards for tensile test specimen [127]
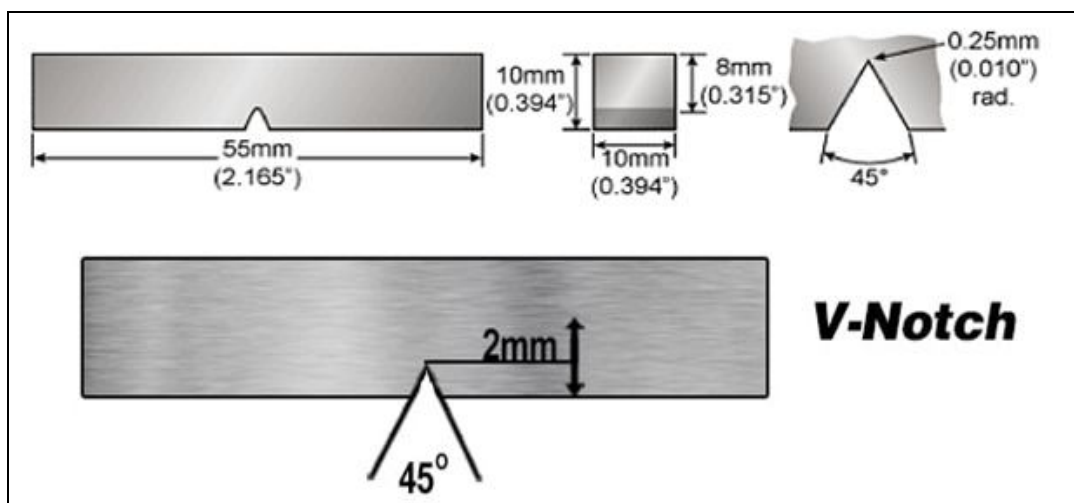
Figure 2.16: ASTM standard for V-notch Charpy impact test

G.Madhusudan Reddy et.al [1] used Electron beam and friction welding for similar and dissimilar welds of austenitic stainless steel (AISI304), ferritic stainless steel (AISI 430), and duplex stainless steel (AISI 2205) . During electron beam welding, elements moved in significant amounts, but during friction welding, they moved in small amounts. Mechanical behaviour was investigated using residual stress, impact toughness, hardness, and tensile strength tests. The duplex stainless steel was shown to bear higher compressive loads than the austenitic stainless steel. Duplex–austenitic stainless-steel joints exhibited the greatest capability in terms of strength. Electron beam weldments have a greater impact strength and notch tensile strength than friction weldments. Electron beam and friction welds were shown to be less tough than parent metals when evaluated [1]. Saeid Ghorbani, et.al [128] investigated dissimilar metals austenitic stainless steel (304 L) and ferritic stainless steel (430) by GTAW with two types of fillers (316 L and 2594L). Researchers performed an experiment to investigate how heat treatment affects the microstructure, mechanical characteristics, and corrosion properties of a weld. For (304L and 430) filler metal used was 2594 and 316L, range of heat treatment temperature is 860^0 to 960^0 C. As the heat treatment temperature increases from 860 °C to 960 °C, the austenite phase of 430 FSS HAZ of the ferritic steel is stable. Because the size distribution of martensitic regions has improved owing to the dissolving of precipitates and the reduction of ferrite matrix grains, the mechanical properties of the weldment have improved [128].

Table 2.5: ASTM standard specification for tensile test specimen

Dimensions			
	Standard Specimens		Subsize specimen
	For plate type, 40 mm wide	For sheet type, 12.5 mm wide	For plate or sheet type, 6 mm wide
G- Gauge Length	200.0 ± 0.2 mm	50.0 ± 0.1 mm	25.0 ± 0.1 mm
W- Width	40.0 ± 2.0 mm	12.5 ± 0.2 mm	6.0 ± 0.1 mm
T- Thickness	5 mm	19 mm	6 mm
R- Radius of fillet	Min, 25 mm	Min, 12.5 mm	Min,6 mm
L- Overall length	Min, 450 mm	Min, 200 mm	Min, 100 mm
A-Length of reduced section	Min,225 mm	Min,57 mm	Min,32 mm
B- Length of grip section	Min,75 mm	Min,50 mm	Min,30 mm
C- Width of grip section	Approx,50 mm	Approx, 20 mm	Approx,10 mm

2.17 Gaps in Literature review

From Literature it has been found that: -

1. 430 FSS and 316L ASS are welded separately with other popular SS, but the dissimilar joint of 430 FSS and 316L ASS are conducted rarely, which is the area of study for the cost effectiveness.

2. The welding parameter optimization and validation with experimental work are the prime concerned area which is not studied till now.

3. Study on microstructure and mechanical properties of dissimilar welded and heat affected zone of 430 FSS and 316L ASS are still the prime area of research.

4. Corrosion studies on dissimilar weldments of 430 FSS and 316L ASS are not taken into the consideration which is the area of research.

2.18 Aim of Investigation

Due to the different welding requirements for dissimilar weld of 316L ASS and 430 FSS in various industries, especially in petrochemical, shipbuilding and chemical, it was decided to systematically consider the following:

1. Effect of welding of the dissimilar welded joints on the heat affected zone.
2. Effect of various welding methods on the microstructure of dissimilar welded joints.
3. Effect of welding techniques on the dissimilar weld joints mechanical properties.
4. Effect of welding techniques on the dissimilar weld joints intergranular and pitting corrosion properties.

2.19 Research objectives

1. Optimization and validation of welding parameters with experimental work.
2. To investigate and analyse the microstructure of the 316L ASS and 430 FSS dissimilar welded joints.
3. To study the mechanical properties of 316L ASS and 430 FSS weldments.
4. To study the intergranular and pitting corrosion behavior of 316L ASS and 430 FSS weldments.

2.20 Scope of work

1) To optimize the welding parameters with experimental work.
2) To analyze and examine the microstructural changes of the weldment.
3) To investigate the effects on mechanical properties of the weld joint of different welding fillers.
4) To investigate the effects on intergranular corrosion properties of the weld joint of different welding fillers.
5) Potentiodynamic polarization studies on dissimilar welded joints and to investigate the effect of 0.5 M H_2SO_4 and 0.01 M NH_4SCN.
6) Potentiodymaic polarization studies on dissimilar welded joints to investigate the effect of 3.5 wt% NaCl.

7) Single V-butt joint welding of ASS-FSS by conventional GTAW, study microstructural changes, mechanical and corrosion properties of dissimilar welded joint.

8) Single V-butt joint of ASS-FSS by advanced CMT welding, study microstructural changes, mechanical and corrosion properties of dissimilar welded joint.

2.21 Organization of thesis

The thesis is organized into five chapters. The salient features of each chapter have been given in brief as following:

Chapter 1 introduction deals with building background for the work. It gives brief description of austenitic stainless steel, ferritic stainless steel, welding, effect of welding on FSS, welding defect, corrosion of weld joints, dissimilar metal welding and ends with enlisting aim of investigation.

Chapter 2 deals with literature review on ASS and FSS, in which this chapter gives review on the basics of stainless steel and its classification, difference between 200-series and 300-series stainless steel, sensitization of stainless steel, influence of alloying elements on microstructure and properties of stainless steel, welding methods, welding electrode, welding parameters, effect of welding on 316L ASS, effect of welding on 430 FSS, welding of dissimilar metals with electrochemical techniques of corrosion testing including DLEPR and PDP test, mechanical testing of dissimilar joint with ASTM standards. It ends with enlisting scope of investigation.

Chapter 3 deals with experimental work and describes the different welding processes, sample preparation, equipment and tests used for testing.

Chapter 4 deals with results and discussions. The results are systematically presented and discussed in the light of finding reported in the literature.

Chapter 5 presents conclusion of the work.

CHAPTER 3: EXPERIMENTAL WORK

3.1 Preamble

The experimental work began with the purchase of 3 mm thick test steels from the local market, comprising 316L austenitic stainless steel (ASS) and 430 ferritic stainless steel (FSS). The two plates were cut through wire cut Electrical Discharge Machining (EDM) of length 100 mm and width 75 mm. The plates were cleaned, then solution annealing was performed at 1050^0C for 1 hour before being quenched in water. The chemical composition of both the base metal were analyzed and the microstructure investigated. The samples were than welded with single pass Gas Tungsten arc welding (GTAW) and Cold Metal Transfer (CMT) welding with GTAW mode.To determine how welding affects mechanical and corrosion, EDM was used to cut samples for studying microstructure, testing mechanical properties such as hardness, tensile, impact, and electrochemical testing. The double loop electrochemical potentiokinetic reactivation test (DLEPR) was used for finding degree of sensitization (DOS). Finally, the welded test samples were tested for pitting corrosion by potentiodynamic (PDP) test.

3.2 Framework of Experimental work

The experiment began with purchasing of 316L ASS and 430 FSS as test steels from the local market. The solution annealing is used as a heat treatment process which decreases metal crack sensitivity of aged material that needs to be returned to a weldable state. The two test steels were first welded by Gas Tungsten Arc Welding Process (GTAW) and Cold Metal Transfer (CMT) Welding process with GTAW mode with the help of fillers ER316L, ER309L and without filler because these types of fillers are mainly used for stainless steel joint [Table 2.3]. The test samples were cut by Electrical Discharge Machining (EDM) for analysis. The optical microscope was used for microstructural examination. The universal testing machine is used for tensile strength, Charpy Impact Tester for toughness and Vickers hardness tester for testing hardness of the test steel. The potentiostat (Solartron-1285) is used for intergranular corrosion and potentiostat (BIO Logic VMP-300) is used for pitting corrosion. The framework of experimental work is shown in Fig.3.1.

49
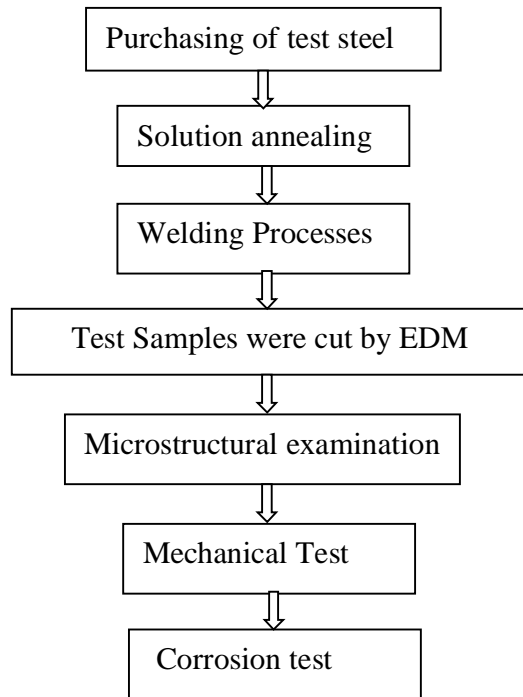
Figure 3.1: Framework of experimental work

3.3 Material

The present research work involves a study of two materials such as 316L ASS and 430 FSS. The chemical composition of the test steel was obtained from Mineral and Metal Testing Services, Hingna, Nagpur (NABL lab) by means of optical emission spectroscopy (OES). The two types of fillers were used and their chemical composition is presented in **table 3.1**.

Table 3.1: Chemical composition (wt.%) of base metal and filler materials

Materials	C	Mn	Si	Cr	P	S	Mo	Ni	Co	Cu	Fe
316L ASS	0.026	1.097	0.354	16.370	0.038	0.002	2.013	10.014	0.168	0.272	Bal.
430 FSS	0.050	0.434	0.479	16.345	0.030	0.007	0.020	0.194	0.011	0.018	Bal.
ER 316L	0.03	1.8	0.5	19	-	-	2.8	11.5	-	0.3	Bal.
ER 309L	0.035	1.58	0.175	23.45	0.024	0.021	0.75	12.6	-	-	Bal.

3.4 Welding

3.4.1 Gas Tungsten arc welding (GTAW) process

The plates of 316L ASS and 430 FSS of dimensions (100 mm x 75 mm x 3 mm) were welded using ER 316L, ER 309L and without fillers (autogenous) material. The welding was carried out with single pass GTAW process (TORNADO TIG 315/500 ACDC,415 V AC, 3Ph, 50Hz). The single butt joint with root gap of 1.2 mm was performed at a constant current of 90 A with electrode having 1.6 mm diameter. Argon gas is used as a shielding gas at a flow rate of 10 l/min. Direct current electrode negative (DCEN) polarity was used. Fig.3.2 shows schematic diagram of GTAW. For repeatability of process the welding was carried out two times with same welding parameters. Table 3.2 shows welding parameters with different filler materials. The heat input (HI) is calculated as

$$HI = \eta \times \frac{V \times I}{W} \text{ KJ/mm} \qquad \text{(eq.3.1)}$$

Where, η – efficiency of GTAW as 0.7, V- voltage in volts (V), I – welding current in amperes (A) and W – welding speed in (mm/s) [129].

Table 3.2 Welding parameters for GTAW processes

Specimen	Filler Material	Current (A)	Voltage (V)	Welding Speed (mm/s)	Heat input (KJ/mm)
316L and 430	ER 316L	90	22	2.0811	0.6659
316L and 430	ER 309L	90	22	1.7427	0.7953
316L and 430	Without filler (autogenous)	90	23.3	2.6946	0.5750

Argon
Gas

Current
selection

Figure 3.2: Welding set-up for Gas Tungsten Arc Welding (GTAW)

3.4.2 Cold Metal Transfer (CMT) Welding process

The plates of 316L ASS and 430 FSS of dimensions (100 mm x 75 mm x 3 mm) were welded using ER 316L, ER 309L and without fillers (autogenous) material with 1.6 mm diameter [30]. The welding was carried out with single pass Cold Metal Transfer Welding (FRONIUS- TPS 430, 3x460 Mains Voltage, 3-430 A Current range,14.2-34.0 Voltage range) with GTAW mode. A constant current of 90 A was used to perform the single butt joint with a root gap of 1.2 mm. Argon gas is used as a shielding gas at a flow rate of 10 l/min. For repeatability of results the welding processes were conducted three times and average value for the specimen were reported. Table 3.3 shows welding parameters with different filler materials. Fig 3.4 shows the welded plate with ER 316L, ER 309L and without filler. Fig. 3.3 consist of welding setup. The heat input was evaluated from current and voltage using eq. 3.1 [130].

Table 3.3: Welding parameters for Cold Metal Transfer Welding with GTAW mode

Specimen	Filler Material	Current (A)	Voltage (V)	Welding Speed (mm/s)	Heat Input (KJ/mm)
316 L and 430	ER316 L	90	8	1.6750	0.30089
316L and 430	ER309 L	90	8	1.8181	0.27721
316L and 430	Without filler (autogenous)	90	9	2.3255	0.24381
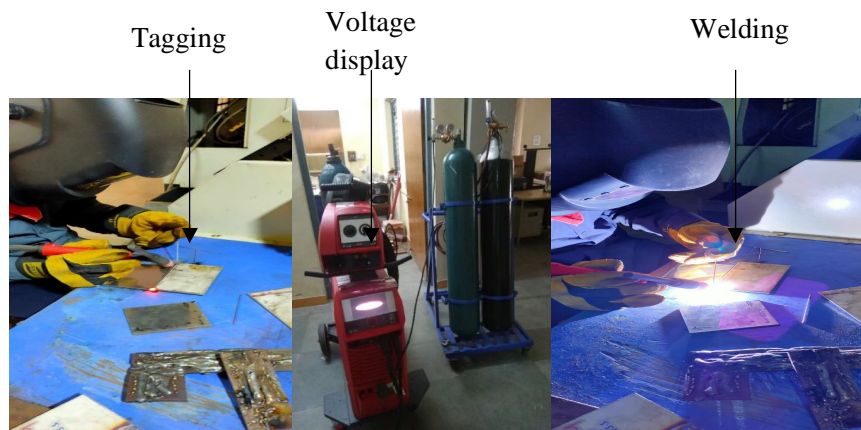
Figure 3.3: Welding set-up for CMT Welding
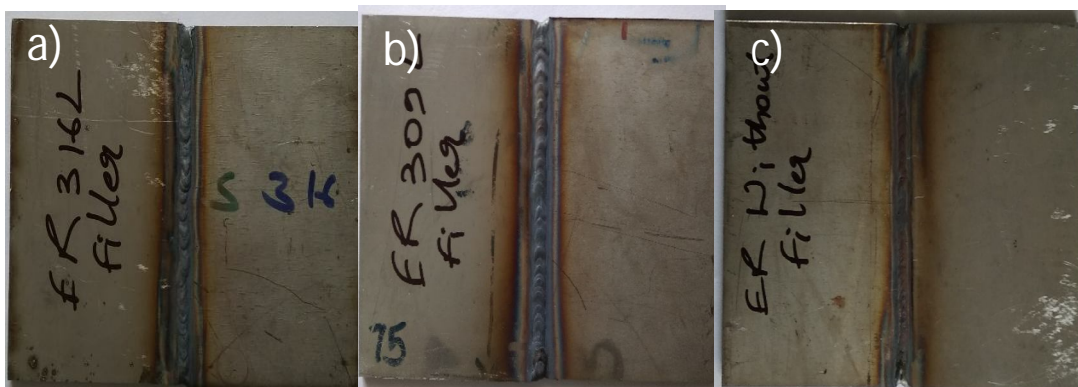
Figure 3.4: a) ER316L b) ER 309L and c) Without Filler weld plate

3.5 Sample preparation

Samples of different sizes were prepared for different tests as shown in Table 3.4. For various specimens for testing, welded plates of (100 mm x 75 mmx 3 mm) were cut from wire cut Electrical Discharge Machine (EDM). The welded specimen for microstructural, tensile, impact, hardness, DLEPR and PDP test are shown in Fig.3.5.

Table 3.4: Specimen size for different samples for testing

Sr.No.	Samples for testing	Dimension of samples
1)	Microstructural observation	30 x 10 x 3 mm^3
2)	Microhardness test	30 x 10 x 3 mm^3
3)	Tensile test	As per ASTM E8
4)	Impact test	55 x 10 x 3 mm^3 with notch angle 45^0
5)	Corrosion test	10 x 10 x 3 mm^3
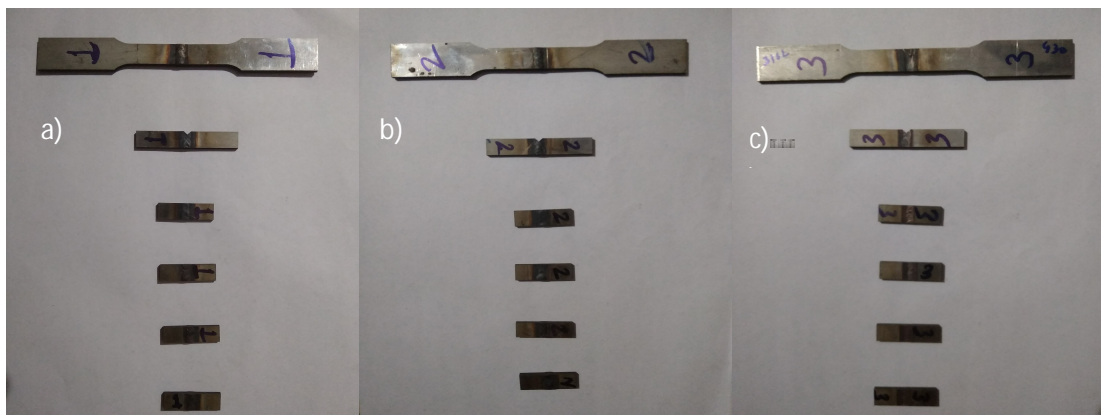
Figure 3.5: Test specimen welded with a) ER316L b) ER 309L and c) Without Filler weld

3.6 Microstructural Examination

After welding, the samples were cut with dimension 30 mm x 10 mm x 3 mm to analyze the microstructure as shown in fig.3.6. All weld samples were polished using a grit sequence of 220,320,400,800,1000,1200,1500,2000 and 2500 followed by cloth polishing with 0.75 µm alumina slurry, and finally the samples were cleaned by ultrasonic machine after polishing. To observe the microstructure of the base metal (BM) and Weld metal (WM) the samples were electrochemically etched in 10 wt.% oxalic acid with a current density of 1 A/cm^2 for 70 s using a Potentiostat (Solartron 1285) [131]. Different welding regions were analyzed and metallographic examination were carried out in Zeiss Axio Lab A1 and optical microscope.
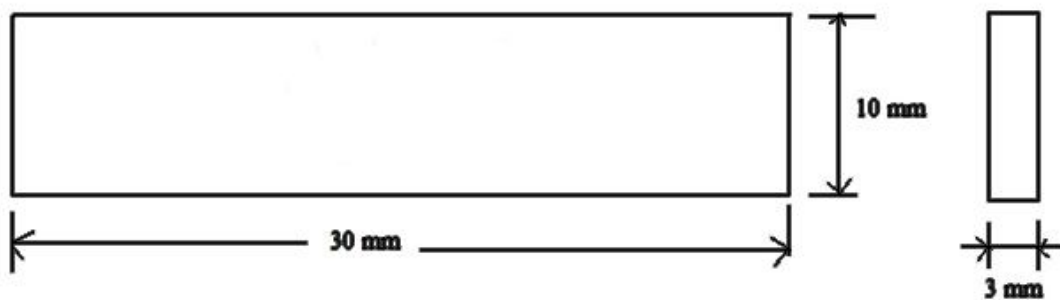
Figure 3.6: Specimen for microstructural observation

3.7 Micro-hardness measurement

The microhardness specimens have been polished with several kinds of emery papers (420, 800, 1000,1500 and 2000 grit) and then finished with cloth smeared with alumina slurry (0.75µm) [132]. The hardness of the weld was measured using a Vickers microhardness testing equipment, which was made by MITUTOYO, Japan. HAZ and base metal by taking the load of 500 gf (gram-force) with dwell time of 10 s across the transverse section and along the length of specimen [133]. The average of three data points is taken at HAZ, WZ and BM in order to maintain reproducibility of results.

3.8 Tensile Test and Fractography

For preparing tensile specimens, the welded joints were cut by EDM wire cut along the transversal direction (perpendicular to welding direction). The ASTM E8 M-04 guidance for preparing and testing tensile specimens was used [134] as shown in fig.3.7. Tensile specimens were fractured in a Universal Testing Machine (UTES-TS) with a cross head speed of 20 mm/min and gauge lengths of 45 mm. Tensile properties like yield strength, ultimate tensile strength and percentage elongation of the joints were evaluated. The fractured surfaces were examined using Scanning electron Microscopy (JEOL's, JSM-7900F). All the specimens were examined at 500X magnification.
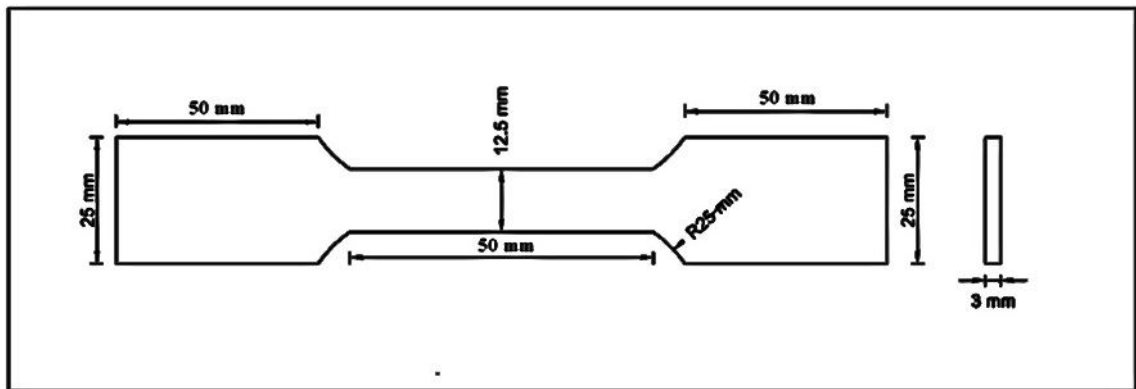
Figure 3.7: Specimen of tensile test as per ASTM E8

3.9 Impact Test

For impact test, ASTM A370 with dimension 55 mm x 10 mm x 3 mm were used as shown in fig.3.8. V-notch Charpy impact test (IT-30) was performed at room temperature for evaluating toughness value at notch angle 45^0 with 2 mm depth [135]. SEM was used to examine the broken surface of the impact specimen.
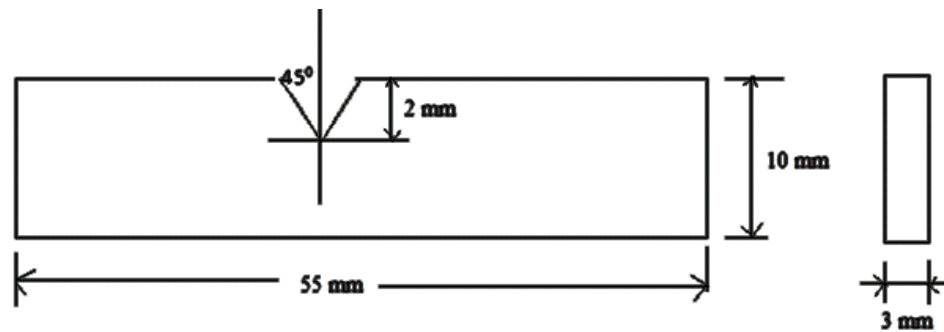
Figure 3.8: Specimen of impact test as per ASTM A370

3.10 Double loop electrochemical potentiokinetic reactivation (DLEPR) test

Double loop electrochemical potentiokinetic reactivation (DLEPR) test was performed as per ASTM G108-07 standard. The test was carried out in potentiostat (Solartron- 1285) with 0.5 M H_2SO_4 (Sulfuric acid) + 0.01 M NH_4SCN (Ammonium thiocyanate) solution. The three electrochemical cells were used, first the working electrode (were sample is placed), second the reference electrode (saturated calomel electrode) and third the counter electrode (platinum guaze) as shown in Fig.3.9.
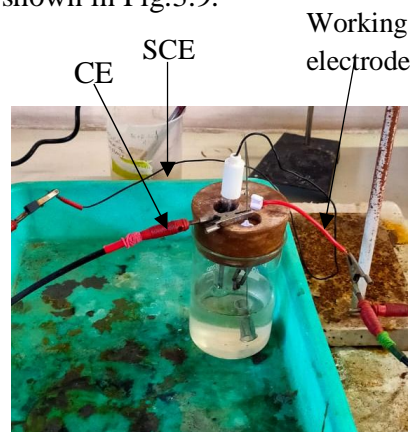
Figure 3.9: Sample for DLEPR test in Solatron-1285

In the beginning the oxide layer is removed from the surface of working electrode for 120 s at -0.5 V in the same solution. The surface of the sample in working electrode is then stabilized by open circuit potential (OCP) for 30 min. Finally, at constant scanning rate of 1.667 mV/s forward and reverse scan is implemented. The potential range of -0.5 V (SCE) to +0.5 V (SCE) was applied to get forward scan and the potential is reversed to -0.5 V in

reverse scan. Forward and backward scans were used to determine the peak activation current density (Ia) and peak reactivation current density (Ir). The ratio (Ir/Ia) x 100 was used to calculate the percent degree of sensitization (% DOS) [48]. The mounted samples for testing DLEPR and PDP test are shown in Fig.3.10.

Single strand copper wire

Cold setting mounting
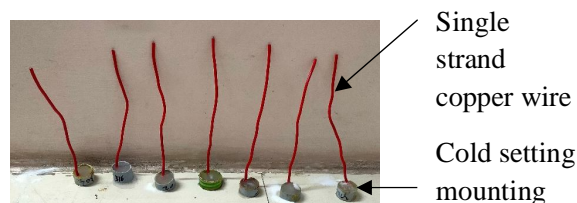
Figure 3.10: Mounted Samples for DLEPR and PDP test

3.11 Potentiodynamic Polarization (PDP) test

Potentiodynamic polarization (PDP) tests were performed on a potentiostat (BIO Logic VMP-300) using a standard cell arrangement. First cell - consist of working electrode (WE), second – reference electrode (RE) and third – counter electrode (CE) in 3.5 % NaCl solution as shown in fig.3.11. The open circuit potential (OCP) was measured 1h while the potential stabilized during PDP test. The tests were performed in the potential range of -0.7 V (vs SCE) to 1.2 V (SCE) at a scan rate of 0.5 mV/sec [136]. The test was conducted at room temperature with a surface area of 0.50 cm^2 (weld area only). The obtained data was analyzed using EC-lab software. Corrosion potential (Ecorr), corrosion current density (Icorr) and pitting potential (Epit) were evaluated using PDP test. After conducting tests for microstructural examination, mechanical and corrosion properties. The results are analyzed and conclusions are drawn.

Counter Electrode

Reference electrode

Working electrode
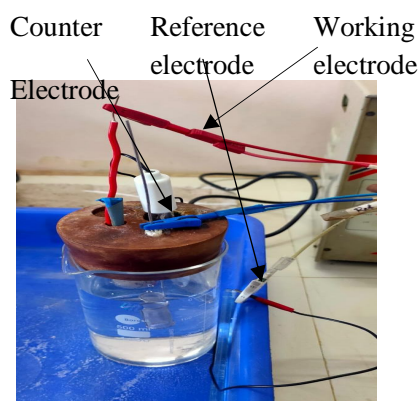
Figure 3.11: Sample for PDP test in BIO logic VMP-300

CHAPTER 4: RESULTS AND DISCUSSION

4.1 Preamble

The chapter is organized to show the findings, as well as analyse and discuss them. To begin with the microstructure of test steels are presented. This microstructure will be used as a base for discussing the effect of various welding parameters. The results of dissimilar welding of 316L austenitic stainless steel (ASS) and 430 ferritic stainless steel (FSS) are presented to show the effect of welding processes and welding current on microstructure, microhardness, tensile, impact and corrosion test by Gas Tungsten arc welding process (GTAW) and Cold Metal Transfer (CMT) welding processes with GTAW mode were presented.

4.2 Dissimilar welding of 316L ASS and 430 FSS by GTAW process

4.2.1 Microstructural examination

The microstructure of weldments of Base Metals (BM), Unmixed Zone (UMZ), Weld Metal (WM) and Heat Affected Zone (HAZ) is shown in fig 4.1. From the microstructure, it was observed that the 316L ASS BM represents an austenitic phase matrix mainly containing intergranular ferrite, whereas, 430 FSS BM represents a ferrite matrix containing intergranular martensite. Furthermore, because of the low cooling rate and the long diffusion time the considerable heat input results in substantial martensite formation during cooling [130,137].The composition of fillers plays an important role in the formation of the WM microstructure. The microstructure of ER316L WM is made up of an austenite (white) matrix and skeletal ferrite phase (dark etched phase) Fig.4.1(a), intermediate cooling rate and Cr_{eq}/Ni_{eq} ratio under the ferrite-austenite (FA) series to support the skeletal phase [135]. After solidification, ferrite separates from the austenite mainly due to their chemical composition and the cooling rate of 316L ASS [135]. UMZ is observed on the interface around 316L ASS BM. It can be formed due to its very thin and low thermal conductivity (8.54 w/mK), which causes low thermal conductivity and high volumetric heat capacity (3,966 $cm^{-3}K^{-1}$) [138]. The same was observed for ER309L and autogenous weld interface side (316L ASS BM and 430 FSS BM side). There is no difference between the two because the heat input does not change significantly. All welds

in different phase formations behave strangely. The ER309L weld (Fig.4.1 b) also solidifies in the ferrite- austenite (FA) mode and exhibits a slightly higher Creq/Nieq ratio (˂1.66) than ER316L weld Creq/Nieq ratio (˂1.61) [139].

ER309L weld formed vermicular ferrite with dendritic spacing of 18.22 µm and primary arm of 4.13 µm. The vermicular ferrite in ER 309L weld was produced due to the development of chromium (Cr) and nickel (Ni) enriched and depleted regions at the cores of the cellular dendritic sub grain [139]. No other precipitates were observed in ER316L and ER309L welds. In autogenous weld (without filler), since no filler was used, lathy ferrite was observed with a martensite phase, rich in Chromium (Cr) and carbon (C), and only compositions 430 FSS and 316L ASS were mixed and solidify into lathy ferrite and martensite morphology (Fig. 4.1 c).
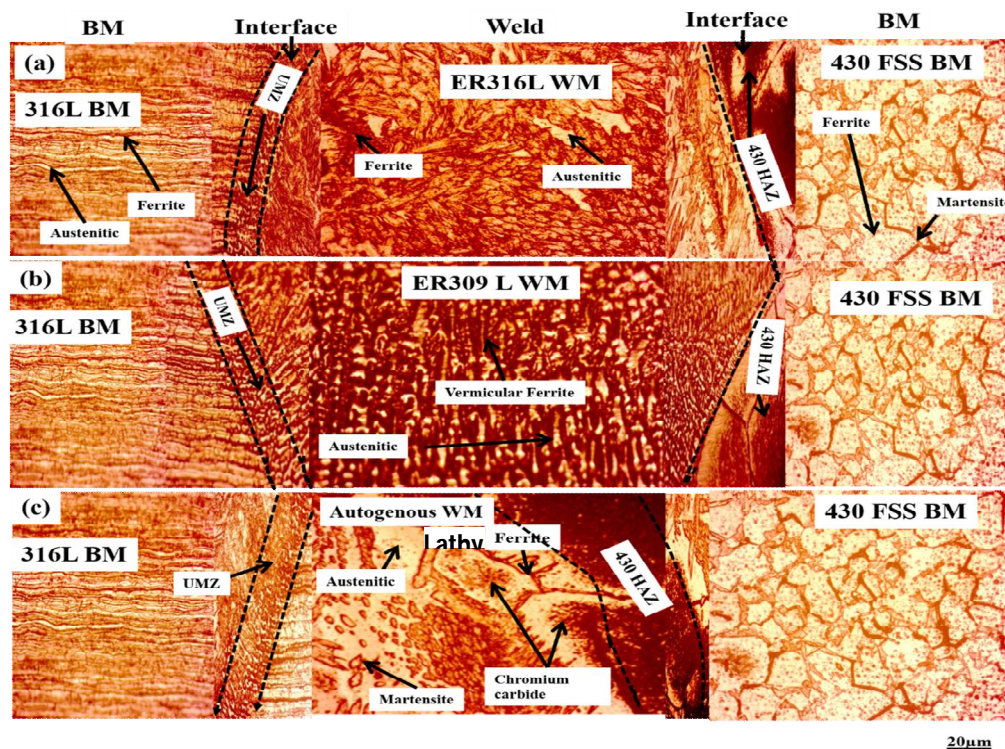
Figure 4.1: Optical Micrograph of weldments a) ER 316L filler weld, b) ER 309L filler weld, c) without filler (autogenous weld) for GTA welding

Chromium carbide was also observed in the weld, SEM/EDS analysis (Fig 4.2) shows the presence of chromium carbide deposits during autogenous welding. EDS analysis showed that the chromium (Cr) content in the chromium carbide ($Cr_{23}C_6$) range is higher than that of the ferrite phase, indicating the presence of carbides. This type of precipitate is formed when carbon is saturated with a ferrite phase at high temperatures. 430 FSS is enriched with Cr and C which is ferrite-forming elements, however 316L ASS is enriched with Ni (austenite former) and Cr (ferrite former) accelerates carbide precipitates, but amount of heat input maximizes carbon dissolution, and in the ferrite-matrix corresponding to the more supersaturation sites and subsequently much more chromium carbide precipitate [57,139]. The formation of chromium carbide is supposed to affect the corrosion resistance of autogenous weld.

Element	wt (%)
Fe	85.1
Cr	17.9
C	44.7
Mn	1.1
Ni	5.79

Element	wt (%)
Fe	77.7
Cr	19.1
C	47.75
Mn	0.9
Ni	2.79
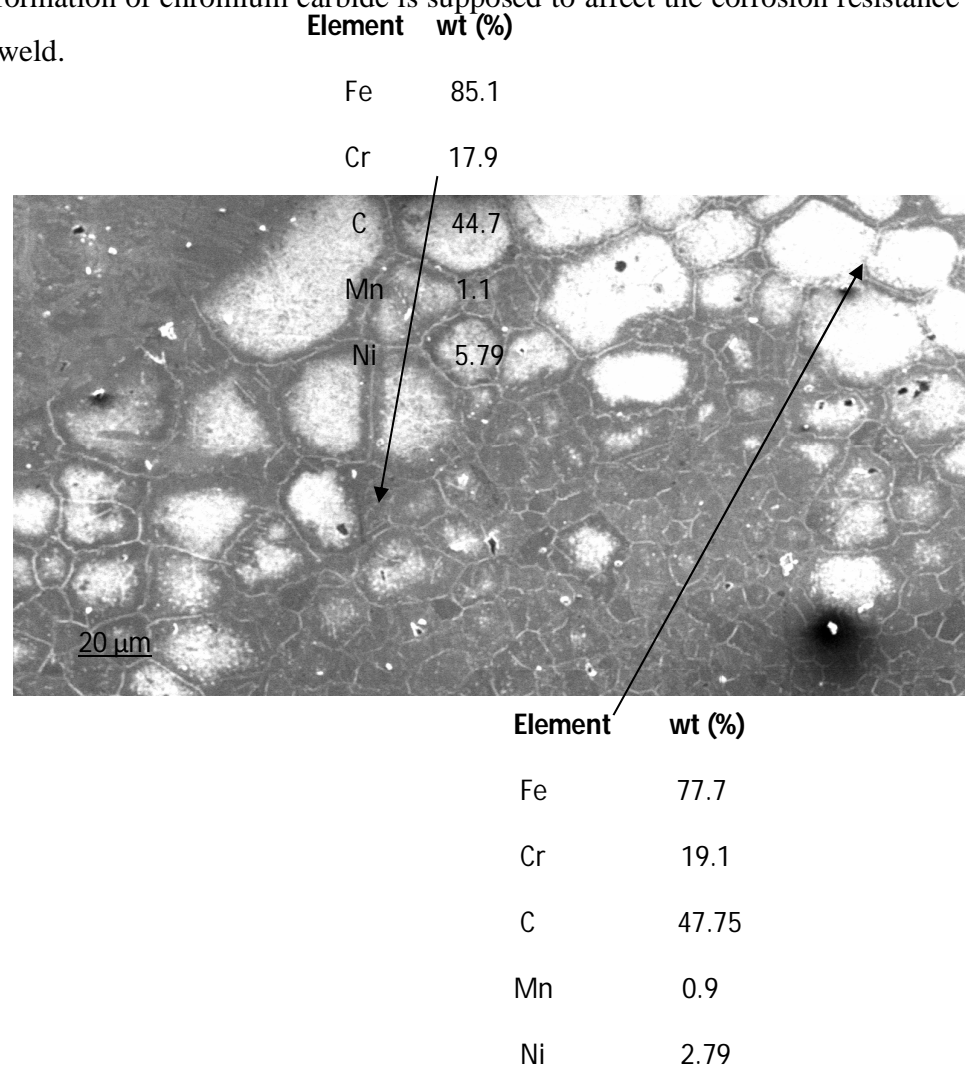
Figure 4.2: SEM/EDS analysis of autogenous weld

61

4.2.2 Micro-hardness Test

As shown in Fig 4.3, weld cross-section hardness test was performed on BM 316L ASS, 316L UMZ, WM, 430 HAZ and BM 430 FSS. The three readings are taken at one point and average of three values are indicated in different regions of the specimen. The values are indicated at BM 316L ASS, 316L UMZ, Weld Zone, 430 HAZ and BM 430 FSS. The average hardness at the 316L ASS BM is (avg.179.1 HV). The hardness increases from the 316L UMZ and it is highest at the weld zone. Then after this, the hardness decreases from the weld zone to the 430 HAZ. It was found that the highest hardness for without filler (autogenous) weld (avg.317.0 HV) as related to ER 316L weld (avg.263.6 HV) and ER 309L filler weld (avg.242.6 HV). The average hardness at BM 430 FSS is (avg.135.9 HV). The hardness first increases (316L ASS BM, 316L ASS UMZ, Weld Metal (WM)) and decreases from (430 FSS HAZ and BM 430 FSS). The more percentage of carbon in the weld zone imparts higher hardness. Therefore, the increase in hardness in autogenous weld may be due to the formation of martensite and chromium carbide deposits. Cooling causes nuclei to expand, resulting in an increase in dendritic size and a reduction in hardness during solidification [140]. On the other hand, ER 316L weld has higher hardness than ER 309L filler weld due to the higher percentage of molybdenum (Mo) content than ER 316L, the higher the ferrite phase, but the Cr_{eq} / Ni_{eq} ratio is small, so it was supposed that the less martensite and / or precipitate can increase the microhardness [57]. In the temperature range, the heat affected zone (HAZ) is heated and cooled, thus the increase in the hardness is due to the formation of chromium carbides. On the other hand, BM 316L ASS and 316L UMZ shows avg.176.7 HV and 197.4 HV hardness respectively. The more hardness in 316L UMZ is due to the starting of transformation of austenite to ferrite and then into martensite.
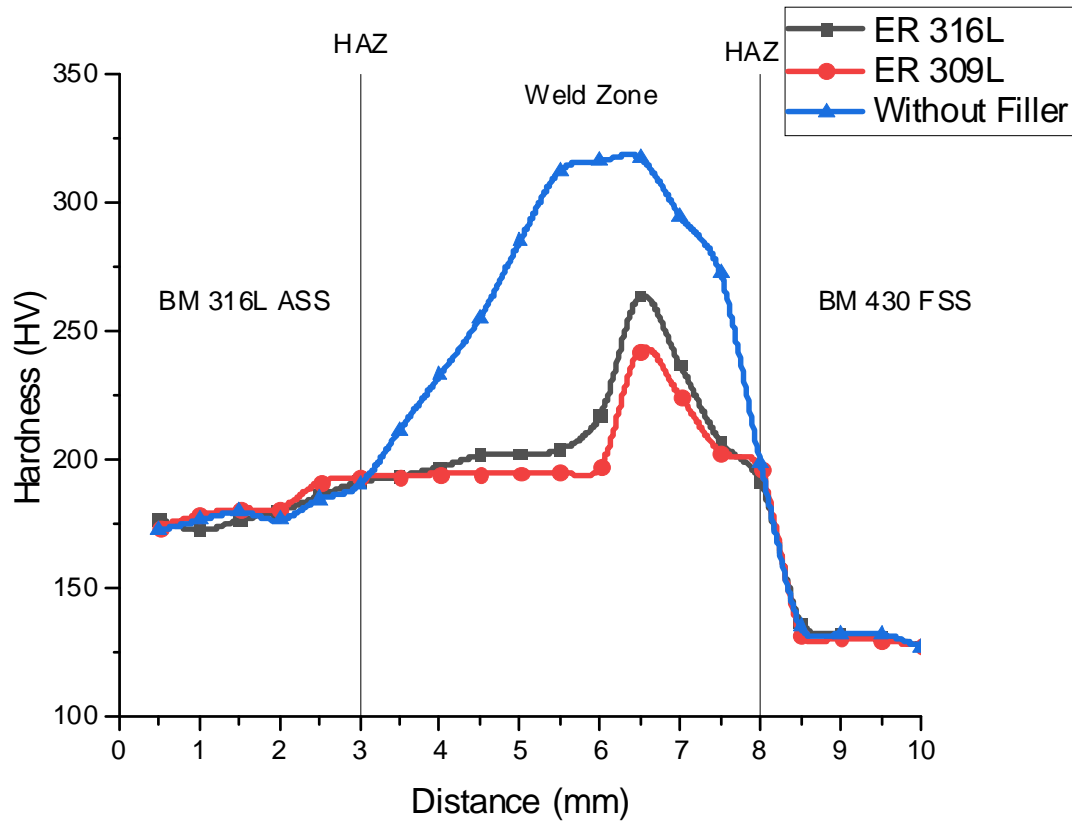
Figure 4.3: Microhardness results across various zones for GTA welding

4.2.3 Analysis of Tensile Test

Tensile tests were performed for dissimilar welds as shown in Fig 4.4a and samples were prepared according to ASTM E8. Strain rate taken as 1.5 mm/min or 2.5 x 10^{-2} mm/s (cross head speed). Stress-strain curves for all samples are shown in Fig 4.4b. The average values of three samples were tested for each specimen. All tensile test pieces failed on the 430 FSS BM side of the weld, indicating that the dissimilar welds were strong enough. The discussion on the weld strength is inconclusive because the failure occurred with the 430 FSS BM. However, weld strength variations can be associated with solid solution hardening of different filler compositions [113,141]. In order to diversify the strength, the filler and BM compositions are important. The yield strength of BM 316L ASS (~ 361

63

MPa), BM 430 FSS (~ 319 MPa), ER 316L filler weld (~ 342 MPa), ER 309L filler weld (~ 353 MPa) and without filler weld (~ 334 MPa). The yield strength of ER 309L filler weld shows (~ 353 MPa) which is greater than the 430 FSS BM (~ 319 MPa) which indicates that the weld joint is stronger. This is due to the chemical composition of filler metal ER 309L which contains Cr (23.45 %) and Ni (12.6 %). The tensile strength of BM 316L ASS (~ 570 MPa), BM 430 FSS (~ 438 MPa), ER 316L filler weld (~ 452 MPa), ER 309L filler weld (~ 435 MPa) and without filler weld (~ 438 MPa). It indicates that the tensile strength of ER 316L filler weld (~ 452 MPa) is greater than the weaker base metal of dissimilar metal i.e., BM 430 FSS (~ 438 MPa) this indicates that the strength of the weld joint of ER 316L filler weld is stronger. The reason behind this is the chemical composition of the filler, as in ER 316L filler has higher percentage of Mo (2.8 %) than ER 309L filler (0.75 %) [142]. The percentage elongation of BM 316L ASS (54 %), BM 430 FSS (27%), ER 316L filler weld (21%), ER 309L filler weld (23%) and without filler weld (23%). Fig 4.5 shows the changes obtained by comparing the yield strength, tensile strength and percentage of elongation, as a result of solid solution strengthening of welds.

The fractography of the weld specimen was analyzed using SEM (fractography were shown in Fig 4.4 (c-e). From fractography results, it was found that the fracture types were mostly cleavage / flat facet and river pattern.
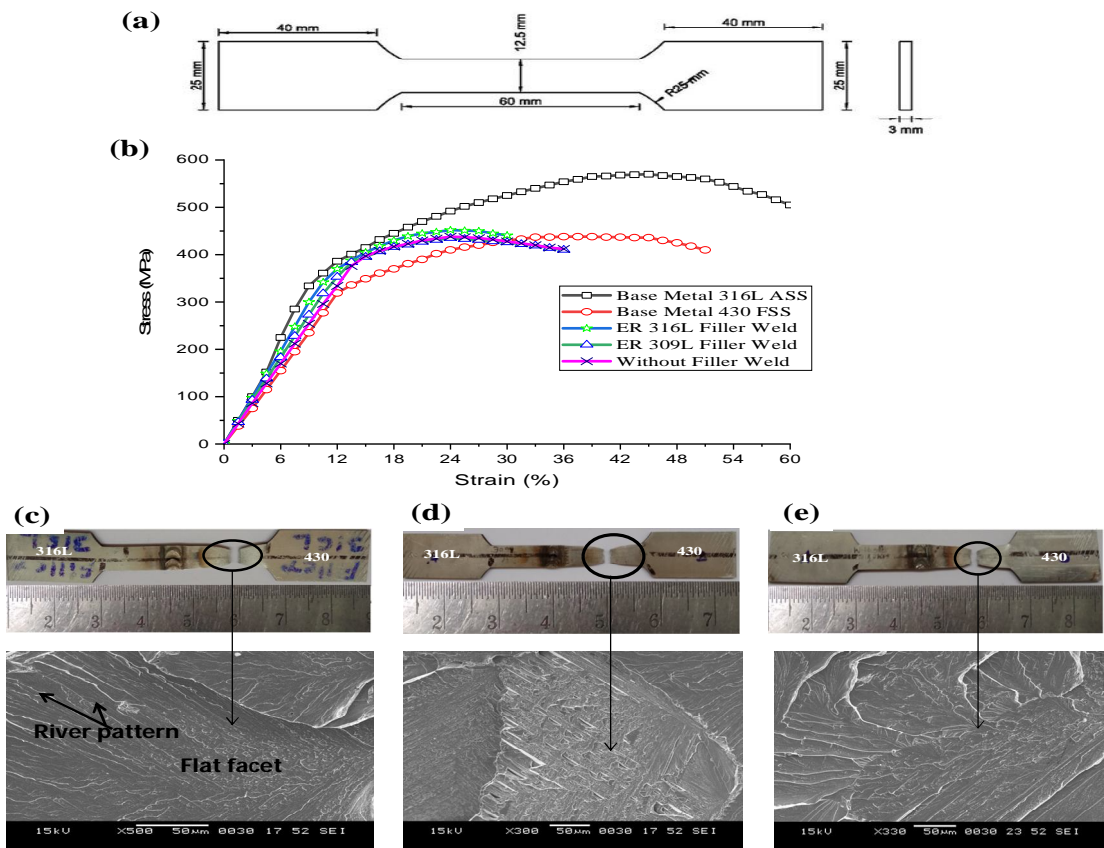
Figure 4.4: Tensile test (a) schematic illustration of specimen, (b) stress strain curve, (c-e) fractography of BM 430 FSS.
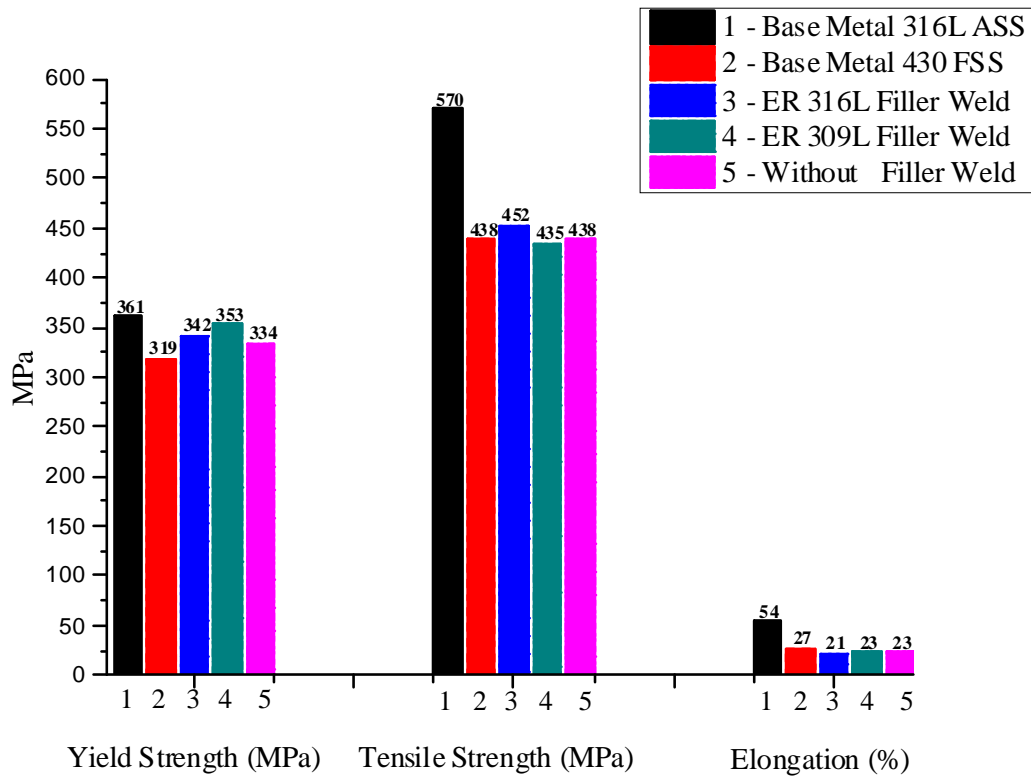
Figure 4.5: Comparison of Yield Strength, Tensile Strength and Percentage Elongation

4.2.4 Analysis of Impact Test

The Charpy V notch impact test was performed at room temperature with a sample size of 55 mm x 10 mm x 3 mm, a notch angle of 45^0 and a depth of 2 mm. Fig.4.6 shows the comparison of the toughness of the Base metal and the weldments of the filler weld metal. BM 316L ASS and BM 430 FSS showed impact toughness values of ~ 55 J and ~ 29 J. In contrast to ER 316L weld, the obtained impact strength values where ~ 44 J. ER 309L weld, on the other hand exhibits an impact energy of ~ 22 J, but the autogenous weld impact toughness is ~15 J.This is due to the low ferrite content, high Ni content in ER 316L filler weld increases toughness [8,9] and lowers ER 309L filler impact energy due to the high ferrite content as compared to autogenous weld where there is formation of martensite and chromium carbide.

The fractured surface of the impact sample was analysed using SEM. Fractography of three samples are shown in Fig 4.7 a-c, shows ductile and semi-cleavage mode.
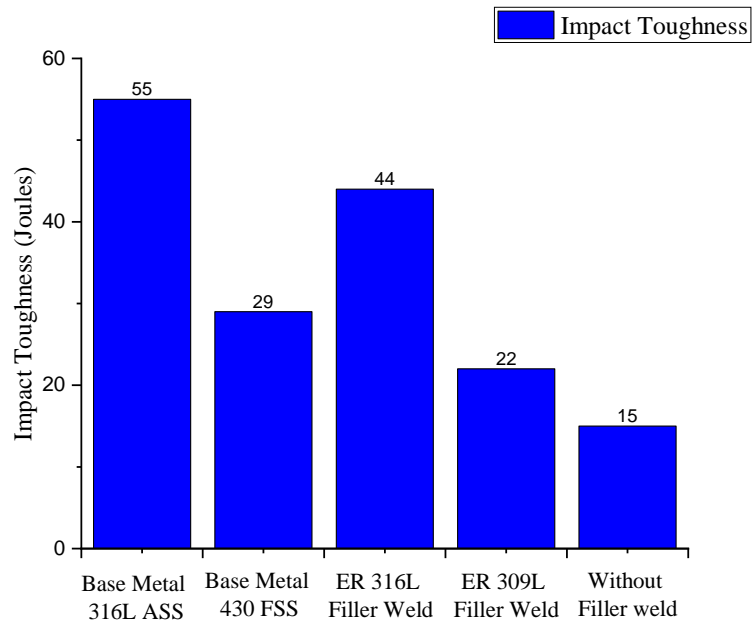
Figure 4.6: Comparison of toughness of the Base Metal and Weldments of GTAW
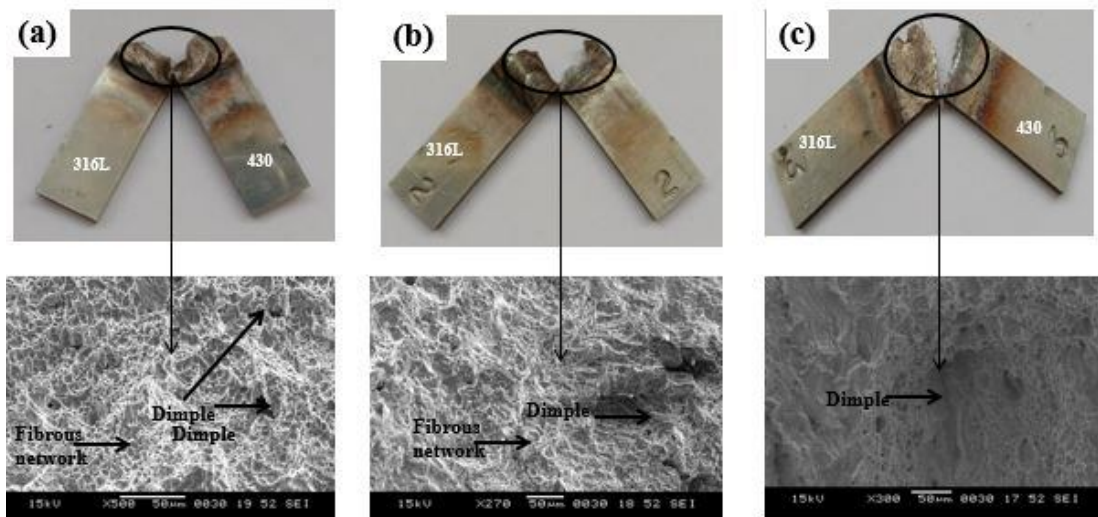
Figure 4.7: Fractography of impact test for a) ER316L, b) ER 309L and c) autogenous weld

4.2.5 Double Loop Electrochemical Potentiokinetic Reactivation (DLEPR) Test for intergranular corrosion

Welded joints are susceptible to corrosion as a result of metallurgical changes, and the potential variations between grain and grain boundaries are significant. The development of a Cr-depleted zone has been found to accelerate corrosion [142]. Therefore, to estimate the life of the welding process in aggressive environments, it is extremely essential to assess the corrosion resistance of the weld process. The double loop electrochemical potentiokinetic reactivation (DLEPR) test was carried out in potentiostat (Solartron-1285) using a solution of 0.5M H_2SO_4 + 0.01M NH_4SCN. The adopted surface area was 0.45 cm^2 (weld area) for the test performed at room temperature. First, the oxide layer was removed from the working electrode at -0.5V for 120 sec in the same solution. The surface of the working electrode sample was stabilized by the open circuit potential (OCP) for 30 min. Finally, forward and backward scans are implemented with a constant scan rate of 1.667 mV/s. For a forward scan, apply a potential range of -0.5 V (SCE) to +0.5 V (SCE) and apply a reverse scan to bring the potential back to -0.5 V. Fig. 4.8 (a) and (b) shows DLEPR curves for base metals (BMs) (316L ASS and 430 FSS). Fig. 4.8 (c-e) shows DLEPR curves for weld metals (WMs) (ER316L, ER309L and autogenous weld). Among the welds, autogenous weld was the most sensitive and shows highest degree of sensitization, followed by ER309L weld and the least sensitive was ER316L weld. The sensitivity of an autogenous weld is increased when martensite and chromium carbide precipitate are present. Due to variations in the activation energies of ferrite, martensite, and austenite, the austenite phase is less sensitive, while the ferrite and martensite phases are more sensitive, according to the literature [2,142]. The degree of sensitization is accelerated when carbide deposits are present [2,142]. On the other hand, the BM 430 FSS showed higher sensitivity than the BM 316L ASS. The presence of martensite and a smaller percentage of alloying elements may cause a high sensitivity in 430 FSS BM, while the sensitivity of 316L ASS BM is lower than that of 430 FSS BM due to the higher Cr concentration [57,141,142]. Table 4.1 shows the percentage degree of sensitization (DOS) of weldments.

Table 4.1: Percentage degree of sensitization of weldments

Sample	Ia (A/cm^2)	Ir (A/cm^2)	Ir/Ia (% DOS)
ER316L Filler Weld	0.0064	0.00028	4.34
ER309L Filler Weld	0.0094	0.00055	5.81
Without Filler Weld	0.0185	0.01226	66.24
(Autogenous)			
316L ASS BM	0.0021	0.00006	2.66
430 FSS BM	0.1710	0.09000	52.00
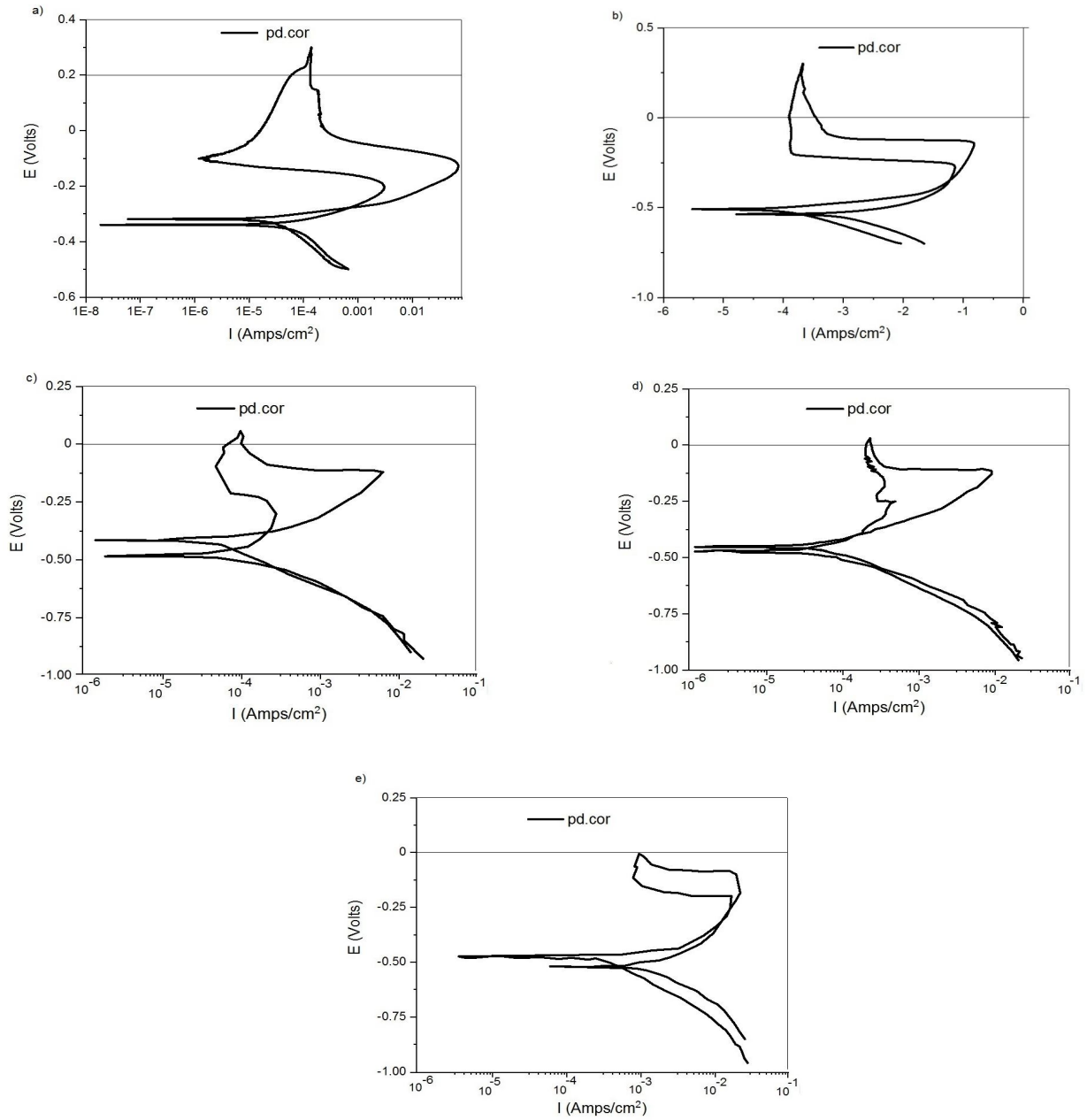
Figure 4.8: DLEPR curves of a) 316L ASS BM, b) 430 FSS BM, c) ER316L weld, d) ER309L weld and e) Autogenous weld

4.2.6 Potentiodynamic Polarization (PDP) Test for pitting corrosion

Potentiodynamic polarization (PDP) tests were performed at a potential of -0.7 V (vs SCE) to 1.2 V (vs SCE) at a sampling rate of 0.5 mV/sec. The approximate test area is 0.45 cm^2 (weld area only) and is carried out at room temperature. The data obtained was analyzed using EC-lab software. Corrosion potential (E_{corr}), corrosion current density (I_{corr}) and pitting potential (E_{pit}) were represented in Table 4.2. The polarization curves of dissimilar weld of 316L ASS and 430 FSS produced by two different fillers ER316L, ER309L and without filler in 3.5 % NaCl solution as shown in Fig 4.9 and the values are presented in Table 4.2. The corrosion potential (E_{corr}) values of BM 316L ASS is (-235.2 mV), BM 430 FSS is (-304.8 mV), ER 316L filler weld (-271.415 mV), ER 309L filler weld (-248.0 mV) and Without filler (Autogenous) weld (-356.851 mV). The corrosion potential value was found to be highest for autogenous weld and lowest for ER 309L filler weld. The corrosion current density (I_{corr}) for BM 316L ASS (0.110 μA/cm^2) , BM 430 FSS (0.34 μA/cm^2), ER 316L filler weld (1.22 μA/cm^2) , ER 309L filler weld (0.771 μA/cm^2) and without filler (autogenous) weld (3.566 μA/cm^2).The corrosion current density was highest for autogenous weld and lowest for ER 309l filler weld. The pitting potential (Epit) for BM 316L ASS (-0.086510 mV), BM 430 FSS (-0.3925 mV), ER 316L filler weld (0.021578 mV), ER 309L filler weld (0.086077 mV) and without filler (autogenous) weld (-0.018582 mV). The highest pitting potential was measured with ER309L filler weld followed by ER316L filler weld and lowest pitting potential with autogenous weld. It has been shown by autogenous weld that the presence of martensitic phases (low in Cr and Mo content) and chromium carbide causes stronger pitting formation resulted in more pits. Due to the higher Cr_{eq} / Ni_{eq} ratio, the pitting potential measured by the ER309L filler weld is higher than that of ER316L filler weld. It is reported that the pit nucleated when discontinuity forms in the passive film [141,142] due to lower Cr content. When the sample is exposed to chloride, the cathode surface layer of Cl$^-$ is stabilized and pitting are formed [2]. The higher Cr content, better the pitting [141] 316L BM exhibited better pitting potential than 430 FSS BM due to the variation in composition. Autogenous weld and 430 FSS BM observed heavy pits.

Table 4.2: Pitting Corrosion of ER316L, ER309L and without filler weld

Sample	Ecorr (mV)	Icorr (μA)	Epit (mV)
ER316L Filler Weld	-271	1.22	0.0216
ER309L Filler Weld	-248	0.77	0.0861
Autogenous Weld	-357	3.56	-0.0186
316L ASS BM	-235	0.11	-0.0865
430 FSS BM	-305	0.34	-0.3925
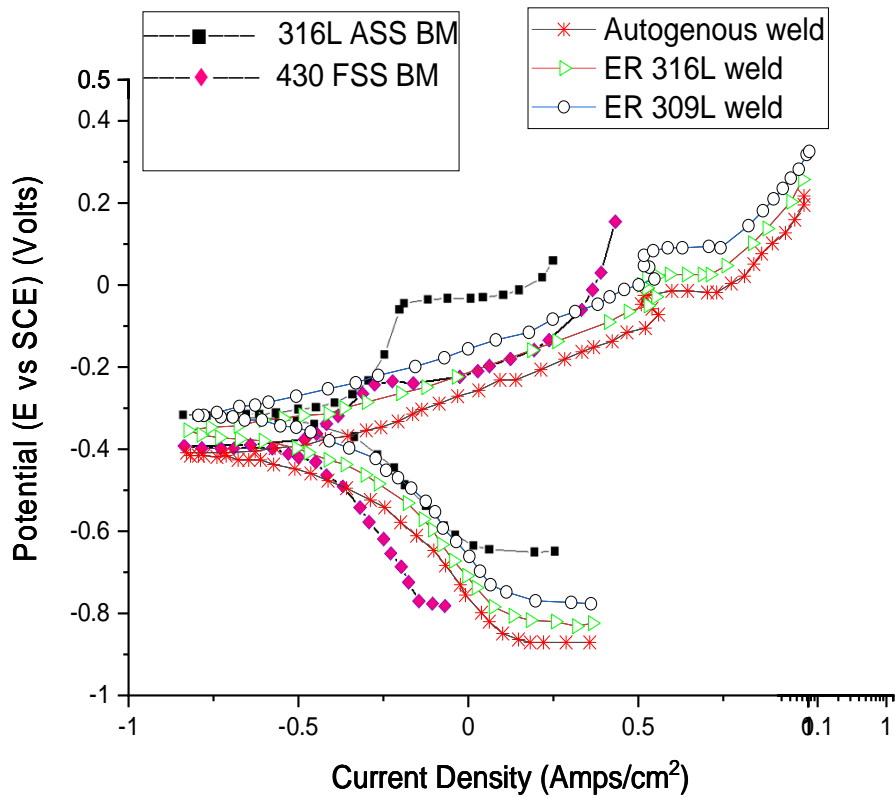
Figure 4.9: Potentiodynamic polarization plots of 316L ASS BM, 430 FSS BM, ER316L, ER309L filler and without filler weld

4.3 Dissimilar welding of 316L ASS and 430 FSS by Cold Metal Transfer (CMT) Welding with GTAW mode

4.3.1 Microstructural Examination for CMT welding

The microstructure of weldments of Base Metals (BM), Unmixed Zone (UMZ), Weld Metal (WM) and Heat Affected Zone (HAZ) is shown in fig 4.10. From the microstructure, it was observed that the 316L ASS BM represents an austenitic phase matrix mainly containing intergranular ferrite, whereas, 430 FSS BM represents a ferrite matrix containing intergranular martensite. Composition of fillers has a significant influence in the development of the WM microstructure. ER316L WM has a microstructure composed of a martensite phase (white) (Fig.4.10 (a)). After solidification, ferrite separates from the austenite particles mainly due to their chemical composition and the cooling rate of 316L ASS [3]. UMZ is observed on the interface around 316L ASS BM. All welds in different phase formations behave strangely. The ER309L weld (Fig.4.10 b) also solidifies in the Ferrite-austenite (FA) mode and exhibits a slightly higher Creq/Nieq ratio (~ 1.66) than ER316L weld Creq/Nieq ratio (~1.61) [139].

The formation of chromium (Cr) enriched and nickel (Ni) depleted regions at the centers of the cellular dendritic sub grain in ER 309L weld virtually continuous networks of vermicular ferrite [57]. No other precipitates were observed in ER316L and ER309L welds. In autogenous weld (without filler), since no filler was used, lathy ferrite was observed with a martensite phase, rich in Chromium (Cr) and carbon (C), and only compositions 430 FSS and 316L ASS were mixed and solidify into lathy ferrite and martensite morphology (Fig. 4.10 c).
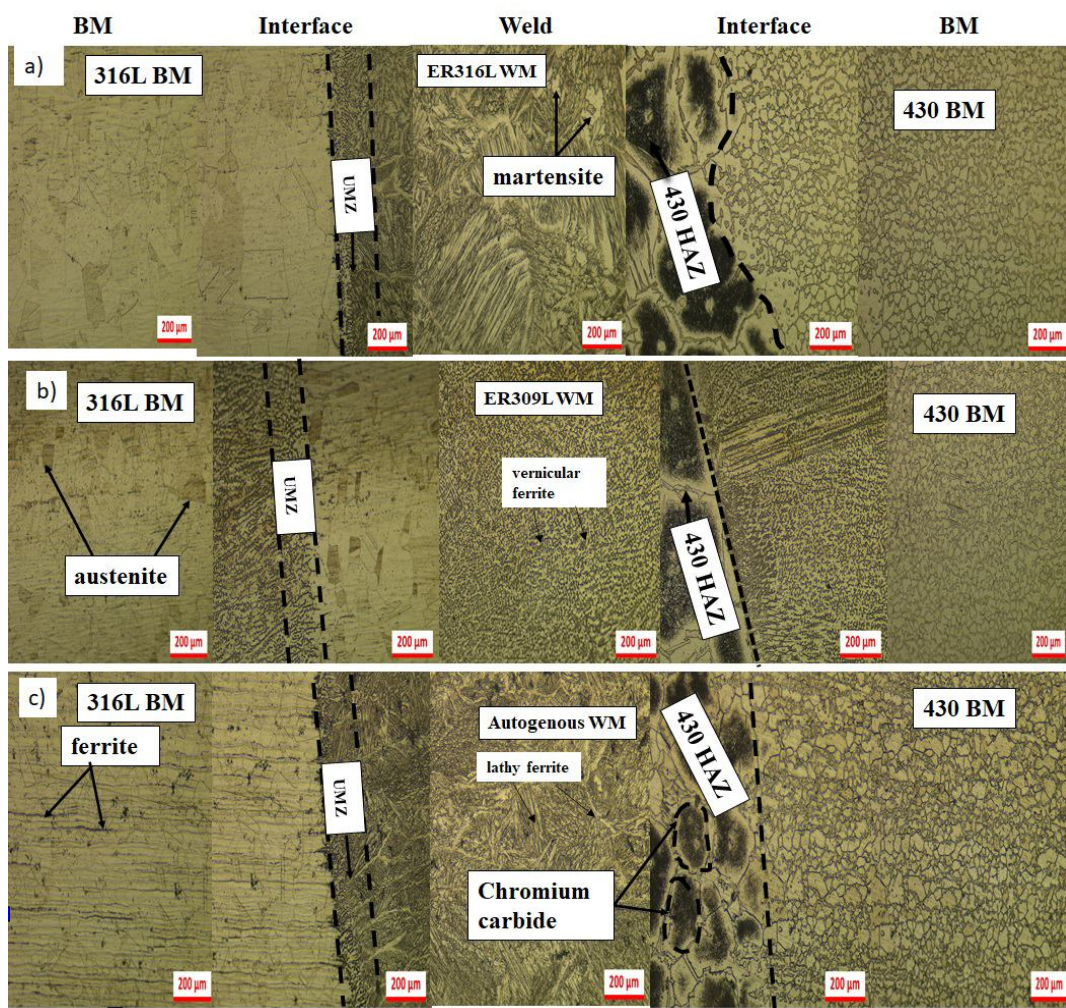
Figure 4.10: Optical Micrograph of weldments a) ER 316L filler weld, b) ER 309L filler weld, c) without filler (autogenous weld) for CMT Welding

Increase in carbon and chromium wt (%) was observed in the SEM/EDS analysis (Fig 4.11) which shows the presence of chromium carbide during autogenous welding. EDS analysis showed that the chromium (Cr) content in the chromium carbide ($Cr_{23}C_6$) range is higher than that of the ferrite phase, indicating the presence of carbides.

This type of precipitate is formed when carbon is saturated with a ferrite phase at high temperatures. 430 FSS is enriched with Cr and C which is ferrite-forming elements, however 316L ASS is enriched with Ni (austenite former) and Cr (ferrite former) accelerates carbide precipitates, but amount of heat input maximizes carbon dissolution,

and in the ferrite-matrix corresponding to the more supersaturation sites and subsequently much more chromium carbide precipitates [57,139].

Element	wt (%)
C	28.56
Cr	7.39
Fe	19.77
Ni	42.03
Mo	2.26

Element	wt(%)
C	39.87
Cr	15.18
Fe	22.78
Ni	19.16
Mo	3

Figure 4.11: SEM/EDS analysis of CMT autogenous weld

4.3.2 Micro-hardness Test for CMT welding

As shown in Fig 4.12, weld cross-section hardness test was performed on BM 316L ASS, 316L UMZ, WM, 430 HAZ and BM 430 FSS. The three readings are taken and average of three values are indicated in different regions of the specimen. The values are indicated in the sequence BM 316L ASS, 316L UMZ, Weld Zone, 430 HAZ and BM 430 FSS. The average hardness at BM 316L ASS is (avg.178.75 HV). The hardness increases from 316L UMZ and it is highest at the weld zone than it decreases from weld zone to 430 HAZ. Microhardness measurement results were measured and found that the highest hardness for 316L filer weld (avg.208.67 HV) as related to ER 309L weld (avg.203.00 HV) and without filler weld (avg.201.00 HV). The average hardness at BM 430 FSS is (avg. 146.66 HV).ER 316L filler weld has a higher hardness than ER 309L filler weld due to the higher percentage of molybdenum (Mo) content than ER 316L, the higher the ferrite phase, but the Cr_{eq} / Ni_{eq} ratio is small [57]. However, in BM 430FSS side, the lowest value was obtained in without filler weld (avg. 141.33 HV); the absence of filler may cause the lowest value in autogenous weld. Because the heat-affected zone is heated and cooled across a wide temperature range, an increase in hardness is caused by the development of martensite in this area. On the other hand, among all the three samples, the 316L HAZ side (316L filler weld sample) highest hardness (avg.204.67 HV) was measured as shown in Fig 4.12. Higher value of hardness was found in ER 316L filler weld this may be due to the larger grains formation which leads to formation of martensite as compared to 309L filler and without filler weld.
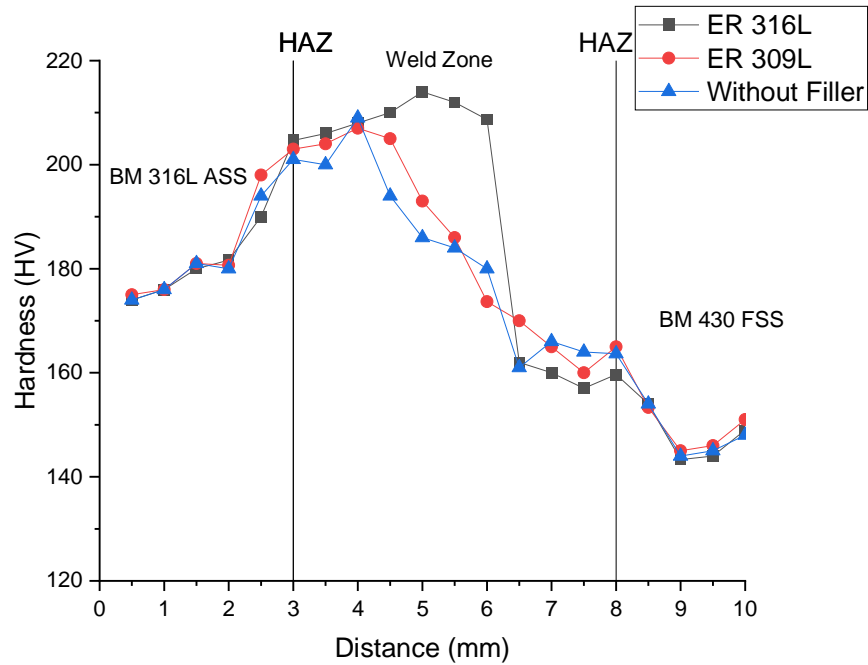
Figure 4.12: Microhardness results across various zones for CMT welding

4.3.3 Tensile Test for CMT welding

Tensile tests were performed to join dissimilar welds as shown in Fig 4.14a and samples were prepared according to ASTM E8. Strain rate taken as 20 mm/min or 3.3 x 10^{-2} mm/s (cross head speed). Stress-strain curves for all samples are shown in Fig 4.14 b. Fracture samples of ER316L, ER309L and Without Filler (Autogenous) weld is shown in Fig 4.14 c. For each specimen, the average values of three samples are taken. All tensile test pieces failed on the 430 FSS BM side of the weld, indicating that the dissimilar welds were strong enough. The discussion on the weld strength is inconclusive because the failure occurred with the 430 FSS BM. However, weld strength variations can be associated with solid solution hardening of different filler compositions [113,141]. In order to diversify the strength, the filler and BM compositions are critical. The yield strength of BM 316L ASS (~ 361 MPa), BM 430 FSS (~ 319 MPa), ER 316L filler weld (~ 377 MPa), ER 309L filler weld (~ 375 MPa) and without filler weld (~ 398 MPa). The tensile strength of BM 316L ASS (~ 570 MPa), BM 430 FSS (~ 438 MPa), ER 316L filler, ER 309L filler and

autogenous weld shows ~ 573 MPa, ~ 568 MPa and ~ 542 MPa, respectively. It indicates that the ER 316L filler weld has a higher tensile strength than the weaker base metal 430 FSS. This indicates that the weld strength of ER 316L filler weld is higher than ER 309L filler and autogenous weld. The weld strength by CMT welding (~ 573 MPa) with ER 316L filler weld is higher than conventional GTAW (~ 452 MPa). The percentage elongation of BM 316L ASS (54 %), BM 430 FSS (27 %), ER 316L Filler weld (21%), ER 309L filler weld (20 %) and without filler (autogenous) weld (20 %). Fig 4.13 shows the changes obtained by comparing the yield strength, tensile strength and percentage of elongation, as a result of solid solution strengthening of welds.

The fractography of the weld specimen was analyzed using SEM (fractography were shown in Fig 4.14 (c). From fractography results, it was found that the fracture types were mostly dimple which indicates that the fracture is ductile in nature.
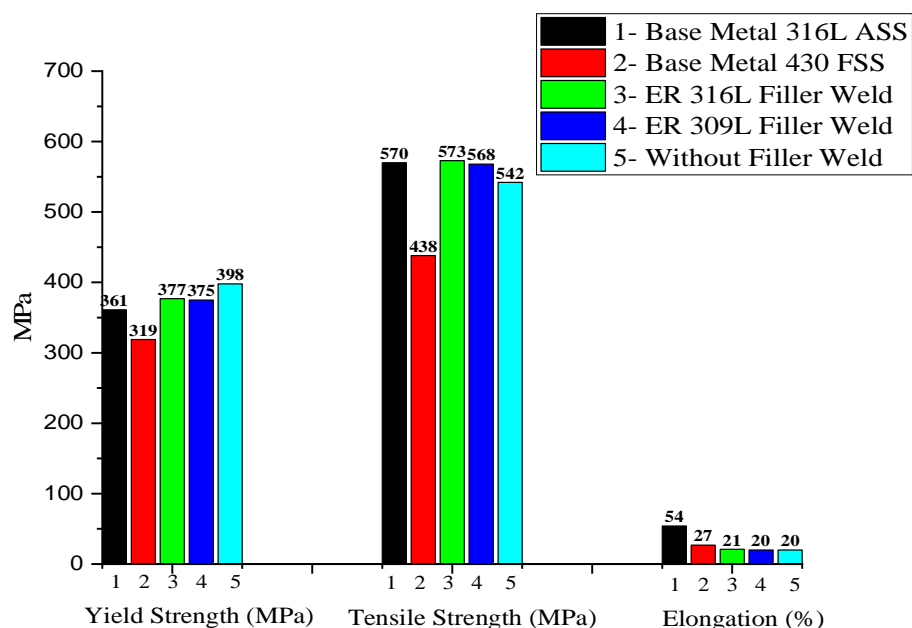
Figure 4.13: Comparison of Yield Strength, Tensile Strength and Percentage Elongation
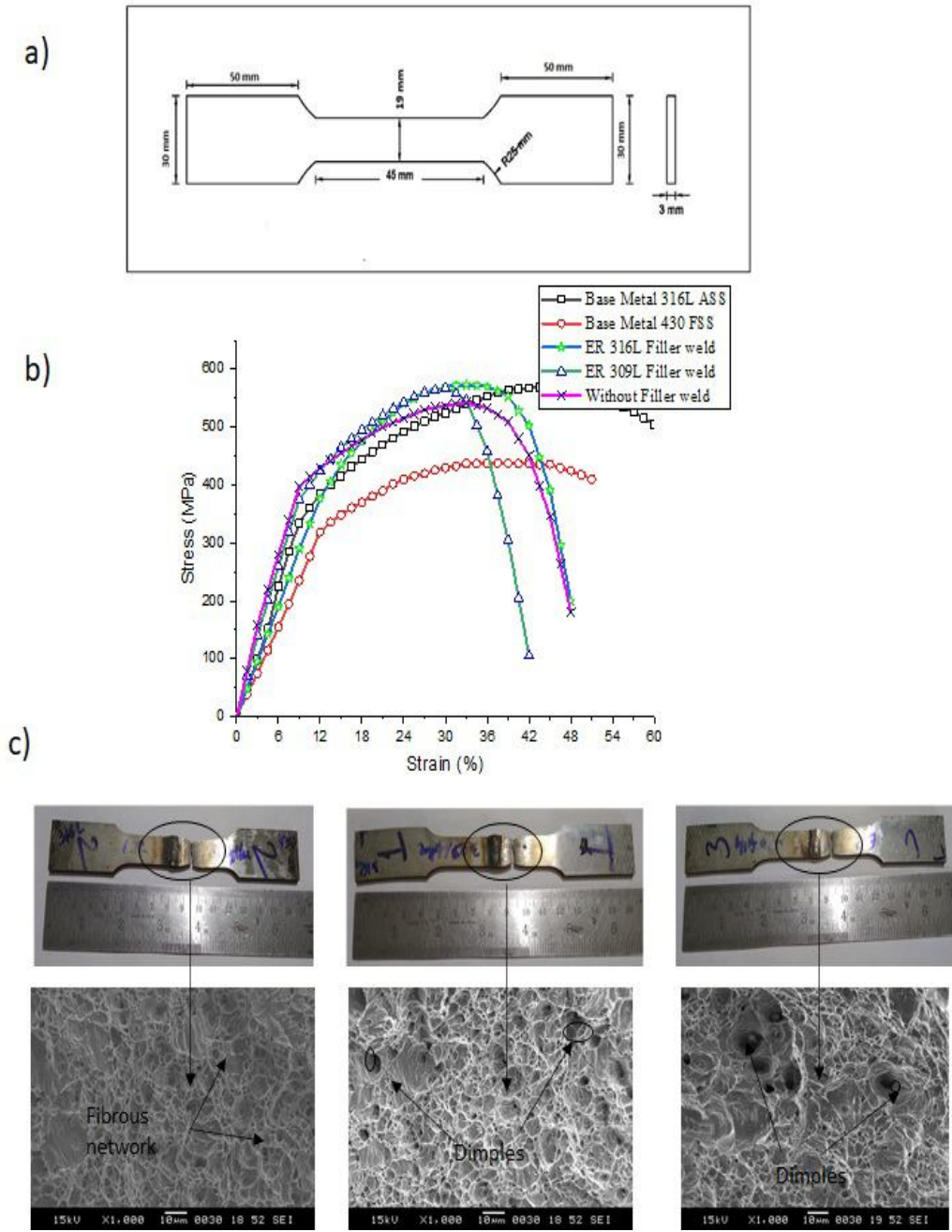
Figure 4.14: Tensile test (a) schematic illustration of specimen, (b) stress strain curve, c) fractured specimen of all weldments.

4.3.4 Impact Test for CMT welding

The Charpy V notch impact test was performed at room temperature with a sample size of 55 mm x 10 mm x 3 mm, a notch angle of 45^0 and a depth of 2 mm. The fractured specimen is shown in Fig 4.15. BM 316L ASS and BM 430 FSS showed impact toughness values of ~ 55 and ~ 29 J. In contrast to ER 316L filler weld, the obtained impact strength values were ~ 47 J. ER 309L weld, on the other hand exhibits an impact energy of ~ 27 J, but the autogenous weld impact toughness is ~ 20 J as shown in Fig.4.16. It was due to the low ferrite content, high Ni content in ER 316L filler weld increases toughness [8,9] and lowers ER 309L filler impact energy due to the high ferrite content as compared to autogenous weld where there is formation of chromium carbide. The values for toughness in CMT welding is greater than ER 316L filler weld (~ 44 J), ER 309L filler weld (~ 22 J) and autogenous weld (~15 J) of GTAW. The fractured surface of the impact sample was analysed using SEM. The fractography of three samples are shown in Fig.4.15 a-c, which shows mostly cleavage / flat facet.
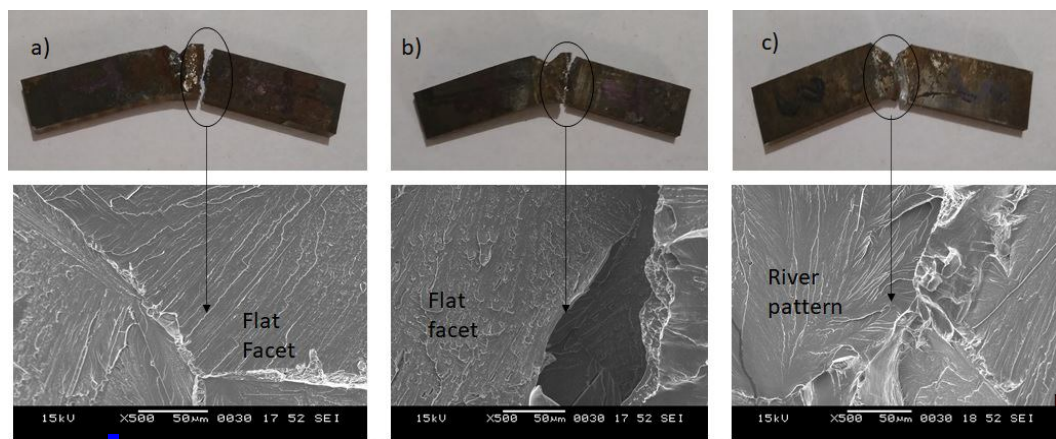
Figure 4.15: Fractography of impact specimen of a) ER 316L, b) ER 309L and c) Without Filler (Autogenous) weld
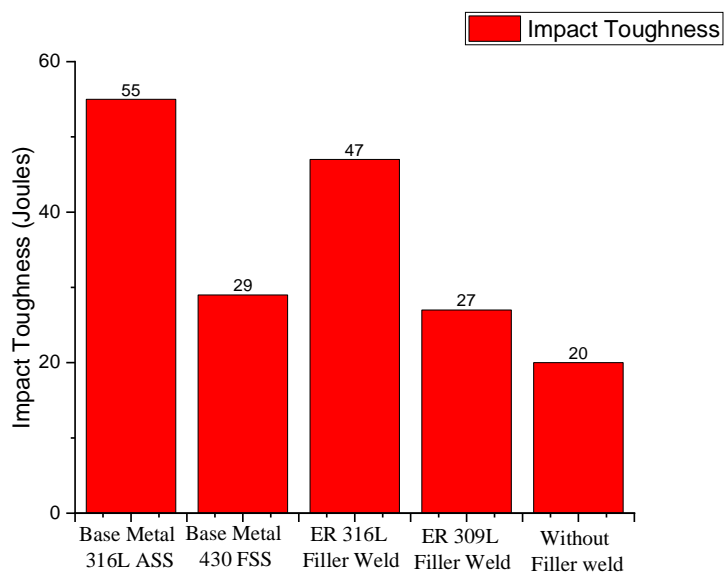
Figure 4.16: Comparison of Impact toughness of weldments

4.3.5 Double Loop Electrochemical Potentiokinetic Reactivation (DLEPR) Test for CMT welding process

Due to metallurgical changes, welded joints are prone to corrosion, and the potential differences between grain and grain boundaries are significant. The development of a Cr-depleted zone has been shown to accelerate corrosion [2]. The strength of a weld will deteriorate more quickly when exposed to extreme conditions, thus assessing the weld's corrosion resistance is important for estimating the life of the weld process. The DLEPR test was carried out in potentiostat (Solartron-1285) using a solution of 0.5M H_2SO_4 + 0.01M NH_4SCN solution. The adopted surface area was 0.45 cm^2 (weld area) for the test performed at room temperature. First, the oxide layer was removed from the working electrode at -0.5V for 120 sec in the same solution. The surface of the working electrode sample was stabilized by the open circuit potential (OCP) for 30 min. Finally, forward and backward scans are implemented with a constant scan rate of 1.667 mV/s. For a forward scan, apply a potential range of -0.5 V (SCE) to +0.5 V (SCE) and apply a reverse scan to bring the potential back to -0.5 V. Fig. 4.17 (a-e) showed DLEPR curves BMs (316L ASS

and 430 FSS) and WMs (ER316L, ER309L and autogenous weld). Among the welds, autogenous weld was the most sensitive and shows highest degree of sensitization, followed by ER309L weld and the least sensitive was ER316L weld. The presence of chromium carbide precipitate increases the sensitivity of autogenous weld. Due to variations in the activation energies of ferrite, martensite, and austenite, the austenite phase is less sensitive, while the ferrite and martensite phases are more sensitive, according to the literature [2,143]. The presence of carbide deposits accelerates the degree of sensitization [2,142]. On the other hand, the BM 430 FSS showed higher sensitivity than the BM 316L ASS. The high sensitivity of 430 FSS BM may be due to the presence of martensite and lower proportion of alloying elements, but the sensitivity of 316L ASS BM is lower than that of 430 FSS BM due to the higher Cr content [2,57,142]. Table 4.3 shows the percentage degree of sensitization (DOS) of weldments by CMT welding. Fig 4.17 (a-b) shows the DLEPR curves of BM 316L ASS and 430 FSS and Fig 4.17 (c-e) shows DLEPR curves for fillers ER 316L, ER 309L and without filler (autogenous) weld. It was observed that the DOS obtained with CMT welding is less than GTAW.

Table 4.3 Percentage degree of sensitization of weldments by CMT welding

Sample	Ia (A/cm^2)	Ir (A/cm^2)	Ir/Ia (% DOS)
ER316L Filler Weld	0.0584	0.00205	3.51
ER309L Filler Weld	0.0783	0.00387	4.95
Autogenous Weld	0.0551	0.02516	45.62
316L ASS BM	0.0021	0.00006	2.66
430 FSS BM	0.1700	0.09000	52.00
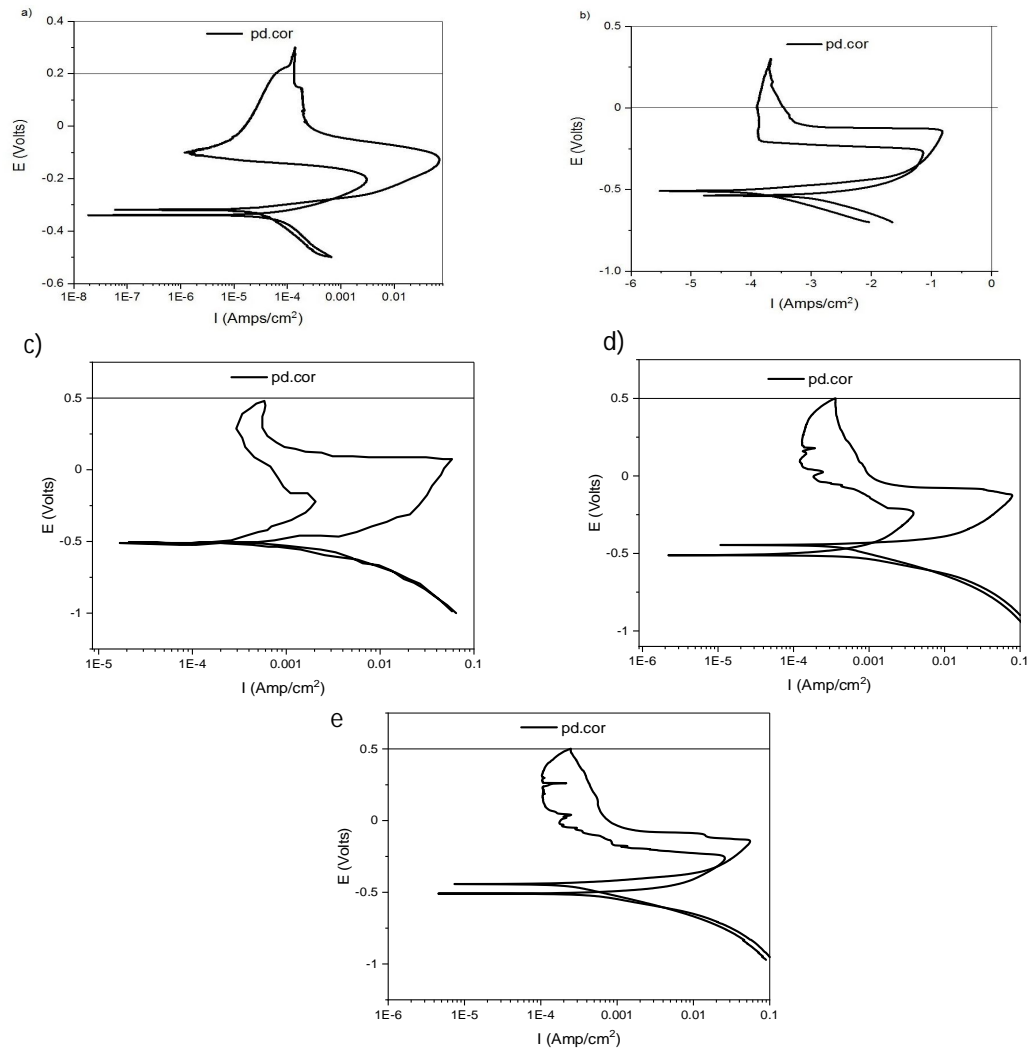
Figure 4.17: DLEPR curves of a) 316L ASS BM, b) 430 FSS BM, c) ER316L weld, d) ER309L weld and e) Autogenous weld

4.3.6 Potentiodynamic Polarization (PDP) Test

Potentiodynamic polarization (PDP) tests were performed at a potential of -0.7 V (vs SCE) to 1.0 V (vs SCE) at a sampling rate of 0.5 mV/sec. The approximate test area is 1.0 cm^2 (weld area only) and is carried out at room temperature. The data obtained was analyzed using EC-lab software. Corrosion potential (E_{corr}), corrosion current density (I_{corr}) and pitting potential (E_{pit}) were represented in Table 4.4. The polarization curves of dissimilar weld of 316L ASS and 430 FSS produced by two different fillers ER316L, ER309L and without filler in 3.5 % NaCl solution as shown in Fig 4.18. The corrosion potential (E_{corr}) values of BM 316L ASS is (-235.2 mV), BM 430 FSS is (-304.8 mV), ER 316L filler weld (- 456.78 mV), ER 309L filler weld (-402.008 mV) and without filler (autogenous) weld (- 531.279 mV). The corrosion potential value was found to be highest for autogenous weld and lowest for ER 309L filler weld. The corrosion current density (I_{corr}) for BM 316L ASS (0.110 µA/cm^2), BM 430 FSS (0.34 µA/cm^2), ER 316L filler weld (0.000016 µA/cm^2), ER 309L filler weld (0.000009 µA/cm^2) and autogenous weld (0.001 µA/cm^2). The pitting potential (E_{pit}) for BM 316L ASS (-0.086510mV) , BM 430 FSS (-0.3925 mV) , ER 316L Filler weld (-0.355104 mV) , ER 309L filler weld (-0.0731724 mV) and autogenous weld (-0.999182 mV). The Highest pitting potential was measured with ER309L filler weld followed by ER316L filler weld and lowest pitting potential with autogenous weld. It has been shown by autogenous weld that the presence of chromium carbide causes stronger pitting formation. Due to the higher Cr_{eq} / Ni_{eq} ratio, the pitting potential measured by the ER309L filler weld is higher than that of ER316L filler weld. It is reported that the pit nucleated when discontinuity forms in the passive film [141,142] due to lower Cr content. When the sample is exposed to chloride, the cathode surface layer of Cl$^-$ is stabilized and pitting are formed [143]. The higher the Cr content, better the pitting [141] 316L BM exhibited better pitting potential than 430 FSS BM due to the variation in composition. Autogenous weld and 430 FSS BM observed lower pitting potential.

Table 4.4: Pitting Corrosion of ER316L, ER309L and without filler weld by CMT welding

Sample	Ecorr (mV)	Icorr (µA)	Epit (mV)
ER316L Filler Weld	-457	0.000016	-0.3551
ER309L Filler Weld	-402	0.000009	-0.0731
Autogenous Weld	-531	0.001	-0.9992
316L ASS BM	-235	0.110	-0.0865
430 FSS BM	-305	0.34	-0.3925
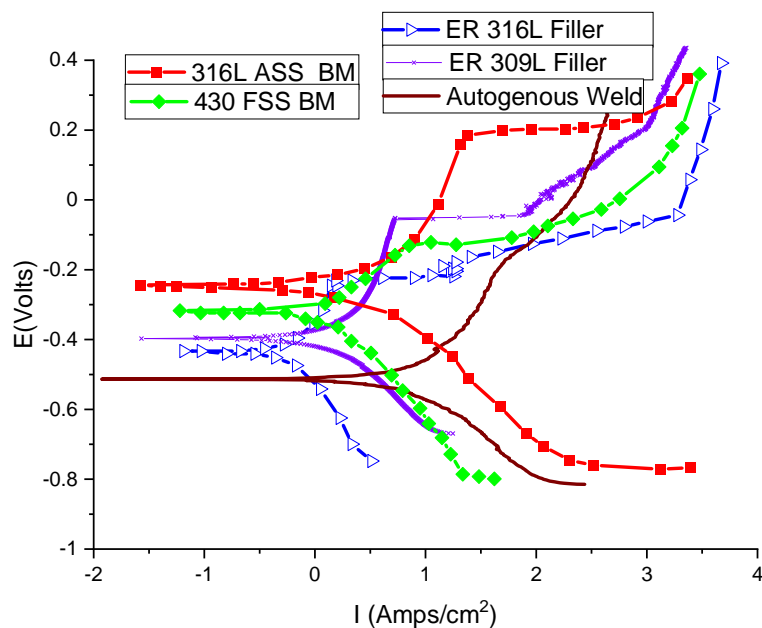
Figure 4.18: Potentiodynamic polarization plots of CMT welding 316L ASS BM, 430 FSS BM, ER316L, ER309L filler and without filler weld

85

CHAPTER 5: CONCLUSIONS

The 316L ASS and 430 FSS welded by conventional GTAW and Cold Metal Transfer welding with GTAW mode with ER 316L, ER 309L and without filler, following important conclusions are drawn from these two welding processes:

1. The 316L ASS BM shows an austenitic phase matrix that contains intergranular ferrite and 430 FSS BM shows ferrite matrix that contains intergranular martensite. ER 316L WM composed of a matrix of austenite (white) and skeletal ferrite phase (dark etched phase) intermediate cooling rate and Cr_{eq}/Ni_{eq} ratio under the ferrite-austenite (FA) series to support the skeletal phase.

2. In ER309L WM, continuous vermicular ferrite networks are the result of deposition in the cells of cellular dendritic subgrains of enriched chromium (Cr) and of depleted regions of nickel (Ni).

3. In autogenous weld (without filler), since no filler is used, lathy ferrite was observed with a martensite phase, rich in Chromium (Cr) and carbon (C), and only compositions 430 FSS and 316L ASS were mixed and solidify into lathy ferrite and martensite morphology.

4. ER 316L weld by CMT welding shows highest tensile strength (~ 573 MPa) which is higher than GTAW (~ 452 MPa) due to the low ferrite and high Ni content as compared to ER 309L weld by CMT welding (~ 568 MPa) which is higher than GTAW (~ 435 MPa), which contains high ferrite as autogenous weld by CMT welding (~ 542 MPa) as compared to (~ 438 MPa) by GTAW which shows lower tensile strength due to the formation of martensite and chromium carbide and due to the solid solution hardening of different filler compositions.

5. The fractography results shows mostly cleavage and flat facet in GTAW which indicates that the fracture is brittle in nature whereas in CMT welding it shows mostly dimple structures.

6. ER 316L filler weld has higher toughness (~ 47 J) by CMT welding as compared to (~ 44 J) by GTAW due to the low ferrite and high nickel content in ER 316L filler material whereas, ER 309L filler by CMT welding shows (~ 27 J) as compared to

(~ 22 J) by GTAW process due to the high ferrite content as compared to autogenous weld where the toughness (~20 J) by CMT welding is higher than (~15 J) by GTAW process due to the formation of chromium carbide.

7. The fractography results of toughness shows ductile and semi- cleavage mode in GTAW whereas in CMT welding shows flat facet.

8. In GTAW, autogenous weld shows higher hardness (avg.317.0 HV) as compared to ER 316L weld (avg.263.6 HV) and ER 309L weld (avg.242.6 HV) due to the formation of martensite and chromium carbide formation in autogenous weld whereas in CMT welding, ER 316L weld (avg.208.67 HV) shows higher hardness due to the larger grains formation which leads to the formation of martensite as compared to ER 309L (avg.203.00 HV) and autogenous weld (avg.201.00 HV).

9. In DLEPR test, the degree of sensitisation (DOS) of dissimilar weld with autogenous weld shows highest sensitisation (45.6223 %) as compared to ER 309L filler weld (4.9504 %) and ER 316L filler weld (3.5073 %) which is least sensitive due to the presence of martensite and chromium carbide precipitate in autogenous weld as compared to GTAW process where autogenous weld shows higher sensitisation (66.2435 %) than ER 309L filler weld (5.8073 %) and ER 316L filler weld (4.3441 %). The 430 FSS (52 %) is more sensitive than BM 316L ASS (2.66 %) due to the presence of martensite and presence of lower alloying elements.

10. In PDP test, the highest pitting potential was observed in GTAW process with ER 309L filler weld (0.086077 mV) as compared to ER 316L (0.021578 mV) and autogenous weld (-0.018582 mV) whereas in CMT welding ER 309 filler weld (-0.0731724 mV) as compared to ER 316L filler weld (-0.355104 mV) and autogenous weld (-0.999182 mV). The ER 309L filler weld shows higher Cr_{eq} / Ni_{eq} ratio which is higher than ER 316L filler weld. When the sample is exposed to chloride, the cathode surface layer of Cl^- is stabilized and pitting is formed. The 316L ASS BM shows better pitting potential than 430 FSS BM due to the high Cr content.

11. The tensile strength of ER 316L filler, ER 309L filler and autogenous weld with CMT welding is higher than tensile strength welded with GTAW. Therefore, it was

concluded that the weld strength obtained with CMT welding is highest than GTAW.

12. The toughness values of ER 316L filler, ER 309L filler and autogenous weld with CMT welding shows higher toughness than GTAW.

13. The hardness values of ER 316L filler, ER 309L filler and autogenous weld shows lower hardness than CMT welding.

14. The degree of sensitisation of ER 316L filler, ER 309L filler and autogenous weld with CMT welding is less as compared to GTAW due to less formation of chromium carbide precipitate in CMT welding.

15. The pitting potential of ER 309L filler weld found highest in both CMT and GTAW as compared to ER 316L filler and autogenous weld.

16. Therefore, it was concluded that welding with CMT shows better microstructural, mechanical and corrosion properties as compared to GTAW as weld defect such as spattering is less in CMT welding.

CHAPTER 6: SCOPE FOR FUTURE RESEARCH

The thesis contains some basic questions about real world interests. It also creates additional tools and space for future / future research. Here are some generous suggestions:

1) There is a scope of welding dissimilar joint by different advanced welding process such as laser beam welding, ultrasonic welding, friction stir welding, etc.

2) Welding effect with various types of fillers, which are used in industrial applications to build boilers, valves, oil pipelines, etc.

3) Corrosion resistance of dissimilar weld metals can be evaluated with other organic environments.

4) The dissimilar joint can be immersed in different organic acids with different immersion times to see the effect of the joint.

5) Passivation film formation studies can be evaluated under various conditions by welding with advanced welding techniques.

6) The dissimilar solid rods of 316L ASS and 430 FSS can be welded by means of friction welding for applications in power and process industries.

7) The hybrid welding process can be used to examine the dissimilar weld of 316L ASS and 430 FSS.

8) The thermal profile of the welded joint can be analysed by various advanced software's such as MATLAB which can be used to optimize the various welding parameters.

Bibliography

1. G.M. Reddy, T. Mohandas, A.S. Rao, and Y. V. Satyanarayana, "Influence of Welding Processes on Microstructure and Mechanical Properties of Dissimilar Austenitic-Ferritic Stainless-Steel Welds", Mater. Manuf. Process., 2005, 20(2), 147–173.

2. J. Verma, R. V Taiwade, R. Kataria, and A. Kumar, "Welding and Electrochemical Behavior of Ferritic AISI 430 and Austeno- Ferritic UNS 32205 Dissimilar Welds", J. Manuf. Process., Elsevier, 2018, 34, 292–302.

3. M. Dadfar, M.H. Fathi, F. Karimzadeh, M.R. Dadfar, and A. Saatchi, "Effect of TIG Welding on Corrosion Behavior of 316L Stainless Steel", 2007, 61, 2343–2346.

4. C.N. Gonçalves, G.M. de A. Carvalho, J.S. Siqueira, and R.Â. Renzetti, "Influence of Nb Content on Sensitization and Pitting Corrosion of Welded AISI 430 Ferritic Stainless Steel", Soldagem & Inspecao,2019, 24.

5. G. Mallaiah, A. Kumar, P. Ravinder Reddy, and G. Madhusudhan Reddy, "Influence of Grain Refining Elements on Mechanical Properties of AISI 430 Ferritic Stainless Steel Weldments - Taguchi Approach", Mater. Des., Elsevier Ltd, 2012, 36, 443–450.

6. R. Ghasemi, B. Beidokhti, and M. Fazel-Najafabadi, "Effect of Delta Ferrite on the Mechanical Properties of Dissimilar Ferritic-Austenitic Stainless-Steel Welds", Arch. Metall. Mater., 2018, 63(1), 437–443.

7. Md Razaullah Khan, A. K. Pathak, Umasankar Das, and Dhirendra Tiwari, "Study of Microstructure and Mechanical Properties of Feritic Stainless Steel (AISI 430) Weldment Using ER309L and ER430 Electrodes by MIG Welding Process", Int. J. Eng. Res., 2016, 5(01), 312–318.

8. H.T. Serndag and Guam, "Microstructure and Mechanical Properties of Gas Metal Arc Welded AISI 430/AISI 304 Dissimilar Stainless Steels Butt Joints, J. Phys. Conf. Ser., 2021, 1777(1).

9. Sindo Kou, "Welding Metallurgy," Second, John Wiley & Sons, Inc, 2003.

10. S.K. Bhambri, "Intergranular Fracture in 13 Wt% Chromium Martensitic Stainless Steel", J. Mater. Sci., 1986, 21(5), 1741–1746

11. D. Jeraldnavinsavio, A.M. Farid, E.V. V Ramanamurthy, S. Porchilamban, and S. Ravikumar, "Evaluation of Mechanical Properties and Micro Structural Charecterization of Dissimilar TIG Welded AISI 316L and AISI 430 Plates Using ER310 and ER2594 Filler", Mater. Today, Proc., Elsevier Ltd., 2019, 16, 1212–1218.

12. A. Hdhibi," Effect of Single Oxide Fluxes on Morphology and Mechanical Properties of ATIG on 316 L Austenitic Stainless-Steel Welds", 2018, 8(3), 3064–3072.

13. A.S. Azar, "A Heat Source Model for Cold Metal Transfer (CMT) Welding, J. Therm. Anal. Calorim., Springer Netherlands, 2015, 122(2), 741–746.

14. D.C. Oliver and M. Sephton, "External Corrosion Resistance of Steel and Ferritic Stainless Steel Exhaust Systems", J. South African Inst. Min. Metall., 2003, 103(2), 93–100.

15. A.K. Lakshminarayanan and V. Balasubramanian, "An Assessment of Microstructure, Hardness, Tensile and Impact Strength of Friction Stir Welded Ferritic Stainless-Steel Joints", Mater. Des., Elsevier Ltd, 2010, 31(10), 4592–4600.

16. A.K. Lakshminarayanan and V. Balasubramanian, "Evaluation of Microstructure and Mechanical Properties of Laser Beam Welded AISI 409M Grade Ferritic Stainless Steel", J. Iron Steel Res. Int., Central Iron and Steel Research Institute, 2012, 19(1), 72–78.

17. A.K. Lakshminarayanan, V. Balasubramanian, and G. Madhusudhan Reddy, "Microstructure and Mechanical Properties of Electron Beam-Welded AISI 409M-Grade Ferritic Stainless Steel", Int. J. Adv. Manuf. Technol., 2011, 55(1–4), 153–162.

18. A.K. Lakshminarayanan, K. Shanmugam, and V. Balasubramanian, "Effect of Welding Processes on Tensile and Impact Properties, Hardness and Microstructure of AISI 409M Ferritic Stainless Joints Fabricated by Duplex Stainless Steel Filler Metal", J. Iron Steel Res. Int., Central Iron and Steel Research Institute, 2009, 16(5), 66–72.

19. R.S. Parmar, "Welding Engineering and Technology," Second, Khanna Publication, New Delhi, India, 2010.

20. Lochhead, J. C., and Rodgers, K. J., Weld. J., 78: 49, 1999.

21. M.G Fontana, Corrosion Engineering, Corrosion Engineering Science and Technology, McGraw Hill, New York, 1986, 445–502.

22. J.C.Scully, "The Fundamentals of Corrosion, The Fundamentals of Corrosion, Pergamon Press, England", 1990, 165–176.

23. M.O.H. Amuda and S. Mridha, "Analysis of Sensitization Profile in Medium Chromium Ferritic Stainless Steel (FSS) Welds", 2011, 3(1), 17–22.

24. T. Murakami, K. Nakata, H. Tong, and M. Ushio, "Dissimilar Metal Joining of Aluminum to Steel by MIG Arc Brazing Using Flux Cored Wire, ISIJ Int., 2003, 43(10), 1596–1602.

25. M.L. Zhu and F.Z. Xuan, "Correlation between Microstructure, Hardness and Strength in HAZ of Dissimilar Welds of Rotor Steels", Mater. Sci. Eng. A, 2010, 527(16–17), 4035–4042.

26. M.L. Zhu and F.Z. Xuan, "Effects of Temperature on Tensile and Impact Behavior of Dissimilar Welds of Rotor Steels", Mater. Des., 2010, 31(7), 3346–3352.

27. C.R. Das, A.K. Bhaduri, G. Srinivasan, V. Shankar, and S. Mathew, "Selection of Filler Wire for and Effect of Auto Tempering on the Mechanical Properties of Dissimilar Metal Joint between 403 and 304L(N) Stainless Steels", J. Mater. Process. Technol., 2009, 209(3), 1428–1435.

28. V. V. Satyanarayana, G.M. Reddy, and T. Mohandas, "Dissimilar Metal Friction Welding of Austenitic-Ferritic Stainless Steels", J. Mater. Process. Technol., 2005, 160(2), 128–137.

29. E.J. Barnhouse and J.C. Lippold, "Microstructure/Property Relationships in Dissimilar Welds between Duplex Stainless Steels and Carbon Steels", Weld. J. (Miami, Fla), 1998, 77(12), 477–489.

30. C. Tembhurkar, R. Kataria, S. Ambade, J. Verma, A. Sharma, and S. Sarkar, "Effect of Fillers and Autogenous Welding on Dissimilar Welded 316L Austenitic and 430 Ferritic Stainless Steels", J. Mater. Eng. Perform., Springer US, 2021, 30(2), 1444–1453.

31. S. Porchilamban and J.R. Amaladas, "Structural Relationships of Metallurgical and Mechanical Properties Influenced by Ni-Based Fillers on Gas Tungsten Arc Welded Ferritic / Austenitic SS Dissimilar Joints", 2019, 13(1), 1–22.

32. R. Neissi, M. Shamanian, and M. Hajihashemi, "The Effect of Constant and Pulsed Current Gas Tungsten Arc Welding on Joint Properties of 2205 Duplex Stainless Steel to 316L Austenitic Stainless Steel", J. Mater. Eng. Perform., Springer US, 2016, 25(5), 2017–2028.

33. G. Madhusudan Reddy and K. Srinivasa Rao, "Microstructure and Mechanical Properties of Similar and Dissimilar Stainless Steel Electron Beam and Friction Welds", Int. J. Adv.Manuf. Technol., 2009, 45(9–10),875–888.

34. A. J. Sedriks: Corrosion of Stainless Steels, 2nd ed., John Wiley & Sons, New York, 1996.

35. John C. Lippold and Damian J. Kotecki: Welding Metallurgy and Weldability of Stainless Steels, 1st ed., John Willey & Sons, New York, 2005.

36. G. George and H. Shaikh: Corrosion of Austenitic Stainless Steels: Mechanism, Mitigation and Monitoring, ed. by H. S. Khatak and Baldev Raj, Woodhead Publishing House, Cambridge, England. 2002, 1–36.

37. M. G. Fontana, Corrosion Engineering, Eighth. Tata McGraw-Hill Edition 2005, 2009, 282–291.

38. K.V. Kasiviswanathan, N.G.Muralidharan, N. Raghu, R. K. Dayal and Hasan Shaikh: Mechanism, Mitigation and Monitoring. ed. by H. S. Khatak and Baldev Raj, Woodhead Publishing and Alpha Sci. Int. Ltd., Cambridge, England, 2002, 314.

39. B. Ravi Kumar, Sailaja Sharma, Parikshit Munda, R.K. Minz, "Structure and microstructure evolution of a ternary Fe–Cr–Ni alloy akin to super martensitic stainless steel", Materials and Design,2013, 50, 392–398.

40. Ceyhun Kose, Ramazan Kacar, "The effect of preheat & post weld heat treatment on the laser weldability of AISI 420 martensitic stainless steel", Materials and Design, 2014,64, 221–226.

41. Metals Handbook: Corrosion, 9th ed., Gulf Professional Publishing, 13,1987.

42. ASM Metals Handbook: ASM International, Materials Park, OH, 3,1992.

43. ASM Metals Handbook: ASM International, Materials Park, OH, 1,1990.

44. J.D. Tucker, "Assessment of thermal embrittlement in duplex stainless steels 2003 and 2205 for nuclear power applications", Acta Materialia, 2015,87, 15–24.

45. C.H. Sarlak, M. Atapour, M. Esmailzadeh, "Corrosion behavior of friction stir welded lean duplex stainless steel", Materials and Design, 2015, 66, 209–216.

46. T. Tański, Fatigue behaviour of sintered duplex stainless steel, Procedia Engineering 2014, 74, 421 – 428.

47. M. Thomas, R. V. Prakash, S. Ganesh Sundara Raman, M. Vasudevan, High Temperature Fatigue Crack Growth Rate Studies in Stainless Steel 316L(N) Welds Processed by A-TIG and MP-TIG Welding. MATEC Web Conf., 2018,165.

48. Ravindra V. Taiwade, Rohan Shukla, Himanshu Vashishtha, "Effect of Grain Size on Degree of Sensitization of Chrome- Manganese Stainless Steel", ISIJ International, 2013, 53, 2206–2212.

49. R.V.Taiwade, S.J.Patre, A.P.Patil, "Studies on welding and sensitization of chrome-manganese Austenitic stainless steel", TIIM, 2011, 64, 513-518.

50. Ravindra V. Taiwade, Awanikumar P. Patil, Ravindra D. Ghugal, "Effect of Welding Passes on Heat Affected Zone and Tensile Properties of AISI 304 Stainless Steel and Chrome-Manganese Austenitic Stainless Steel", ISIJ International, 2013, 53, 102-109.

51. L. Ceschini and G. Minak, Fatigue Behaviour of Low Temperature Carburised AISI 316L Austenitic Stainless Steel, Surf. Coatings Technol., 2008, 202(9), 1778–1784.

52. A.K Lakshminarayan, K. Shanmugam, V. Balasubramanian," Fatigue crack growth behavior of AISI 409M grades ferritic stainless steel welded joints using Austenite Ferritic and Duplex stainless-steel electrodes"; ISIJ International, 2008,48, 1640-46.

53. A.K. Lakshminarayanan, V. Balasubramanian, G. Madhusudhan Reddy, "On the fatigue behavior of electron beam and gas tungsten arc weldments of 409M grade ferritic stainless steel" Materials and Design, 2012,35, 760-69.

54. A.K. Lakshminarayanan, V.Balasubramanian, "Assessment of sensitization resistance of AISI 409M grade ferritic stainless steel joints using Modified Strauss test", Materials and Design, 2012, 39, 175-185.

55. M. O. H. Amuda and S. Mridha, Research Article, "An Overview of Sensitization, Dynamics in Ferritic Stainless-Steel Welds", Hindawi Publishing Corporation, International Journal of Corrosion, 2011, Article ID 305793, 9.

56. C.A.Loto, R.T.Loto, "Electrochemical corrosion resistance evaluation of ferritic stainless steel", International journal of electrochemical science,2012,7, 11011-11022.

57. Sarkari Khorrami, M. A. Mostafaei, H. Pouraliakbar, and A. H. Kokabi, "Study on microstructure and mechanical characteristics of low-carbon steel and ferritic stainless steel joints," Materials Science and Engineering: A, 2014, 608, 35–45.

58. J. R. Davis: Corrosion of Weldment, ASM International, Materials Park, OH, 2006.

59. New 200-series steels: An Opportunity or A Threat to the Image of Stainless Steel? International Stainless-Steel Forum (ISSF), 2005.

60. Steel Authority of India Limited. 200 and 300-series Technical Data [R]. Salem, 2004.

61. X. Li, Y. Wei, Z. Wei, and J. Zhou, "Effect of Cold Rolling on Microstructure and Mechanical Properties of AISI 304N Stainless Steel," IOP Conference Series: Earth and Environmental Science, 2019,252, 022027.

62. S.Chaudhari: Heat Treatment of Stainless Steels, Practical Heat Treating, 2020, 233–283.

63. E. Kocsisová, M. Tománková, I. Slatkovský, and M. Sahul, "Study of the Sensitization on the Grain Boundary in Austenitic Stainless Steel Aisi 316," Research Papers Faculty of Materials Science and Technology Slovak University of Technology, 2014, 22, 341, 131–136.

64. R. K. Dayal, N. Parvathavarthini and Baldev Raj: International Materials Reviews, 2005, 50, 3, 129.

65. E. C. Bain, R. H. Aborn, J. J. B. Rutherford: Trans. Am. Soc. Steel Treating, 1993, 21(1), 481.

66. C. Stawstrom, M. Hillert: J. Iron Steel Inst, 1969, 207, 77.

67. R. L. Fullman: Acta Metallurgical, 1982, 30 (7), 1407.

68. Ernest L. Hall and Clyde L. Briant: Metallurgical Transactions A, 1984, 15 A, 793.

69. H. Sahlaoui, K. Makhlouf, H. Sidhom, J. Philibert: Material Science and Engineering A, 2004, 372 (1-2), 98.

70. H Sahlaoui, H Sidhom, J Philibert: Acta Materialia, 2002, 50 (6), 1383.

71. C. S. Tedmon Jr., D. A. Vermilyea, and J. H. Rosolowski: J. Electrochemical Soc., 1971, 118, 192.

72. W. O. Binder, C. M. Brown and R. Franks: ASM Trans. Q., 1949, 41, 1301.

73. H. Uno, A. Kimura, and T. Misawa: Corrosion, 1992,48, 467.

74. Y. Watanabe, V. Kain, T. Tonozuka, T. Shoiji, T. Kondo and F. Masuyama: Scripta Mater., 2000,42, 307.

75. U. Kamachi Mudali, R. K. Dayal, J. B. Gnanamoorthy and P. Rodriguez: Metall. Trans. A, 1996,27, 2881.

76. R. S. Dutta, P. K. De and H. S. Gadiyar: Corros. Sci., 1993,34, 51.

77. V. S. Raja and A. Ramkumar: Br. Corros. J., 1996 ,31, 153.

78. N. Parvathavarthini, R. K. Dayal: Journal of Nuclear Materials, 2002,305, 209.

79. E. A. Trillo, R. Beltran, J. G. Maldonado, R. J. Romero, L. E. Murr, W.W. Fisher, A. H. Advani: Materials Characterization, 1995, 35,99.

80. E. A. Trillo, L. E. Murr: Acta Mater. ,1999, 47 (1), 235.

81. F. B. Pickering: The Metallurgical Evolution of Stainless Steels, American Society for Metals, Metals Park, Ohio, England, 1979, 1.

82. 200 Series Stainless Steel CrMn Grades: ASSDA Technical Bulletin,1st ed., Australia, 2006.

83. Austenitic Chromium-Manganese Stainless Steels: A European Approach, 1st ed. Materials and Applications Series, 2012,12, 2.

84. Jacques Charles: The New 200-series, An Alternative answer to Ni. Surcharge? Dream or Nightmare, Stainless steel' 05 Science and Market, Seville, 2005, 19.

85. P. C. Pistorius and M. du Toit: Low Nickel Austenitic Stainless Steels, Metallurgical Constraints, the 12th Ferroalloy Congress Sustainable Future, Finland, 2012.

86. C. P. Cutler, G. E. Coates, D. C. Jenkinson: Nickel in Stainless Steels, 6th European Stainless Steel Conference, Science and Market, Helsinki, Finland, 2008.

87. Jacques Charles, J. D. Mithieux, J. Krautschick, N. Suutala, J. Antonio Simon, B. Van Hecke and T. Pauly: A New European 200 Series Standard to Substitute 304 Austenitics, 6th European Stainless-Steel Conference, Science and Market, Helsinki, Finland, 2008.

88. G. E. C. Bell, P. F. Tortorelli, E. A. Kenik, R. L. Klueh: Journal of Nuclear Materials, 1991,615,179-181.

89. R. Beneke and R. F. Sander Berg: Corros. Sci.,1989, 29, 543.

90. N. Parvathavarthini, U. Kamachi Mudali, Lilyana Nenova, Chavdar Andreev, and Baldev Raj: Metallurgical and Materials Transactions A ,2012, 43 (6), 2069.

91. T. A. Mozhi, W. A. T. Clark, K. Nishimoto, W. B. Johnson and D. D. Macdonald: Corrosion, 1985 ,41, 555.

92. A. P. Majidi and M. A. Streicher, Corrosion, 1984, 40 (11), 584.

93. W. A. T. Clark, A. T. Mozhi and D. D. MacDonald: report DOE/ ER/10972–T2,1983.

94. N. Parvathavarthini: Mechanism, Mitigation and Monitoring. ed. by H. S. Khatak and Baldev Raj, Wood-head Publishing and Alpha Sci. Int. Ltd., Cambridge, England, 2002, 117.

95. G. H. Aydogdu, M. K. Aydinol: Corrosion Science, 2006, 48, 3565.

96. Revised Committee draft ISO/CD-12372 for a proposed standard on 'Method for EPR test', ISO-Technical Committee 156, Seventh revised version; 1998.

97. Z. Fang, L. Zhang, Y. S. Wu, J. Q. Li, D. B. Sun, C. Jiang and Z. M. Cui: Corrosion, 1995, 51, 124.

98. A. S. Lima, A. M. Nascimento, H. F. G. Abreu, P. De Lima-Neto: Journal of Material Science, 2005, 40, 139.

99. A. Kriaa, N. Hamdi, H. Sidhom: Protection of Metals, 2008, 44 (5), 506.

100. W. J. Lorenz and F. Mansfield: Corrosion Science, 1981, 21, 647.

101. F. Mansfeld, M. W. Kendig and S. Tsai: corrosion, 1982, 38, 570.

102. Craig Stinchcomb: Welding Technology Today, Principles and Practices, Prentice Hall, Englewood Cliffs, New Jersey, 1989.

103. Welding Handbook: Materials and Applications, Part 2, 8th ed. Miami, FL, American Welding Society,1991,2.

104. Jean Cornu: Advanced Welding Systems- Consumable Electrode Processe, Jaico Publishing House, Bombay, India, 1994.

105. Sindo kou: Transport Phenomena and Materials Processing, John Wiley & Sons, Inc., New York, 1996.

106. Stuart W. Gibson: Advanced welding, Macmillan Press Ltd., Houndmills, Basingstoke, Hampshire RG21 6XS and London, 1997.

107. Modern Arc Welding Technology: ADOR Welding ltd, Oxford & IBH Publishing Co. Pvt. ltd, New Delhi, India, 2008.

108. Y.Q. Zhang, H.-Q. Zhang, I.-F. LIU and R. Wei, J. Iron Steel Res., 2009, 16, 73.

109. Fontana. M.G "Corrosion engineering" McGraw Hill, New York ,1986, 445-502.

110. H. Inoue, T. Koseki, S. Okita & M. Fuji: Solidification and transformation behaviour of austenitic stainless steel weld metals solidified as primary austenite: Study of solidification and subsequent transformation of Cr-Ni stainless steel weld metals (1st Report), Welding International, 1997, 11 (12), 195.

111. H. Inoue, T. Koseki, S. Okita & M. Fuji: Solidification and transformation behaviour of austenitic stainless steel weld metals solidified as primary austenite: Study of solidification and subsequent transformation of Cr-Ni stainless steel weld metals (2nd Report), Welding International, 1997, 11 (12), 937.

112. M.Zietala,T.Durejko,M.Polanski,I.Kunce,T.Plocinski,W.Zielinski,M.Lazinska,W.Step niowski, T.Czujko , K.J.Kuezydlowski and Z.Bojar," The microstructure, mechanical properties and corrosion resistance of 316L stainless steel fabricated using laser engineered net shaping", Materials Science and Engineering:A, 2016, 677,1-10 .

113. J.Verma and R.V. Taiwade, " Effect of Austenitic and Austeno- Ferritic Electrodes on 2205 Duplex and 316L Austenitic Stainless Steel Dissimilar Welds", Journal of materials Engineering and Performance, 2016, 25 (11),4706-4717.

114. G.H.Aydogdu and M.K.Aydinol,"Determination of susceptibility to intergranular corrosion and electrochemical reactivation behaviour of AISI 316L type stainless steel," Corrosion Science,2006, 48 (11),3565-3583.

115. P.Pant, J.Verma,R.V.Taiwade,K.V. Phani Prabhakar, "Influence of advanced laser-arc hybrid welding and conventional MIG process on microstructure, mechanical properties and corrosion resistance of dissimilar joints", Materials Research Express, 2018, 5(6),066558.

116. S.Bose and S.Das , "Experimental investigation on bead-on-plate welding and cladding using pulsed GTAW process", Indian welding journal,2021,54(1).

117. L.O.Osoba,J.O.Okeniyi,B.I.Pogoson and O.A.Fasuba, "Effects of single pass and multipass welding on austenitic stainless steel corrosion in aggressive environments",GU J Sci ,2017,30(4),514-529.

118. M. Du Toit, G.T. Van Rooyen, and D. Smith, "An Overview of the Heat Affected Zone sensitization and stress corrosion cracking behavior of 12% chromium type 1.4003 ferritic stainless steel", IIW Doc IX-H-640, 2006.

119. A.K. Lakshminarayana and V. Balasubramanian, "Use of DLEPR test to asses sensitization resistance of AISI 409M grade ferritic stainless steel", Journal of Materials Engineering and performance, 2013, 22, 2293-2303.

120. Himanshu Vashishtha, Ravindra V. Taiwade, "Welding behavior of low nickel chrome-manganese stainless steel", ISIJ International, 2014, 54, 1361-1367.

121. S. Aguilar, R. Tabares, and C. Serna, "Microstructural Transformations of Dissimilar Austenite-Ferrite Stainless Steels Welded Joints", Journal of Materials Physics and Chemistry,2013, 1(4), 65–68.

122. N. Bensaid, M.hadji,R, Badji, M.F.Benlamnouar, T.Saadi, Y.L.dit Lakshir and S.Senouci," Microstructure and Mechanical Behavior of AISI 430 FSS welds Produced with different elelmental metal powder addition" Sloid State Phenomena , 2019, 297 , 195-203.

123. M. Alizadeh-Sh, S. P. H. Marashi, and M. Pouranvari, "Resistance spot welding of AISI 430 ferritic stainless steel: Phase transformations and mechanical properties," Materials & Design (1980-2015), 2014,56, 258–263.

124. A.M. Barrios, L.M.Burgos, E.E.Niebles-Nunez, L.A.Espitia, J.Unfried-Silgado," Influence of Immersion Corrosion on Mechanical Properties of AISI 430/AISI 316L Dissimilar Welded Joints", International Journal of Engineering,2021,34(5).

125. N. Hackerman, R. M. Hurd, and R. R. Annand, "Some structural effects of organic N-containing compounds on corrosion behaviour," Corrosion NACE, 1962, 18, 37–42.

126. D A. Jones, "Principles and Prevention of Corrosion", 2nd edn, Macmillan Pub. Co (1996), 292.Solartron Instruments, The Potentiodynamic Polarization Scan, Technical Report 33, Issue 2.0 ,1997.

127. E28 committee. Test Methods for Tension Testing of Metallic Materials, American Association State Highway and Transportation official's standard, 2019.

128. S.Ghorbani, R.Ghasemi, R.Ebrahimi-Kahrizsangi and A.Hojjati-Najafabadi," Effect of post weld heat treatment (PWHT) on the microstructure, mechanical properties, and corrosion resistance of dissimilar stainless steels", Materials Science and Engineering: A,2017, 688,470-479.

129. N. Stenbacka, On Arc Efficiency in Gas Tungsten Arc Welding, 2013, 18, 380–390.

130. J. Verma, R.V. Taiwade, R.K. Khatirkar, S.G. Sapate, and A.D. Gaikwad, "Microstructure, Mechanical and Intergranular Corrosion Behavior of Dissimilar DSS 2205 and ASS 316L Shielded Metal Arc Welds", Trans. Indian Inst. Met., Springer India, 2017, 70(1), 225–237.

131. H. Vashishtha, R. V Taiwade, R.K. Khatirkar, A.S. Dhoble, R. V Taiwade, R.K. Khatirkar, A.S.D., H. Vashishtha, R. V Taiwade, R.K. Khatirkar, and A.S. Dhoble, "Effect of Austenitic Fillers on Microstructural and Mechanical Properties of Ultra-Low Nickel Austenitic Stainless Steel", 2016, 1718.

132. A. V Bansod, A.P.Patil, S.Shukla, " Effect of Heat on Microstructure , Mechanical and Electrochemical Evaluation of Tungsten Inert Gas Welding of Low-Nickel ASS", J.Anti-corrosion Methods Materials, 2018,1-11.

133. H. Vashishtha, R. V. Taiwade, S. Sharma, and A.P. Patil, "Effect of Welding Processes on Microstructural and Mechanical Properties of Dissimilar Weldments between Conventional Austenitic and High Nitrogen Austenitic Stainless Steels", J. Manuf.Process., The Society of Manufacturing Engineers, 2017, 25, 49–59.

134. S. Sharma, R. V. Taiwade, and H. Vashishtha, "Investigation on the Multi-Pass Gas Tungsten Arc Welded Bi-Metallic Combination between Nickel-Based Superalloy and Ti-Stabilized Austenitic Stainless Steel", J. Mater. Res., 2017, 32(16), 3055–3065.

135. J. Verma, R.V. Taiwade, R.K. Khatirkar, and A. Kumar, "A Comparative Study on the Effect of Electrode on Microstructure and Mechanical Properties of Dissimilar Welds of 2205 Austeno-Ferritic and 316L Austenitic Stainless Steel", Mater. Trans., 2016, 57(4), 494–500.

136. J. Verma and R.V. Taiwade, "Dissimilar Welding Behavior of 22% Cr Series Stainless Steel with 316L and Its Corrosion Resistance in Modified Aggressive Environment", J. Manuf. Process., The Society of Manufacturing Engineers, 2016, 24, 1–10.

137. N. Ghosh, P. Kumar Pal, G. Nandi, and R. Rudrapati, "Parametric Optimization of Gas Metal Arc Welding Process by PCA Based Taguchi Method on Austenitic Stainless Steel AISI 316L", Mater. Today Proc., Elsevier Ltd, 2018, 5(1), 1620–1625.

138. N. Ghosh, P. Kumar Pal, G. Nandi, and R. Rudrapati, "Parametric Optimization of Gas Metal Arc Welding Process by PCA Based Taguchi Method on Austenitic Stainless Steel AISI 316L", Mater. Today Proc., Elsevier Ltd, 2018, 5(1), 1620–1625.

139. A. Moteshakker, I. Danaee, S. Moeinifar, and A. Ashrafi, "Hardness and Tensile Properties of Dissimilar Welds Joints between SAF 2205 and AISI 316L", 2015, 00(0),1–10.

140. S.Ambade,A.P.Patil,C.K.Tembhurkar,D.B.Meshram,"Effect of filler and autogenous welding on microstructure,mechanical and corrosion properties of low nickel Cr-Mn ASS",Advances in Materials and Processing Technologies,2021.

141. W. Chuaiphan and L. Srijaroenpramong, "Effect of Filler Alloy on Microstructure, Mechanical and Corrosion Behaviour of Dissimilar Weldment between AISI 201 Stainless Steel and Low Carbon Steel Sheets Produced by a Gas Tungsten Arc Welding", Adv. Mater. Res., 2012, 581–582(1), 808–816.

142. Farhad Ostovan, Ehsan Shafiei, Meysam Toozandehjani, Intan Fadhlina Mohamed, Masoud Soltani,"On the role of molybdenum on the microstructural, mechanical and corrosion properties of the GTAW AISI 316 stainless steel welds, Journal of Materials Research and Technology, Volume 13,2021,2115-2125.

143. L. Guo, G. Hua, B. Yang, H. Lu, L. Qiao, X. Yan, and D. Li, "Electron Work Functions of Ferrite and Austenite Phases in a Duplex Stainless Steel and Their Adhesive Forces with AFM Silicon Probe", Nat. Publ. Gr., Nature Publishing Group, 2016, 1–7.

LIST OF PUBLICATIONS

International Journal / e-journal / e- book

1. Advances in Materials Processing, Springer Publications, "Transient Analysis of GTA-welded austenitic and ferritic stainless steel", SCOPUS, e-book, (2020), 59-65.

2. Journal of Materials Engineering and Performance, Springer Publications, "Effect of fillers and autogenous welding on dissimilar welded 316L austenitic and 430 ferritic stainless steels", SCOPUS, Science Citation Index Expanded, Vol.30 (2) (2021),1444-1453.

3. Lecture Notes on Multidisciplinary Industrial Engineering, Springer Publications, "A critical review on dissimilar joining of ASS and FSS", e-book, (2021).

International and National Conferences

1. International Conference on Functional Materials, Manufacturing and Performances (ICFMMP-2019), School of Mechanical Engineering, Lovely Professional University, Phagwara, Punjab, India. Presented Paper Title: *Transient Analysis of GTA Welded Austenitic and Ferritic Stainless Steel,12-13 September,2019.*

2. International Conference on Industrial and Manufacturing Systems (CIMS-2020), Department of Industrial and Production Engineering, Dr.B.R.Ambedkar National Institute of Technology, Jalandhar, Punjab, India. Presented Paper Title: *A critical review on dissimilar joining of ASS and FSS, 9-11 October,2020.*

3. 2nd International Conference on Functional Materials, Manufacturing and Performances (ICFMMP- 2021), School of Mechanical Engineering, Lovely Professional University, Phagwara, Punjab, India. Presented   Paper Title: *Spot Welding analysis of dissimilar joint by finite element analysis, 17-18 September,2021.*

.